DOCTORAATSPROEFSCHRIFT

Faculteit Wetenschappen

TOPICS IN NONEQUILIBRIUM STATISTICAL MECHANICS :

I. COLLECTIVE BEHAVIOR OF COUPLED PARAMETRIC OSCILLATORS

II. HYDRODYNAMIC FLUCTUATIONS IN KOLMOGOROV FLOW

Proefschrift voorgelegd tot het behalen van de graad van
Doctor in de Wetenschappen, richting Natuurkunde,
te verdedigen door

IOANA BENA

Promotor : Prof. dr. C. Van den Broeck

2001

LIMBURGS UNIVERSITAIR CENTRUM
IN HET CENTRUM VAN DE KENNIS

UNIVERSITEITSBIBLIOTHEEK LUC
03 04 0063423 1

010480

BIBLIOTHEEK L.U.C.

17 APR. 2001

531
BENA
2001

luc.luc

D O C T O R A A T S P R O E F S C H R I F T

Faculteit Wetenschappen

TOPICS IN NONEQUILIBRIUM STATISTICAL MECHANICS :

I. COLLECTIVE BEHAVIOR OF COUPLED PARAMETRIC OSCILLATORS

II. HYDRODYNAMIC FLUCTUATIONS IN KOLMOGOROV FLOW

Proefschrift voorgelegd tot het behalen van de graad van
Doctor in de Wetenschappen, richting Natuurkunde,
te verdedigen door

010480

IOANA BENA

BIBLIOTHEEK L.U.C.

17 APR. 2001

Promotor : Prof. dr. C. Van den Broeck

2001

LIMBURGS UNIVERSITAIR CENTRUM
IN HET CENTRUM VAN DE KENNIS

According to the guidelines of the Limburgs Universitair Centrum, a copy of this publication has been filed in the Royal Library Albert I, Brussels, as publication D/2001/2451/7

Mamei

Acknowledgments

My warmest thanks go to my advisor, Professor Christian Van den Broeck, for giving me the opportunity to work with him at the Limburgs Universitair Centrum. I am deeply grateful to him for his stimulating and careful guidance, his wonderful scientific approach, and his amiable accessibility, that were essential for the accomplishment of this work.
I am deeply indebted to my "second advisor", Professor Mamad Malek Mansour of the Université Libre de Bruxelles, who guided me in elaborating the second part of this thesis. His high scientific and didactic abilities are matched by his gentle kindness and patience. I thank him for his warm and constant encouragement.
I owe the fruition of this thesis project to Professor Grégoire Nicolis. I express my gratitude to him for his welcome when I arrived in Belgium, for his continual encouragement, and for the opportunity he gave me to be in contact with the atmosphere of scientific enthusiasm he maintains in the Service de Chimie - Physique II de l'Université Libre de Bruxelles.
Professor Ryoichi Kawai, in true masterly fashion, patiently initiated me to FORTRAN 90. I am very grateful to him for his constant help in the computational part of this work, for his kindness and accessibility, as well as for the fruitful discussions we had during my visit to Alabama University.
Special thanks go to Professor V. Balakrishnan for his help in polishing the ideas and the English of this thesis. I enjoyed the fascinating discussions with him on various subjects. I value his friendship highly.
Professor Florence Baras greatly helped me throughout my work on this thesis. I owe her (and Professor Malek Mansour) some of the most involved computer simulations reported in the second part of the thesis. Her meticulousness and sense of scientific clarity have been a model to me.
I thank Professor Radu Bălescu for his kindness, keen interest in my work, and encouragement. Through his books, I also owe him much of my scientific education.
Professor E. G. D. Cohen and Professor John Turner are acknowledged for very helpful discussions.
My thanks go also to Professor Katja Lindenberg and Dr. Mauro Copelli, with whom I had useful exchange of ideas on the first part of this thesis.
I would like to thank my colleague Bart Cleuren for his amicable company,

encouragement, and valuable help.
Jérôme Déthier, David Hanon, and Peter Leoni were constantly badgered by me with questions on computers, and I thank them for their unfailing patience and prompt help.
For their continual assistance with various administrative matters and for all their help, I am thankful to: Ms. Hilde Wijnen, Ms. Conny Wijnants, Ms. Viviane Mebis, Ms. Annemie Hermans and Ms. Martine Machiels at LUC; and Ms. Irène Saverino, Ms. Sonia Wellens and Ms. Mireille Kies at ULB.
I gratefully acknowledge financial support from the Belgian IUAP program (Prime Minister's Office).

Finally, my thanks to all who are dear to me and who live deep in my heart and mind.

Abstract

This thesis is divided into two parts. The first part is devoted to the study of an analytically solvable model of coupled parametric oscillators. The model comprises an infinite set of globally coupled harmonic oscillators whose frequencies are subjected to time-periodic, piecewise-constant modulations with randomly distributed quenched phases. This system exhibits a variety of amplitude instabilities. In addition to the familiar parametric instability of the individual oscillators, two kinds of collective instabilities are identified. In one, the mean amplitude diverges monotonically, while in the other the divergence is oscillatory. The frequencies of the collective oscillatory instabilities bear no simple relation to the natural frequency of the individual oscillators, or to the frequency of the external modulation. A phase diagram is constructed to delineate the extent of the different regimes in the space of the parameters of the perturbation (its amplitude and period). Some of the features of the collective instabilities in the mean field model are already present in the simple system of just two coupled parametric oscillators with out-of-phase perturbations. It is also shown that the above phenomena are robust, in the sense that they do not depend crucially on the details of the model. Numerical simulations support the theoretical predictions.

The second part of the thesis uses the framework of the Landau-Lifshitz fluctuating hydrodynamics in order to study the statistical properties of Kolmogorov flow. A detailed analysis of the linearized fluctuation spectrum is carried out from the near-equilibrium regime up to the vicinity of the first convective instability threshold (that corresponds to the appearance of rotating convective patterns). It is shown that in the long-time limit the flow behaves as an incompressible fluid, regardless of the value of the Reynolds number. This is not the case for the short-time behavior, where the incompressibility assumption leads in general to an incorrect form of the static correlation functions, except near the instability threshold. However, in this latter region, nonlinear effects have to be taken into account appropriately. We derive the normal form amplitude equation for an incompressible fluid, and construct the velocity field close to, and just above, the threshold. The compressible case is analyzed as well. Using a perturbative technique, it is

shown that close to the instability threshold the stochastic dynamics of the system is governed by two coupled nonlinear Langevin equations in Fourier space. The solution of these equations can be cast in the form of the exponential of a Landau-Ginzburg functional, which proves to be identical to the one obtained for the case of an incompressible fluid. The theoretical predictions are confirmed by numerical simulations of the full fluctuating hydrodynamic equations. It is also shown that the results of particle simulations of Kolmogorov flow are vitiated by a spurious diffusion of the center of mass in phase space. The analytical expression for the corresponding diffusion coefficient is derived, using which we show that the effect is negligible in a macroscopic system.

Samenvatting

Het eerste deel van dit werk behandelt de studie van een analytisch oplosbaar model van gekoppelde parametrische oscillatoren. Dit systeem is samengesteld uit een oneindig groot aantal globaal gekoppelde oscillatoren, waarbij de frekwenties periodisch gemoduleerd worden met een willekeurige beginfase. Dit systeem vertoont een breed spectrum van amplitude instabiliteiten. Naast de welbekende parametrische instabiliteit worden twee andere collectieve instabiliteiten aan het licht gebracht. In het ene geval is er een monotone divergentie van de gemiddelde amplitude, terwijl de divergentie oscillerend is in het andere geval. De frekwenties van deze oscillaties worden in verband gebracht met deze van de individuele oscillatoren en van de modulatie. De verschillende gebieden in de parameterruimte van de modulatie (amplitude en periode) worden in een fasediagram voorgesteld. Enkele eigenschappen van de collectieve instabiliteiten in het gemiddelde veld model zijn reeds aanwezig in een eenvoudig systeem van twee gekoppelde oscillatoren waarbij de modulatie in tegenfase verloopt. Verder wordt er aangetoond dat de bovenstaande eigenschappen niet afhangen van specifieke details in het model. Numerieke simulaties bevestigen de theoretische voorspellingen.

Het tweede deel handelt over de statistische eigenschappen van de Kolmogorov stroom, steunend op de Landau-Lifshitz theorie voor fluctuerende hydrodynamica. Een gedetailleerde analyse van het gelineariseerde fluctuatie spectrum wordt uitgevoerd, vanuit evenwicht tot in de buurt van de eerste convectieve instabiliteit (die correspondeert met rotationele convectieve patronen). Voor lange tijden gedraagt deze stroom zich als een onsamendrukbare vloeistof, onafhankelijk van het Reynolds getal. Voor korte tijden daarentegen leidt de onsamendrukbaarheid tot een verkeerde vorm voor de statische correlatie functies, behalve in de buurt van de instabiliteit. In dit gebied daarentegen moet er weer rekening gehouden worden met niet lineaire effecten. De normaalvorm amplitude vergelijking voor een onsamendrukbare vloeistof wordt afgeleid, samen met het snelheidsveld dicht boven de instabiliteitsgrens. In geval van een samendrukbare vloeistof wordt aangetoond, gebruikmakend van storingsrekening, dat dicht bij de instabiliteitsgrens de stochastische dynamica van het systeem bepaald wordt door twee gekoppelde niet lineaire Langevin vergelijkingen in de Fourierruimte. De oplossing van deze vergelijkingen kan geschreven worden als de

exponentiële van een Landau-Ginzberg functionaal, die overeenkomt met deze voor het geval van een onsamendrukbare vloeistof. De theoretische voorspellingen worden bevestigd door numerieke simulaties van het volledig stel hydrodynamische vergelijkingen. De simulaties van de deeltjesbeweging worden verstoord door een valse diffusie van het massamiddelpunt in de faseruimte. De analytische uitdrukking voor deze diffusie coëfficient wordt afgeleid.

Contents

Part I

Collective Behavior of Coupled Parametric Oscillators

Chapter 1

Introduction

Over the past two decades there has been an increasing interest in the non-equilibrium behavior of spatially extended systems modeled as ensembles of simple dynamical units coupled to each other. The collective evolution of such discrete coupled systems often exhibits qualitatively different behavior from that of the single units.
An example of a system that has attracted a great deal of attention is a collection of a large number of coupled limit-cycle (phase) oscillators with randomly distributed natural frequencies [1]. This system has been invoked as a simple model for coupled chemical, biological or physical oscillators. A most spectacular collective phenomenon discovered with this model is a synchronization phase transition involving mutual entrainment of the oscillators through frequency and phase locking. However, in this model the coupling is assumed to be sufficiently weak so that the amplitude is not affected. As a result, the model cannot describe amplitude instabilities. A system that does exhibit a rich variety of *amplitude instabilities* consists of coupled parametric oscillators and is the subject of this part of the present thesis [2] - [5].

An oscillator under the influence of a parametric (time-periodic) perturbation can undergo an instability known as *parametric resonance.* Such *parametric oscillators* are encountered in a wide variety of physical systems - linear and nonlinear, deterministic as well as stochastic - in various contexts, including simple mechanical systems [6] (where such resonances were first identified), elementary particles [7], astrophysics [8], fluid mechanics [9], magnetism [10], plasma physics [11], electrical and electronic networks [12], optical systems and lasers [13], applied mechanics [14], and biophysics

[15], to cite only a few papers from a huge literature on the subject. A similar (energetic) instability can also arise in oscillators whose frequencies are perturbed in a stochastic manner (see, e.g., [16]), while the effect of thermal fluctuations is also well documented [17]. However, surprisingly little work has been done on systems of *coupled* oscillators with randomly varying or periodically varying natural frequencies - i.e., on *coupled parametric oscillators*. The few cases that we know of deal with a *global* parametric perturbation (i.e., one that acts on all the oscillators in exactly the same way), such as parametrically pumped electrons in a Penning trap [18], pattern formation under global exterior resonant forcing [19], time-periodic loading of an elastic system [20], and nonlinear parametrically driven lattices [21].

The focus of Part I of this thesis is the introduction and study of a simple linear model for coupled parametric oscillators that can be solved in full analytic detail: namely, an infinite set of globally mean-field coupled harmonic oscillators, subject to time-periodic, piecewise-constant modulations with randomly distributed quenched phases [2] - [4]. ("Quenched" in this context means that the phase of the frequency modulation of each oscillator is set at time $t = 0$ and remains unchanged thereafter.) The salient feature is the appearance of *collective parametric instabilities* that manifest themselves through an "explosion" of the mean displacement of the oscillators. Even though each individual oscillator is in its stable parameter domain, the average amplitude of the coupled system may diverge monotonically. This instability is re-entrant with respect to the strength of the spatial coupling of the oscillators, and persists in the overdamped limit. In the presence of a saturating nonlinearity, it generates a pitchfork bifurcation, corresponding to a genuine second-order nonequilibrium phase transition (implying the spontaneous breaking of spatial symmetry and ergodicity). In addition to this instability described by the monotonic growth of the mean amplitude, the globally-coupled infinite system can also undergo transitions to a collective oscillatory instability with an intrinsic frequency that is *not* connected in a simple way with either the frequencies of the individual oscillators, or that of the external modulation. A saturating nonlinearity turns this instability into a Hopf bifurcation, generating a limit cycle with the concomitant breaking of temporal symmetry and ergodicity.

In trying to explain these manifestations of collective behavior, one is struck by the similarities with a simple model introduced recently [5]. This involves *two* coupled parametric oscillators modulated periodically, with a fixed phase

difference τ between their modulations. The behavior of this "dimer" when $\tau = T_p/2$ (T_p is the period of the modulation) is remarkably similar to that of the globally-coupled infinite system, and the roots of the instabilities observed in the latter are already present in this simple system. At an even more primary level, the seeds of these collective instabilities can be traced back to the behavior of single oscillators. In general, an individual oscillator tends to synchronize with the external modulation, whereas the coupling induces mutual synchronization between oscillators. These two tendencies cannot be satisfied simultaneously. Coupling between oscillators can then be seen as leading to a sort of "selection" among the single oscillator modes, enhancing some (destabilization) and smoothing out others (stabilization).

A further remark is in order here about the motivation for the choice of our model. In a number of recent papers [22], several intriguing cooperative phenomena have been reported in spatially extended systems subject to state-dependent (or multiplicative) noise (see [23] for a review). Genuine *nonequilibrium phase transitions* of both first and second order, involving the breaking of time and/or space translation invariance and ergodicity, have been found. Models with state-dependent noise are present in a wide variety of physical systems, e.g., in hydrodynamics [24], growth phenomena [25], lasers [26], etc. (see also [23]). In this context, Van den Broeck and Kawai [27] had the idea of investigating *inertia-less, mean-field coupled* particles subject to a parametrically perturbed elastic force, whose equations of motion look like

$$\gamma\dot{x}(t) + \omega_0^2[1 + \xi(t)]x(t) + k(x - < x >) = 0 \,, \tag{1.1}$$

and examining the effects of various types of perturbations $\xi(t)$ of the restoring force [1]. They compared the effect of a periodic modulation with a phase disorder with the effects of perturbations by white noise and dichotomous Markov noise. Besides the mean field version, which allows a general exact solution in all three cases, they also studied numerically $1D$ and $2D$ systems with first-neighbour coupling between the oscillators.

The main conclusion of their study was that periodic perturbation with

[1] In the thermodynamic limit of an infinite number of coupled particles, the mean $< x >$ over the realizations of the perturbation is equal to the mean over the ensemble of particles. Here x is the coordinate of a typical particle, γ the friction coefficient, and ω_0 corresponds to the unperturbed elastic force; k is the (spatial) coupling constant.

disorder can give rise to what they called "absorption-desorption" *phase transitions* that are similar to those induced by the noise. In particular, in $1D$ and $2D$ systems one can recognize the appearance of long-range spatial correlations in the vicinity of the phase transition. Moreover, they clarified the rather surprising mechanism behind such modulation-induced phase transitions, by tracing it back to the transient increase of the first moment, already observed in other systems with multiplicative noise that exhibit nonequilibrium phase transitions [28]. Indeed, it was shown that the first moment $< x >$ undergoes, for a short time, an increase above its initial value; this is due to a minority of particles with large values of $|x|$. In the case of a sufficiently strong coupling, these members pull the other sites away from the "absorbing state" $x = 0$. However, as these particles start relaxing, other sites take over and pull the system even further away from zero, and so on. This pool of "transiently large-$|x|$" particles changes periodically with time in a complicated manner. The random ingredient contributes to the existence of a broad distribution of $|x|$ values, so that the average can deviate significantly from the typical value. This reasoning is in agreement with the fact that the transition from the absorbing state $< x >= 0$ to an explosive behavior $< x > \rightarrow \pm\infty$ when $t \rightarrow \infty$ is *re-entrant* with respect to the strength k of the coupling. Indeed, when the coupling is too large, the difference between the oscillators is suppressed and the collective instability disappears.

When one takes into account the inertia of the particles, the dynamics becomes considerably richer; in particular, oscillatory modes of behavior are made possible. We therefore investigate the counterpart of eq. (1.1) that takes into account the inertial terms. In the next chapter, we first briefly present some examples of parametric oscillators in various physical contexts (Section 2.1). We then review the behavior of a single parametric oscillator subject to a time-periodic, piecewise-constant modulation of its frequency (Section 2.2 and Appendix A). The elements that will be relevant for the coupled system, as described in the subsequent chapter, are brought to the fore. In Section 3.1 of Chapter 3 we introduce the globally coupled model. Section 3.2 and Appendix B establish the mathematical setting for the analysis of the globally coupled system as a mean-field problem. Typical numerical results are presented in Section 3.3. In Section 3.4 we collect these results in the form of a phase diagram that characterizes the behavior of the coupled system as the modulation parameters are varied. We discuss the boundaries between stable and unstable behavior and also between different

instability regimes. Two interesting limiting cases are discussed in Section 3.5, namely that of inertia-less particles and that of an adiabatic modulation. Finally, Section 3.6 (along with Appendix C) offers a comparison between the mean-field system and the dimer, which leads to a deeper insight into the mechanisms of the collective instabilities. Conclusions and a discussion of the results are presented in Chapter 4.

Chapter 2

The Single Parametric Oscillator

2.1 Parametric Resonance in Different Physical Contexts

Generally speaking, parametric resonance refers to the instability of a system in response to a (time-periodic) modulation of one of its parameters. The simplest and best-studied example is the parametric harmonic oscillator (with a friction coefficient γ and mass $m = 1$), given by

$$\ddot{x} + \gamma\dot{x} + \omega^2(t)x = 0 \ , \tag{2.1}$$

where the frequency $\omega(t)$ varies periodically in time according to

$$\omega^2(t) = \omega_0^2 \ [1 + \xi_\tau(t)] \ . \tag{2.2}$$

Here ω_0 is the proper frequency of the unperturbed oscillator and $\xi_\tau(t)$ is a periodic function of time, $\xi_\tau(t) = \xi_\tau(t + T_p)$, with $\omega_p = 2\pi/T_p$ as the frequency of the perturbation; τ is the initial phase of the perturbation [1].

One of the trademarks of parametric resonance is that the most pronounced instability is induced by a *superharmonic* perturbation with frequency $\omega_p \approx 2\omega_0$. For the harmonic oscillator (with no saturating nonlinear terms

[1] Of course, τ can be set to zero through a suitable choice of the origin of time; however, we prefer to retain it explicitly, in order to make clearer the connection with the coupled system to be considered in the next chapter.

present) one observes an unlimited growth of the amplitude; in contrast to the "usual" resonance phenomena (for an oscillator subject to an *additive* periodic forcing), friction alone cannot limit this growth.

As already mentioned in the Introduction, parametric resonance occurs in a wide variety of physical systems [6] - [15]. The oldest example is the parametrically driven pendulum. The frequency of small oscillations around the vertical resting position is of course $\omega_0 = \sqrt{g/l}$, where g is the acceleration due to gravity and l is the length of the pendulum. It is clear that ω_0 can be perturbed in two ways, by altering l and the effective g, respectively. We first consider a periodic modulation of l. The discovery of this form of parametric resonance dates back to way before the birth of Newtonian mechanics, and was already practised, for instance, in the cathedral of Santiago de Compostela in Spain, in the early Middle Ages. One can understand the concern of the local bishop to make his church smell fresh with incense, while an unending flux of pilgrims, walking all the way south from as far away as Germany and Holland, streamed in daily to pay their respects to the remains of Saint James the Major. A giant censor, called O. Botafumeiro, and weighing about 60 kg, hung from a rope that passed through a roller on the ceiling, 20 m high. By pulling and releasing this rope ($\Delta l \approx 1.5$ m) periodically, with five strong men at the task orchestrated by the initiated priest, the censor could be pumped in 17 cycles to a full swing, nearly touching the ceiling of the cathedral, happily releasing its beatifying odor as it passed 1.5 m above the floor at about 50 km/h. This remarkable and spectacular physical phenomenon is reported and described in a medieval manuscript of 1366. It should be noted that the physics of a pendulum with a time-periodic length is more complicated than that of (2.1), because the time derivative of the impulse $\dot{p} = d(l\dot{\theta})/dt$ will generate a time-dependent friction term. For a detailed treatment including the nonlinear terms, as well as a comparison with the experimental observation in Santiago de Compostela, see [29]. We note also that children have a rather direct experience of this phenomenon, when moving themselves up and down on a swing in order to increase the amplitude of its movement.

The other way to vary the frequency of a pendulum is to modulate the effective acceleration due to gravity. (We know from general relativity that gravitation is locally equivalent to an accelerated frame of reference.) By modulating the acceleration, one can modulate the effective value of g. This can be realized for the pendulum by periodically varying its suspension

point. For a frequency $\omega_p \approx 2\omega_0$ (and low friction), it is found that this induces, above a critical amplitude, a bifurcation to an amplified swinging motion of the pendulum around its equilibrium position. For a nicely documented computer experiment, see [30].

In 1831, Faraday discovered that a layer of fluid can develop surface ripples when the basin that holds it is periodically moved up and down. Faraday instability is another example of parametric instability. The surface of the water can be considered as consisting of an infinite number of harmonic oscillators, namely the surface eigenmodes. In the case of so-called gravity waves (in deep water, neglecting dissipation and surface tension), the dispersion relation expressing the frequency $\omega_0(k)$ of these waves as a function of their wave vector $k = 2\pi/\lambda$ is particularly simple [31] and very similar to that of the pendulum, namely $\omega_0(k) = \sqrt{gk}$. These waves are highly dispersive with a phase velocity $\omega_0(k)/k$ that is twice as large as the group velocity $d\omega_0(k)/dk$. By periodically vibrating the whole basin containing the fluid with frequency ω_p, one is in fact periodically changing g. By parametric resonance, surface waves with frequency $\omega_0 \approx \omega_p/2$ will be most strongly excited.

Perhaps one of the most spectacular illustrations of parametric resonance is the dynamical Casimir effect. We describe here a naive, "classical" picture of the effect. In 1948 Casimir showed [32] that two parallel, perfectly conducting plates in vacuum are subjected to a mutual attractive force given by

$$F = \frac{\pi^2 \hbar c S}{240\, d^4} \,, \tag{2.3}$$

where $\hbar$ is Planck's constant, c the speed of light, S the surface area of each plate and d the distance between them. The origin of the force lies in the vacuum fluctuations of the electromagnetic field. However, these ground state excitations (virtual photons) cannot have arbitrary wavelengths in the region between the plates, since the wavefunction must be exactly zero on the plates. The lowest possible frequency for these virtual photons is thus $\omega_0 = 2\pi c/\lambda = \pi c/d$. Since the virtual photons exert a pressure on the plates, and since all wavelengths are excited outside but not in the region in between the plates, a net force results. Another way to state this is that the energy density is lower in between the plates than in the region outside. The work done by the Casimir force upon separating the plates corresponds

exactly to the energy deficit between the two regions. Of course, the Casimir force also appears in other configurations of conductors, such as a plate and a sphere, or two spheres. Only recently has this phenomenon been observed directly and measured [33], and the results - found to be in agreement with the prediction of the Casimir formula (2.3). From the relation $\omega_0 = \pi c/d$ it is clear that a periodic modulation of the distance d corresponds to a parametric pumping of the modes between the plates: this is called the dynamical Casimir effect. The amplitude instability that one observes classically corresponds to the creation of photons in a quantum mechanical context. One thus expects that the mechanical work corresponding to the oscillation of the plates with frequency $\omega_p = 2\omega_0$, will be transformed into photons with frequency ω_0. Although our "translation" in terms of a classical language is rather heuristic, the results described here are in agreement with the predictions of a more detailed quantum field-theoretic calculation [34].

It is also interesting to note a close connection between the frictionless parametric oscillator and the Bloch theory of electrons in metals [37]. The stationary Schrödinger equation

$$\psi'' + \frac{2m}{\hbar^2}(E - V)\psi = 0\,, \tag{2.4}$$

where V is a spatially periodic potential modelling the attraction of the lattice ions on the electrons, is formally identical to eqs.(2.1) - (2.2), with t replaced by x and γ set equal to zero. The energy values for which the corresponding wave function diverges exponentially with the distance form the forbidden bands and are the equivalent of the regions of parametric resonance in the oscillator problem. A specific square-wave form for the potential (the Krönig-Penney model in solid state physics) is equivalent to the piecewise-linear modulation of the frequency of the parametric oscillator to be considered in the next section.

Finally, further examples of physical systems in which parametric resonance appears [35] include: LCR circuits (C or L oscillates), spiral waves in active media (an applied electrical field oscillates), ferrofluids and $2D$ electron gases (an applied magnetic field oscillates), microwave guides (the temperature oscillates), and even the theory of the early universe (inflationary oscillations).

2.2 The Single Parametric Oscillator

2.2.1 The "Piecewise Constant" Model

Equation (2.1), combined with (2.2), reads

$$\ddot{x} + \gamma\dot{x} + \omega_0^2[1 + \xi_\tau(t)]x = 0 \ . \tag{2.5}$$

This is called Hill's equation [36], and it looks misleadingly simple. In fact, no general explicit solution of this equation is known. For the particular (and extensively studied) case of a sinusoidal perturbation $\xi_\tau(t) = A\sin[\omega_p(t+\tau)]$, it is known as the Mathieu equation. Explicit results are expressed in terms of the Mathieu functions, which are unfortunately quite complicated. We therefore turn to the case of a *piecewise-constant* periodic modulation

$$\xi_\tau(t) = A \ \mathrm{sgn}\,[\sin\omega_p(t+\tau)] \tag{2.6}$$

for which the analysis is more tractable, helping reveal the underlying physics.

Let us focus first on the mechanism of the onset of the instability. For simplicity of exposition, we neglect friction for the moment ($\gamma = 0$). During the time intervals where ξ_τ is constant, (2.5) is the evolution equation of a plain harmonic oscillator, with conservation of the total energy,

$$\frac{\dot{x}^2}{2} + \frac{\omega^2 x^2}{2} = \text{constant} \ . \tag{2.7}$$

Hence the motion lies on ellipses in the phase space $(x, \dot{x})$. Note that flat ellipses correspond to small ω (fig. 2.1). Suppose we start in the low frequency phase ($\xi = -A$) at $x = 0$ with $\dot{x}$ at some initial value (state 1 in fig.2.1). The phase point follows the ellipse until it reaches $\dot{x} = 0$ with a nonzero maximal amplitude x. At this point (state 2), we switch to the higher frequency ($\xi = A$). By doing so, we replace a soft extended spring by a stiff one with the same extension, and therefore we have to pump in an amount of energy equal to the corresponding gain in potential energy. We now proceed with this stiff spring and the phase point moves on a vertically elongated ellipse, until we again reach $x = 0$ with nonzero $\dot{x}$. At this point (state 3), we switch back to the soft spring, but with no cost in energy, since $x = 0$. This enables the oscillator to move to state 4 and so on. Thus energy is pumped in, while covering a full cycle in the perturbation in each half cycle of the oscillator itself. Whenever this condition for the period of

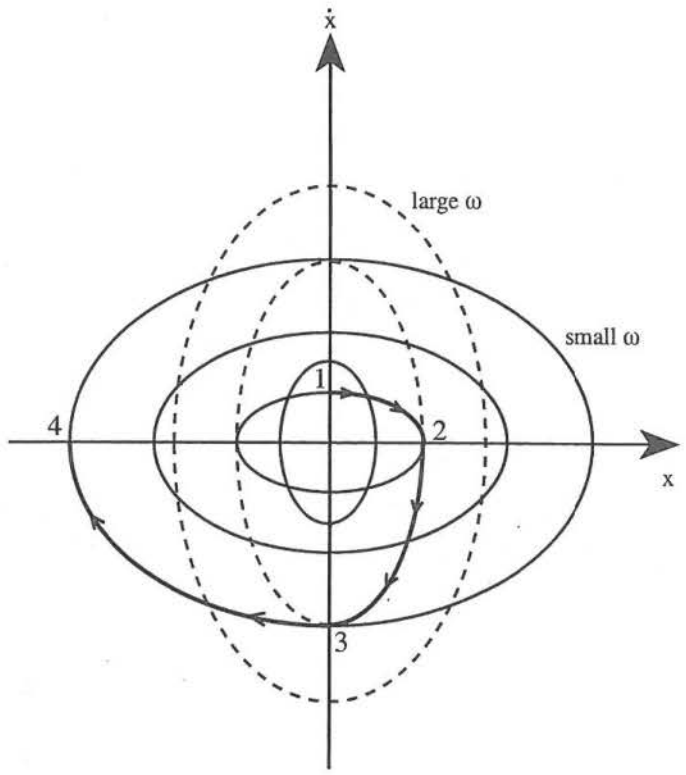

Figure 2.1: A schematic representation of the phase-space trajectory of the parametric oscillator with piecewise linear modulation of its frequency, eqs.(2.5) - (2.6), without friction ($\gamma = 0$).

the perturbation is fulfilled, the instability of the oscillator develops for any amplitude A of the perturbation.

If friction is taken into account, the phase space trajectories of the unperturbed oscillator become spirals that decay to the origin. It is then understandable that the onset of the instability requires not only a definite period for the perturbation, but also an amplitude (of the perturbation) that is larger than a certain value, in order to compensate for the inward spiralling of the unperturbed trajectories.

2.2.2 Analytic Solution

We now turn to an explicit analytic solution for the piecewise constant model. The equation of motion can be solved using Floquet theory and Laplace transform methods, as shown in Appendix A. The temporal behavior of oscillator's amplitude is expressed as a linear superposition of modes,

$$x(t) = \sum_{j \in Z} c_j e^{s_j t} \tag{2.8}$$

where the c_j's are constants determined by the initial conditions. The exponents $s_j = \Lambda_j + i\Omega_j$ $(j \in Z)$ are determined in terms of the *resonance parameter* R defined as

$$R = \cos\left(\frac{\omega_+ T_p}{2}\right)\cos\left(\frac{\omega_- T_p}{2}\right) - \frac{\omega_+^2 + \omega_-^2}{2\omega_+\omega_-}\sin\left(\frac{\omega_+ T_p}{2}\right)\sin\left(\frac{\omega_- T_p}{2}\right) , \tag{2.9}$$

with

$$\omega_\pm = \omega_0\sqrt{1 \pm A - \left(\frac{\gamma}{2\omega_0}\right)^2} . \tag{2.10}$$

The exponents s_j are solutions of the equation

$$\cosh\left[\left(s + \frac{\gamma}{2}\right)T_p\right] - R = 0 . \tag{2.11}$$

Their real parts are explicitly given by

$$\Lambda_j = \begin{cases} -\frac{\gamma}{2} \pm \frac{1}{T_p} \ln\left[-R + \sqrt{R^2-1}\right] & \text{for} \quad R \leq -1 \\ -\frac{\gamma}{2} & \text{for} \quad |R| \leq 1 \\ -\frac{\gamma}{2} \pm \frac{1}{T_p} \ln\left[R + \sqrt{R^2-1}\right] & \text{for} \quad R \geq 1 \end{cases} , \tag{2.12}$$

while the imaginary parts are

$$\Omega_j = \begin{cases} \left(j - \frac{1}{2}\right)\omega_p & \text{for} \quad R \leq -1 \\ j\omega_p & \text{for} \quad R \geq 1 , \end{cases}$$

$$\Omega_j^{\pm} = \left[j \pm \frac{1}{2\pi} \arccos R\right] \omega_p \quad \text{for} \ |R| \leq 1 . \tag{2.13}$$

Here $\arccos R$ lies in the range $[0, \pi]$ and, as already mentioned, j is an integer. Note that the real parts of the exponents are in fact independent of j. One can therefore drop the subscript j on Λ and rewrite the amplitude (2.8) as

$$x(t) = e^{\Lambda t} \sum_{j \in Z} c_j e^{i\Omega_j t} \tag{2.14}$$

(plus another sum of the same type with a second value of Λ, in the cases when there are two possible values for Λ: see below.). Correspondingly, the relative weights of the different modes remain the same for all time, i.e., they all decay ($\Lambda < 0$), or diverge ($\Lambda > 0$), or maintain their initial amplitudes ($\Lambda = 0$). None of them becomes relatively dominant with increasing time. Figure 2.2 illustrates the dependence of the real and imaginary parts of the exponents on the resonance parameter R, for $-2 \leq j \leq 2$.

There are two boundaries to be considered.

a). *The boundary* $|R| = 1$ that separates the regimes where Λ and the Ω_j's are R-dependent from the regimes where they are R-independent. When $|R| < 1$, Λ is R-independent, single-valued, and negative (unless there is no damping, $\gamma = 0$, in which case Λ vanishes and the motion is purely oscillatory). At the bifurcation points $R = \pm 1$ the real part becomes R-dependent and two-valued, but remains negative until $|R|$ reaches the critical value R_c (see below).

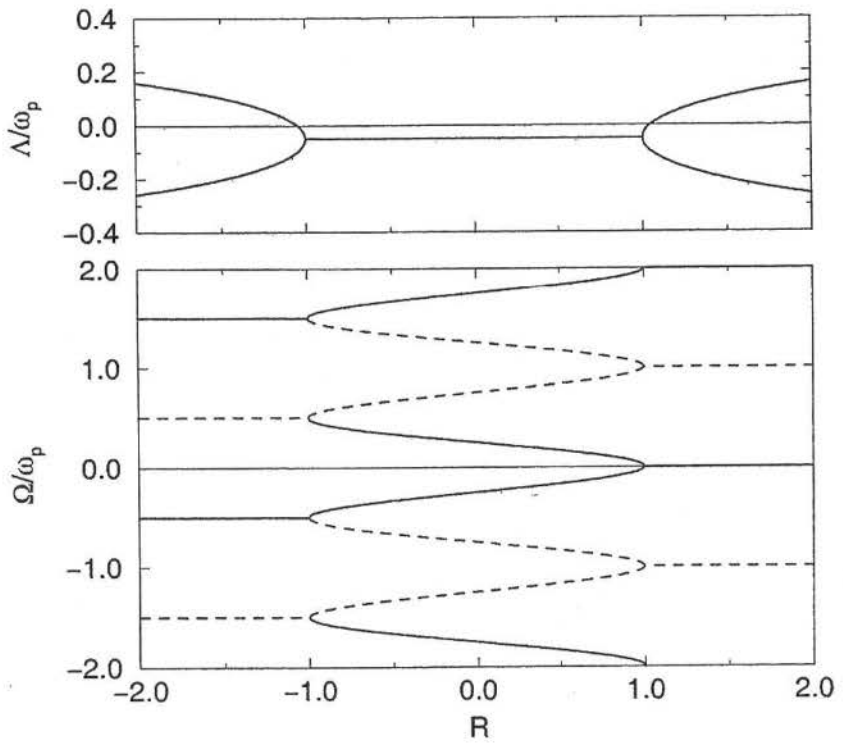

Figure 2.2: Real part (upper graph) and imaginary part (lower graph) of the exponents s_j for $j = -2, \ldots, 2$ as a function of R (for $\gamma/\omega_p = 0.1$). The behavior associated with these exponents is described in detail in the text. Note the significance of the boundaries $R = \pm 1$, and of the boundaries $R = \pm R_c$ where one value of Λ becomes positive. The latter mark the onset of single-oscillator parametric instability.

In contrast, when $|R| < 1$, the oscillator frequencies Ω_j change continuously with R and bear no simple relation to either ω_p or the natural frequency ω_0. On the large-$|R|$ side of this boundary, the frequencies Ω_j are simply proportional to the frequency ω_p of the modulation, $\Omega_j = j\omega_p$ or $\Omega_j = (j - 1/2)\omega_p$, with $j \in Z$.

For $R > 1$ note the existence of a zero-frequency mode of the oscillator, $\Omega_0 = 0$, which simply provides a monotonically decaying contribution (for $\Lambda < 0$) or increasing contribution (for $\Lambda > 0$) to the displacement of the oscillator.

b). *The boundary* $|R| = R_c$, where

$$R_c \equiv \cosh\left(\frac{\gamma T_p}{2}\right) \tag{2.15}$$

which is greater than unity unless $\gamma = 0$. Beyond $|R| = R_c$ one of the Λ's becomes positive, leading to an exponential growth of the oscillator amplitude. The condition $|R| = R_c$ thus corresponds to the onset of the parametric resonance or, more appropriately, the parametric instability. Figure 2.3 depicts the boundaries of instability in the parameter space (A, T_p/T_0) for different values of the friction coefficient. Note that friction has a stabilizing effect, i.e., it reduces (quite dramatically) the extension of the instability regions. In particular, in the absence of friction $\gamma = 0$, and for small amplitudes A of the perturbation, the boundaries of the instability are described simply by

$$T_p/T_0 = n\left(1 \pm A^2/4\right) \quad (n = 1, 2, \ldots) \tag{2.16}$$

and

$$T_p/T_0 = n + 1/2 \pm A/2\pi \quad (n = 0, 1, 2, \ldots)\ . \tag{2.17}$$

The most pronounced and widest region of instability, especially for small A's, is delimited by $T_p/T_0 = 1/2 \pm A/2\pi$, in agreement with the previous qualitative discussion of the mechanism of parametric instability.

An important difference between the present case and that of the usual additive periodic driving (and the usual resonance phenomena) is the fact that here friction does not prevent the divergence of the amplitude when

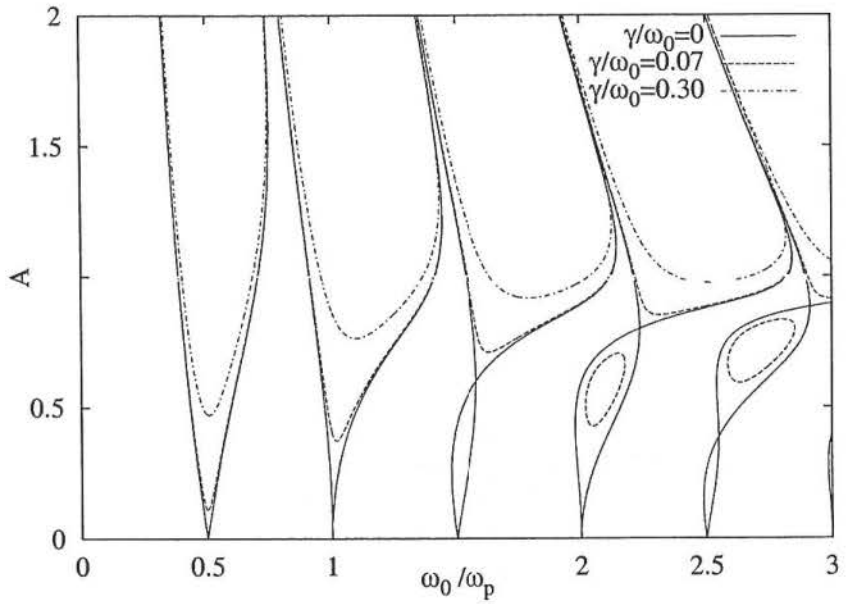

Figure 2.3: The boundaries of the region of parametric resonance for a single oscillator subject to a piecewise linear perturbation (2.6), in parameter space $(A, T_p/T_0 = \omega_0/\omega_p)$, for different values of the friction coefficient γ. Note that the $\gamma = 0$ curves touch the $A = 0$ axis. The domains inside the curves correspond to the region of instability.

one is in an unstable parameter regime. Nonlinear terms, e.g., $-x^3$ in the right hand side of eq.(2.5), are needed to prevent the divergence, but these terms do not modify the appearance and the location of the instability. We also note that in the parametric instability region the oscillator's frequencies Ω_j are simply proportional, through a (half)integer, to the frequency of the modulation, while Λ is strongly R-dependent.

In fig. 2.4 we present the regions in parameter space $(A, T_p/T_0)$ where $|R| > 1$: darker regions for $R > 1$; lighter, for $R < -1$. The stability boundaries $|R| = R_c$ are also indicated by solid lines, the oscillator being unstable inside these boundaries. Note that the $|R| = R_c$ and $|R| = 1$ boundaries almost coincide, because of the very low damping considered, namely $\gamma = 0.01$. For small A's, as is well known, the instability appears in the vicinity of $T_p \approx jT_0/2$ (j a natural number).

Although the boundary $|R| = R_c$ is important in determining the transition from stable to unstable behavior for the single parametric oscillator, we shall see in the next chapter that it does not play the same role for the coupled system, for which the boundary $|R| = 1$ turns out to acquire further significance. Indeed, as we will see in Section 3.2, each individual pole $s_j = \Lambda + i\Omega_j$ gives rise to a "collective" pole in the coupled system, and these collective poles have different Λ's. Some modes may become unstable ($\Lambda > 0$), and therefore dominant, even when $|R| < 1$, while others remain stable ($\Lambda < 0$). The underlying mechanism is that, depending on whether or not the frequencies of the individual oscillators are proportional to the modulation frequency, in the coupled system the oscillators may get synchronized either to the perturbation or to each other (through the mean), and this may result in the "enhancement" of some modes as compared to the others.

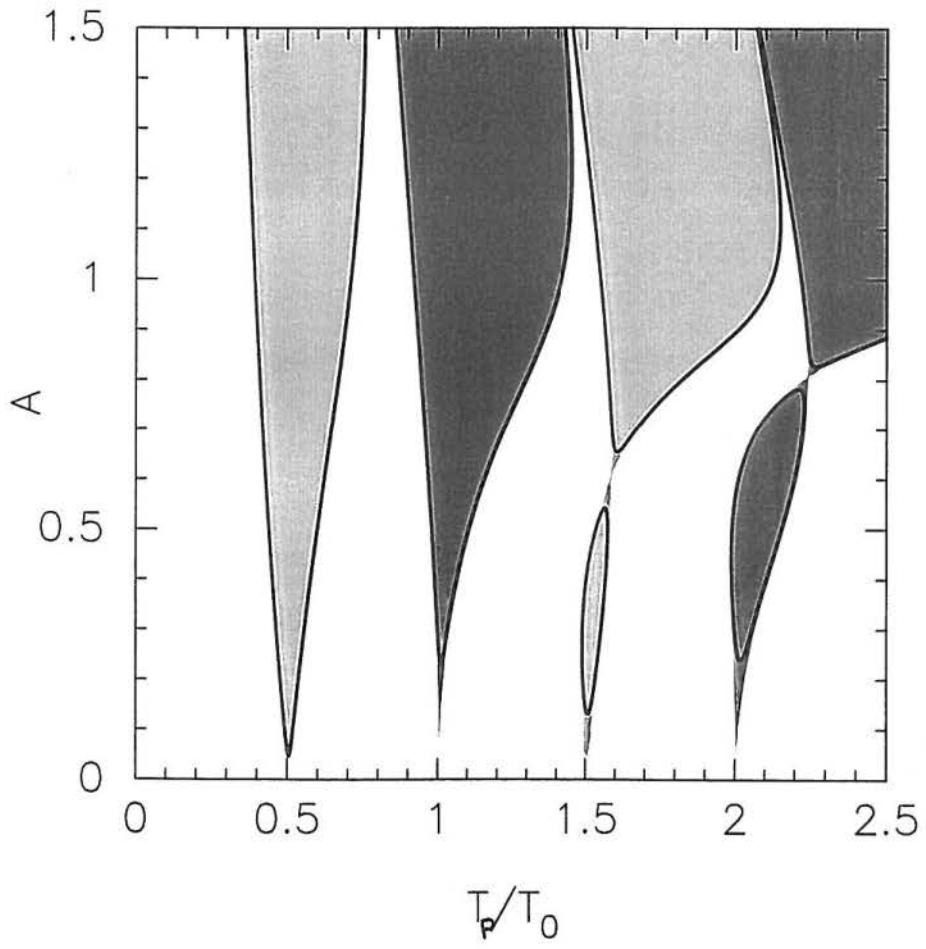

Figure 2.4: Shaded regions indicate $R > 1$ (darker) and $R < -1$ (lighter). Solid lines delineate the boundaries $|R| = R_c$. Damping $\gamma = 0.01$, frequency $\omega_0 = 0.4$.

Chapter 3

Coupled Parametric Oscillators

3.1 The Basic Linear Model

The physics of coupled oscillators has a long and very interesting history - see, e.g., [20]. Of course, the simplest case of a linear chain of harmonically coupled particles is textbook material in introductory physics. In the continuum limit, one gets the non-dispersive wave equation. When in addition each particle is subjected to a harmonic substrate potential, the equation of motion is known as the (discrete version of the) Klein-Gordon equation:

$$\ddot{x}_i + \omega_0^2 x_i = -\frac{k}{2}(2x_i - x_{i+1} - x_{i-1}) \tag{3.1}$$

where x_i is the coordinate of the i-th oscillator, ω_0 the natural frequency, and $k/2$ the "normalized" spring constant coupling neighbouring oscillators. (The mass of each oscillator has been set equal to unity.) A great deal of effort, prompted in part by such surprising discoveries as the KAM theory and the existence of solitons [38], has been devoted to investigating what happens when nonlinear terms are added. Another major direction of research, following the discovery of Anderson localization in linear systems with disorder and the relation to the theory of random matrices, has been the study of the effects of disorder [39].

This part of the thesis is devoted to the analysis of the exact solution for a simple linear model, namely a system of harmonically coupled parametric

oscillators with quenched randomly distributed phases.

Consider a set of N parametric oscillators of unit mass, with displacements $\{x_i\}$, each with a periodically modulated frequency and all of them harmonically coupled to one another. We restrict our analysis to coupled *linear* parametric oscillators. A few comments on the nonlinear case will be presented in Chapter 4. The equation of motion of the i-th oscillator is given by

$$\ddot{x}_i + \gamma\dot{x}_i + \omega_0^2[1 + \xi_i(t)]x_i = -\frac{k}{N}\sum_{j=1}^{N}(x_i - x_j) \ , \tag{3.2}$$

with $i = 1, \cdots, N$. Analytic results are possible with a simple piecewise-constant periodic modulation of the frequency of each oscillator (see Chapter 2) given by

$$\xi_i(t) = A \ \mathrm{sgn}\left[\sin\omega_p(t + \tau_i)\right] \ , \tag{3.3}$$

where $\omega_p = 2\pi/T_p$ (T_p - the modulation period), and the initial phase τ_i is chosen at random for each oscillator from a uniform distribution between 0 and T_p. We are mainly interested in the mean amplitude

$$\langle x\rangle = \frac{1}{N}\sum_{i=1}^{N} x_i \tag{3.4}$$

as a measure of the macroscopic behavior of the system. In the *thermodynamic limit* $N \rightarrow \infty$, the site average (3.4) is equivalent to the average with respect to the random phase τ_i of the displacement of a single oscillator i, namely,

$$\langle x\rangle = \frac{1}{T_p}\int_0^{T_p} x_i \, d\tau_i \ , \tag{3.5}$$

which is independent of i. Equation (3.2) can then be reduced to a single mean-field differential equation,

$$\ddot{x} + \gamma\dot{x} + \omega_0^2[1 + \xi_\tau(t)]x = -k(x - \langle x\rangle) \ , \tag{3.6}$$

where we have dropped the index i, and $\xi_\tau(t)$ denotes modulation with a random initial phase τ (eq.(3.3)). We note that the average $\langle x\rangle$ must be evaluated self-consistently using eqs. (3.5) and (3.6).

3.2 Collective Instabilities

As explained in Appendix B, the first (and rather trivial) effect of the coupling is a *shift in the frequencies* ω_0 and $\omega_\pm$ of the single oscillator, according to

$$\omega_k = \omega_0 \sqrt{1 + \frac{k}{\omega_0^2}} ,$$

$$\omega_\pm = \omega_0 \sqrt{1 \pm A + \frac{k}{\omega_0^2} - \left(\frac{\gamma}{2\omega_0}\right)^2} . \tag{3.7}$$

Correspondingly, all the single oscillator quantities - e.g., the resonance parameter R - must be calculated using these shifted values of the frequencies.

The self-consistent equation for the mean leads, as shown in Appendix B, to a temporal behavior of the form

$$\langle x \rangle (t) = \sum_{l \in Z} c_l e^{r_l t} , \tag{3.8}$$

where the constants c_l are determined by the initial conditions. The exponents $r_l = \Lambda_l + i\Omega_l$ correspond to *pure collective modes.* They are complex solutions of the rather complicated equation

$$F(r;\, T_p,\, A,\, \omega_0,\, \gamma,\, k) \equiv$$

$$T_p\, \omega_+\, \omega_- \left[\cosh\left(\frac{\tilde{\gamma} T_p}{2}\right) - R\right] \times$$

$$\times \left(\omega_+^2 + \frac{\tilde{\gamma}^2}{4}\right)^2 \left(\omega_-^2 + \frac{\tilde{\gamma}^2}{4}\right)^2 \left[\frac{k\left(\omega_+^2 + \omega_-^2 + \frac{\tilde{\gamma}^2}{2}\right)}{2\left(\omega_+^2 + \frac{\tilde{\gamma}^2}{4}\right)\left(\omega_-^2 + \frac{\tilde{\gamma}^2}{4}\right)} - 1\right]$$

$$- k\omega_+ \,(\omega_+^2 - \omega_-^2)^2 \left(\omega_-^2 - \frac{\tilde{\gamma}^2}{4}\right) \sin\left(\frac{\omega_- T_p}{2}\right) \left[\cosh\left(\frac{\tilde{\gamma} T_p}{4}\right) - \cos\left(\frac{\omega_+ T_p}{2}\right)\right]$$

$$- k\omega_- \,(\omega_+^2 - \omega_-^2)^2 \left(\omega_+^2 - \frac{\tilde{\gamma}^2}{4}\right) \sin\left(\frac{\omega_+ T_p}{2}\right) \left[\cosh\left(\frac{\tilde{\gamma} T_p}{4}\right) - \cos\left(\frac{\omega_- T_p}{2}\right)\right]$$

$$- k\omega_+ \omega_- \tilde{\gamma} (\omega_+^2 - \omega_-^2)^2 \sinh\left(\frac{\tilde{\gamma}T_p}{4}\right)\left[2\cosh\left(\frac{\tilde{\gamma}T_p}{4}\right)\right.$$
$$\left. - \cos\left(\frac{\omega_+ T_p}{2}\right) - \cos\left(\frac{\omega_- T_p}{2}\right)\right] = 0 \tag{3.9}$$

where

$$\tilde{\gamma} \equiv \gamma + 2r = \gamma + 2\Lambda + 2i\Omega \; . \tag{3.10}$$

Finding the complex roots of eq. (3.9) is difficult even numerically. Therefore, we investigate the collective modes graphically, as shown in the next section. Graphical inspection not only provides a qualitative understanding of collective modes, but also helps in identifying suitable numerical algorithms.

When $k \to 0$, eq.(3.9) reduces precisely to eq.(2.11), i.e., the collective modes reduce to the single oscillator modes. This suggests that each single oscillator mode s_j is the progenitor of a collective mode r_j with different Λ_j and Ω_j in the coupled system. Much can therefore be learned about these collective modes from the single oscillator modes, as will become clear from what follows. An analysis of the temporal behavior of $\langle x \rangle$, as well as of the behavior of the single oscillators, enables us to identify four different possible regimes in the system:

Regime A :
Each single oscillator with the given shifted parameters is unstable (i.e., $|R| > R_c$), while the mean $\langle x \rangle$ is zero.

Regime B :
Each oscillator is stable, and is in the region where its frequency is determined by the modulation frequency (i.e., $1 < |R| < R_c$), while the mean diverges monotonically in time. This is the first type of collective instability.
This instability of the mean can also appear when each single oscillator is unstable, but the unstable collective mode diverges faster than the single oscillator modes.

Regime C :
Each single oscillator is stable and its shifted frequency bears no simple relation to the natural shifted oscillator frequency or to the modulation frequency (i.e., $|R| < 1$); and the mean oscillates with a diverging amplitude. This is the second type of collective instability.

Regime D :
Each single oscillator is stable and the mean tends asymptotically to zero (the "absorbing state").

In the following section we will present examples of realizations of the first three regimes. A detailed analysis of the behavior of the individual oscillators allows one to clarify the mechanisms behind the different kinds of behavior.

3.3 Results

Before proceeding further, let us emphasize that in the following we make a careful distinction between a *single* oscillator and an *individual* oscillator. The former refers to an independent oscillator with parameters ω_k (shifted proper frequency) and γ, while the latter will refer to one of the oscillators in a coupled system with parameters ω_k, γ, and k.

We present three examples that correspond, respectively, to the first three regimes listed at the end of the last section. Each case is discussed with the help of three corresponding figures. Note that the parameter values $k = 1.28$, $\omega_0 = 0.4$, $\gamma = 0.01$, and $A = 1.0$ are used in all the figures, and that only the shifted proper frequency ω_k of the oscillator is different from one case to another.

The first set of figures represents the exponents of the collective modes. We recall that in order to find the poles $r_l = \Lambda_l + i\Omega_l$ associated with the collective modes one needs to solve the set of coupled equations

$$\text{Re } F(r;\, T_p,\, A,\, \omega_0,\, \gamma,\, k) = 0 \,, \tag{3.11}$$

$$\text{Im } F(r;\, T_p,\, A,\, \omega_0,\, \gamma,\, k) = 0 \tag{3.12}$$

obtained from eq.(3.9). In figure 3.1 we plot the left-hand sides of eqs. (3.11) and (3.12) as contour lines in the space $(\Lambda/\omega_p, \Omega/\omega_p)$ [solid lines for eq.(3.11), and dashed lines for eq.(3.12)]. The thick lines indicate zero contours. The solutions we seek are therefore the intersections of these two sets of thick lines, and are indicated by open circles. The poles of single oscillators with shifted frequency are indicated by solid black circles. There is, of course, an infinite number of exponents, but we only exhibit the relevant ones. In figure 3.2 we depict the corresponding mean amplitude, mean standard deviation $\Delta x = \sqrt{\langle x^2 \rangle - \langle x \rangle^2}$, and the trajectory of an individual oscillator as functions of time. as they serve to characterize the particular situation. Finally, the associated phase trajectories are also presented in figure 3.3. Figures 3.4 - 3.6 and 3.7 - 3.9 represent the corresponding figures for two other values of ω_k, as described below.

Regime A :
Figure 3.1 shows the contours and poles for the case $\omega_k = \omega_p/2$, which corresponds to $R = -1.0062$. Since $R < -1$, the poles of single oscillators appear on the lines $\Omega_j/\omega_p = j - 1/2$, each as a pair because in this regime there are two values of Λ associated with each Ω. Only the poles for $j = 1$ are shown, as the others (and there is an infinite number of them) are off the scale of this figure. Since $|R| > R_c = 1.00077$ for these parameters, one of each pair of poles has a positive Λ. The amplitude of a single oscillator would therefore diverge exponentially. However, as the numerical calculations indicate, all the collective modes have $\Lambda = -\gamma/2$. Therefore, as indicated by eq.(3.8), the mean amplitude decays to zero, despite the instability of single oscillators.

Computer simulation results for various trajectories of a system of 100000 oscillators with these parameters are shown in fig. 3.2. We see that the mean amplitude is indeed zero, and that the standard deviation $\Delta x = \sqrt{\langle x^2 \rangle - \langle x \rangle^2}$ diverges. The inset shows the same two trajectories as well as the diverging trajectory of an individual oscillator.

Phase trajectories of individual oscillators in the coupled system are shown in fig. 3.3. Each circle indicates a snapshot of an individual oscillator. Solid circles represent oscillators with positive modulation and open circles correspond to those with negative modulation at the time of the snapshot. Only 2000 oscillators out of 100000 are shown. The six snapshots show that

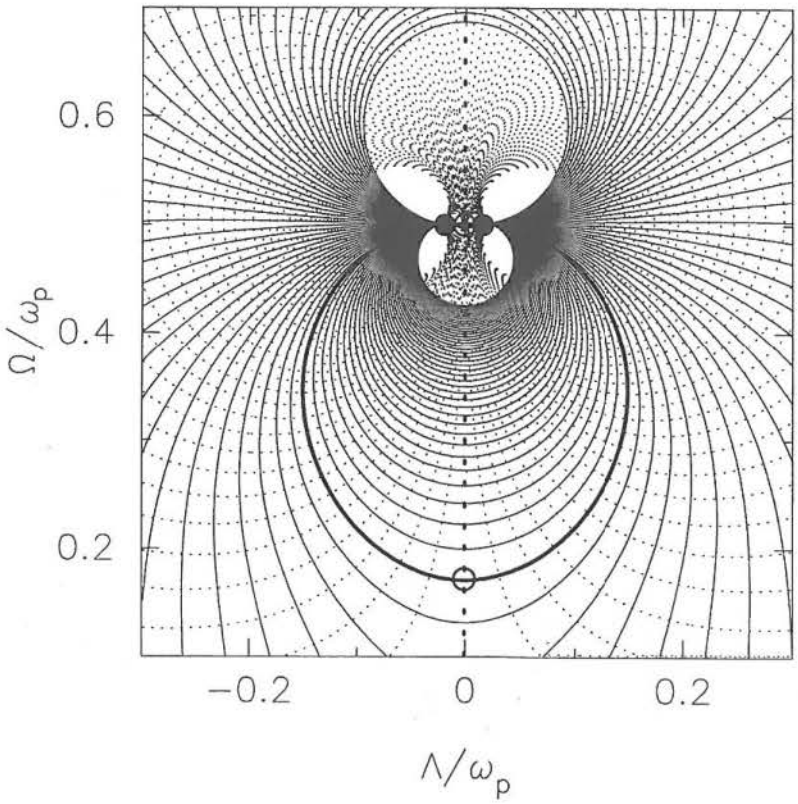

Figure 3.1: Contour plots of the left-hand side of eq. (3.11) (solid lines) and eq. (3.12) (dashed lines) for $\omega_0 = 0.4$, $k = 1.28$, $\gamma = 0.01$, $A = 1.0$, and $T_k = 2\,T_p$, which lead to $R = 1.00617$. Poles of a single oscillator are indicated by solid circles. Thick lines correspond to solutions of eqs. (3.11) (solid) and (3.12) (dashed). The intersections of the solid and dashed thick lines, indicated by open circles, are thus solutions of eq. (3.9). Although there is a single oscillator pole with positive Λ there is no positive-Λ collective mode.

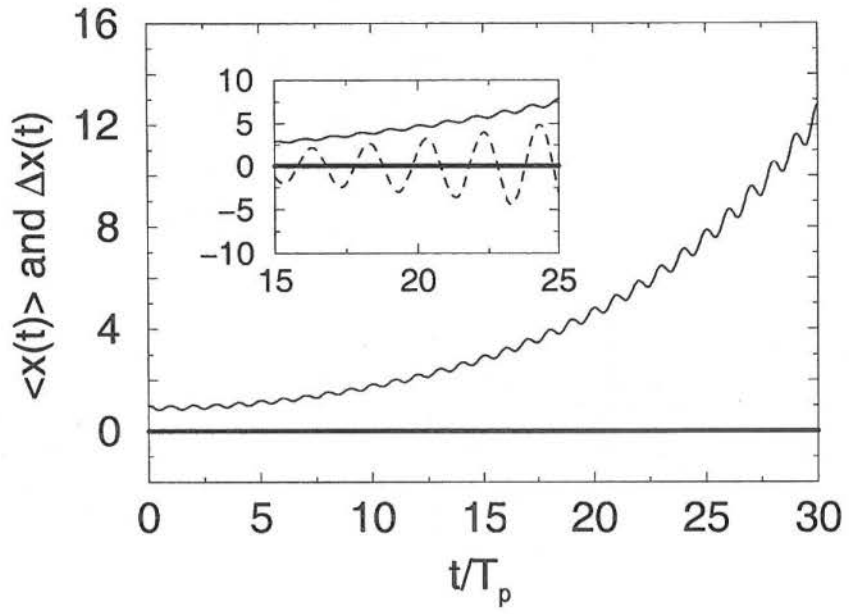

Figure 3.2: Trajectories associated with fig. 3.1. Thick solid line: mean $\langle x \rangle$. Thin solid line: standard deviation Δx. The inset also includes the trajectory x of an individual oscillator (dashed line).

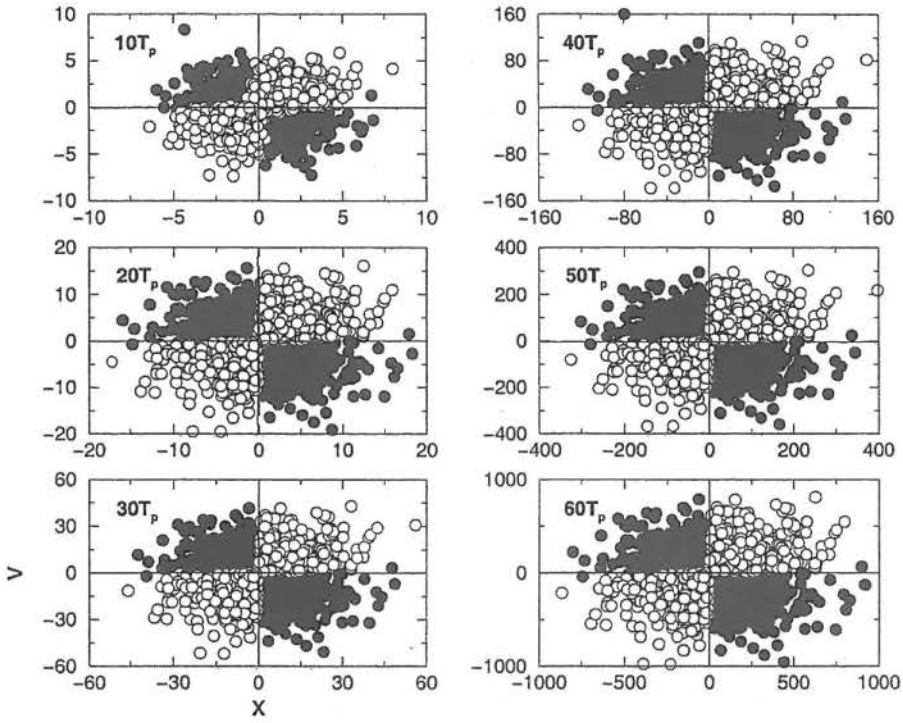

Figure 3.3: Phase point snapshots of 2000 individual oscillators in the system associated with figs. 3.1 and 3.2. Note the scale changes with increasing time.

with increasing time the phase volume increases (note the different scales in each snapshot), which is consistent with the divergent behavior of each oscillator and with the growth of the deviation Δx, and also provide confirmation that there is indeed no mutual synchronisation or other kinds of organized collective motion. The persistent separation of solid and open circles into separate quadrants indicates that individual oscillators are synchronized with the external modulation. Note that any *individual* oscillator moves clockwise, switching colors accordingly. In this case, the only effect of coupling is the frequency shift (3.7).

Regime B :
Interesting behavior is observed when $\omega_k = \omega_p$, that is, the single oscillator frequency is equal to the modulation frequency. The contours and poles for this case are shown in fig. 3.4. Since $R = 1.0001$, the single oscillator has poles at $\Omega_j = j\,\omega_p$. Only the poles for $j = 0$ are shown. R is just below $R_c = 1.0031$, and therefore all the single oscillator modes have negative Λ's (single oscillator trajectories decay to the absorbing state $x = 0$). However, one of the collective modes has a pole with $\Omega = 0$ and a *positive* Λ. All the other collective modes in eq.(3.8) are dominated by this nonoscillatory unstable mode, and therefore the mean amplitude diverges monotonically.

Computer simulation results for the associated trajectories are shown in fig. 3.5. The mean decays slowly at the beginning and then diverges monotonically. The standard deviation diverges as well, and does so more rapidly. The individual oscillator trajectory also diverges; in this instance, although each single oscillator would be stable, the coupling causes individual oscillators in the system to become unstable. In other words, each oscillator is driven by the diverging mean in eq. (3.6).

The phase trajectories in fig. 3.6 show that after an initial transient (first three panels, where the open circles hide most of the solid circles), individual oscillators in the coupled system oscillate with increasing amplitude about $\langle x \rangle$, while the mean $\langle x \rangle$ is moving away from the origin. In the long-time limit, each oscillator "forgets" its initial conditions and is driven by the mean. Therefore, while the phase of each individual oscillator is determined by the phase of the modulation, the amplitude in phase space is determined by the mean. Correspondingly, the oscillators become "amplitude-synchronized" through the mean.

Until the synchronization is well established, the individual oscillators decay because the single oscillator modes have negative Λ. As in the previous case, the phases of all single-oscillator modes with $\Omega_j \neq 0$ become synchronized with the external modulation. However, in contrast with the previous case, there is now a zero-frequency mode which does not have a phase to be synchronized. This mode is therefore not affected by the phase of each oscillator, or by the phase of the modulation. The zero-frequency mode shifts the center of oscillation away from $x = 0$ in either the positive or the negative direction. In the presence of coupling the oscillators tend to follow the mean, and therefore shift in the same direction, thus breaking the sym-

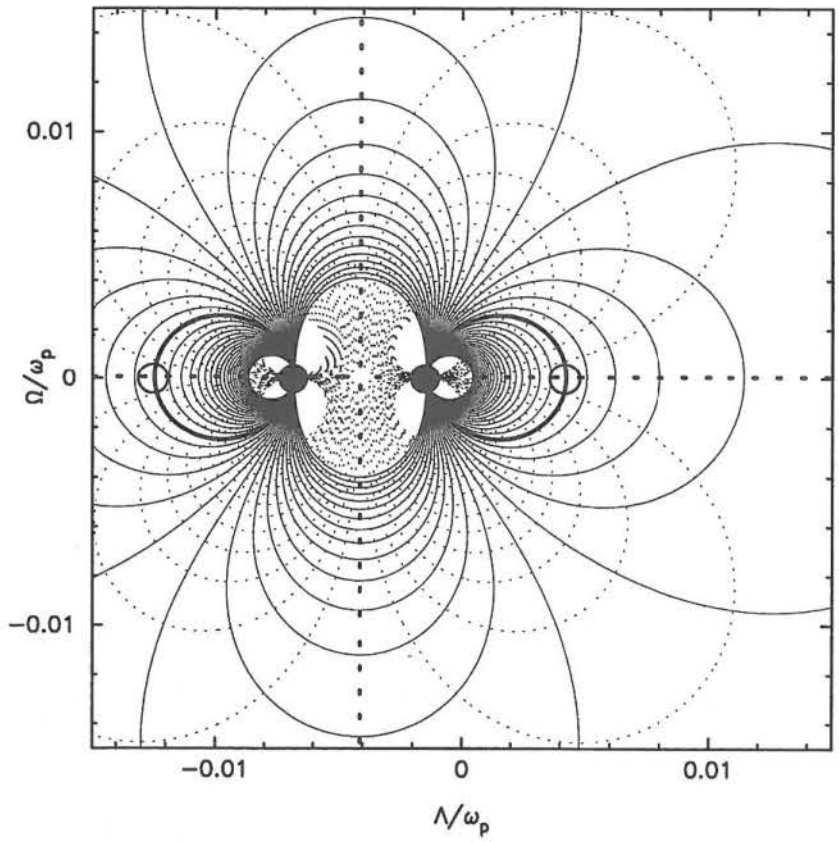

Figure 3.4: Contour plots of the left-hand side of eqs. (3.11) (solid lines) and eq. (3.12) (dashed lines) for $\omega_0 = 0.4$, $k = 1.28$, $\gamma = 0.01$, $A = 1.0$, and $T_k = T_p$, which lead to $R = 1.0001$. Poles of a single oscillator are indicated by solid circles. Thick lines correspond to solutions of eqs. (3.11) (solid) and (3.12) (dashed). The intersections of the solid and dashed thick lines, indicated by open circles, are thus solutions of eq. (3.9). Although the single oscillator poles have all negative Λ, the collective modes include a pole with positive Λ and $\Omega = 0$. This mode diverges exponentially without oscillation.

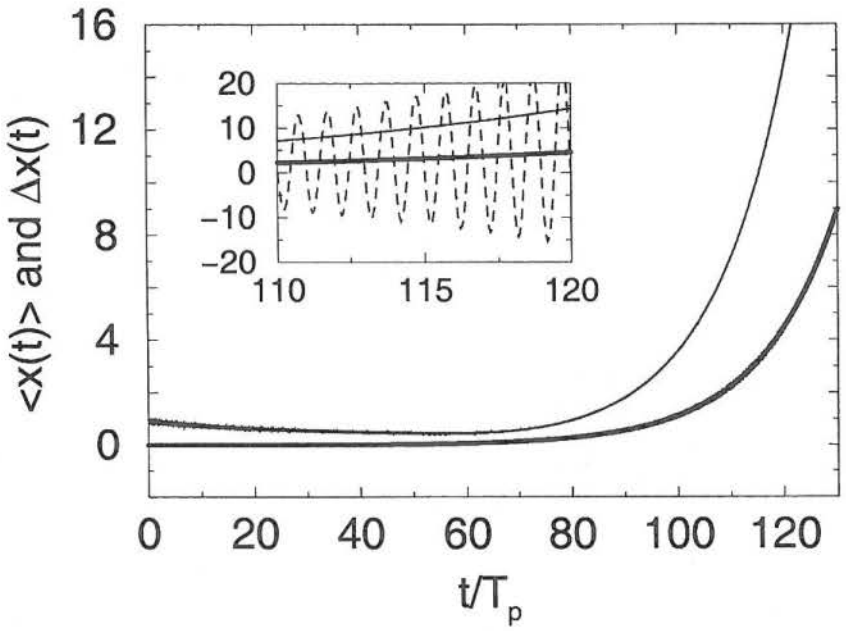

Figure 3.5: Trajectories associated with fig. 3.4. Thick solid line: mean $\langle x \rangle$. Thin solid line: standard deviation Δx. The inset also includes the trajectory x of an individual oscillator (dashed line).

metry of the system. Note that the open and solid circles no long lie entirely in separate quadrants. Thus, in this case the effect of coupling is not only a shift in the frequency according to (3.7), but also the more interesting collective symmetry-breaking monotonic divergence of the mean amplitude and the mutual synchronization of the individual oscillator amplitudes.

One can sometimes encounter this nonoscillatory instability of the mean even if the single oscillators are unstable (i.e., are in their parametric resonance region). In these cases, the positive Λ of the collective mode is always larger than that of the single oscillator modes; the collective mode dominates the dynamics of the mean.

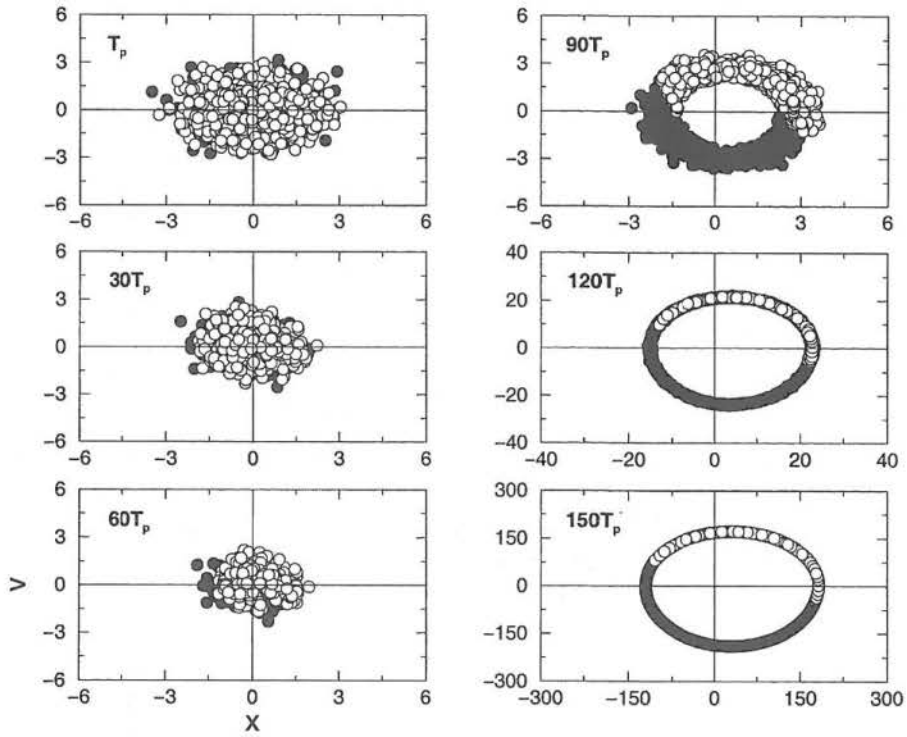

Figure 3.6: Phase point snapshots of 2000 individual oscillators in the system associated with figs. 3.4 and 3.5. Note the scale changes with increasing time.

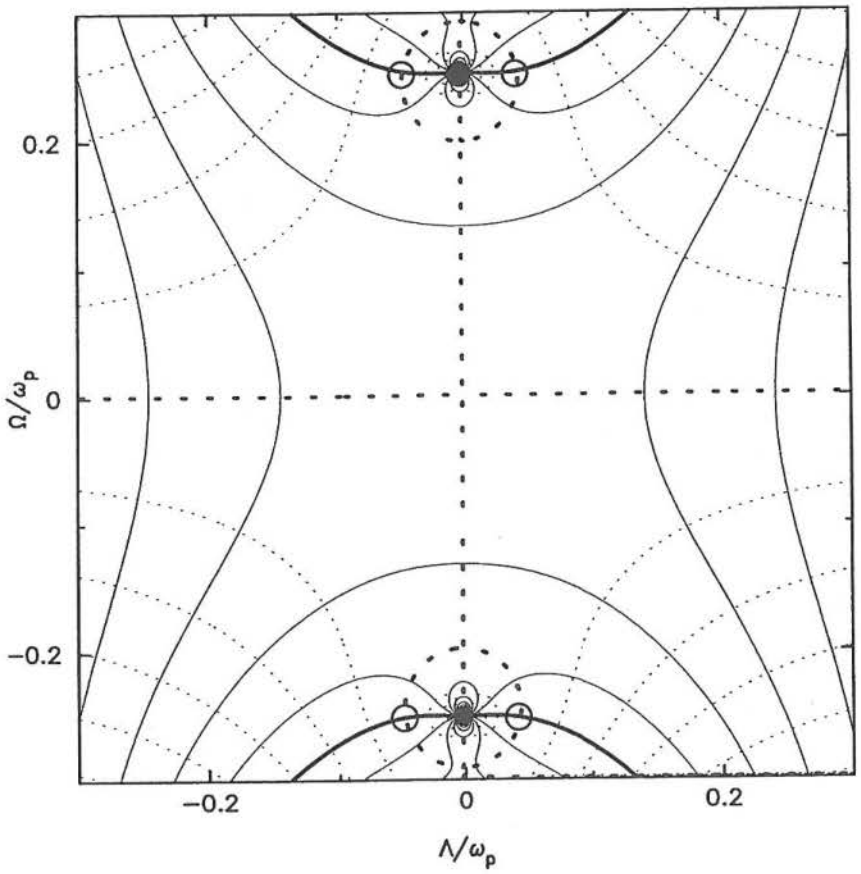

Figure 3.7: Contour plots of the left-hand side of eqs. (3.11) (solid lines) and eq. (3.12) (dashed lines) for $\omega_0 = 0.4$, $k = 1.28$, $\gamma = 0.01$, $A = 1.0$, and $T_k = 4\,T_p/3$, which lead to $R = -0.01037$. Poles of a single oscillator are indicated by solid circles. Thick lines correspond to solutions of eqs. (3.11) (solid) and (3.12) (dashed). The intersections of the solid and dashed thick lines, indicated by open circles, are thus solutions of eq. (3.9). Although the single oscillator poles all have negative Λ, the collective modes include a pole with positive Λ and nonzero Ω. This mode diverges exponentially in an oscillatory manner.

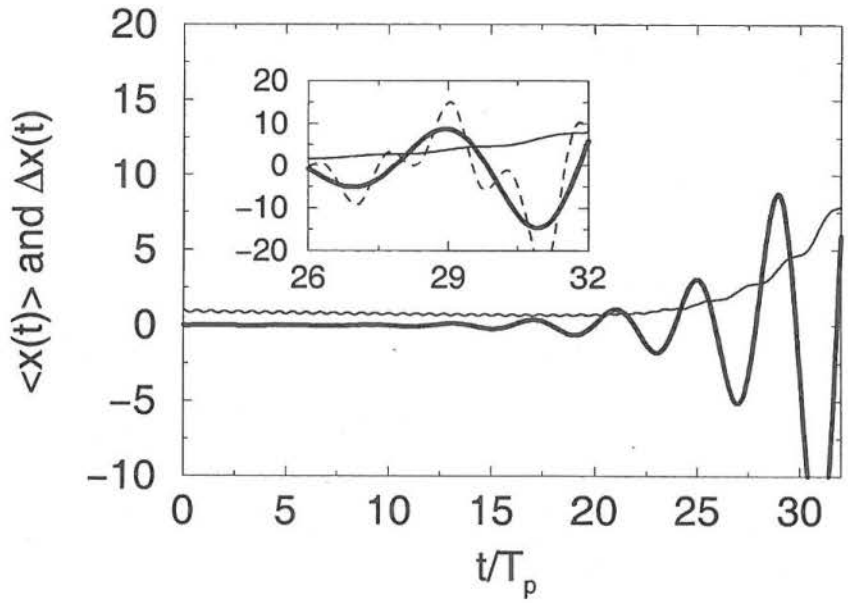

Figure 3.8: Trajectories associated with fig. 3.7. Thick solid line: mean $\langle x \rangle$. Thin solid line: standard deviation Δx. The inset also includes the trajectory x of an individual oscillator (dashed line).

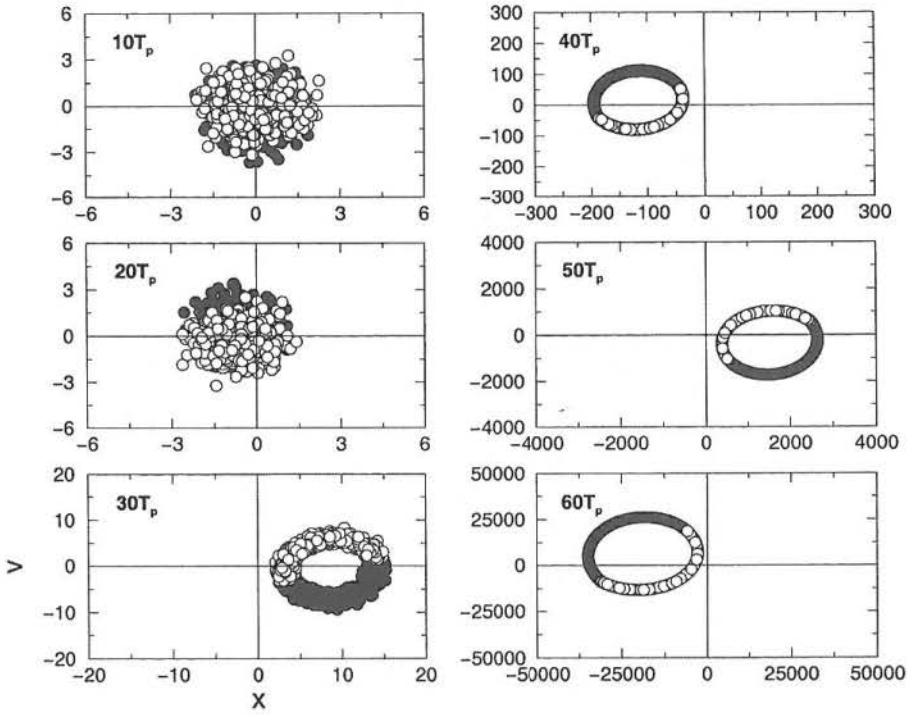

Figure 3.9: Phase point snapshots of 2000 individual oscillators in the system associated with figs. 3.7 and 3.8. Note the scale changes with increasing time.

Regime C:
This occurs, for instance, when $\omega_k = 3\,\omega_p/4$ (which lies in between the two previous cases), so that $|R| < 1$ (and, of course, the single oscillators are not in the parametric resonance situation). However, fig. 3.7 indicates that at least one of the collective modes has a positive Λ as well as a non-zero Ω. Therefore, the mean $\langle x \rangle$ oscillates with a diverging amplitude. Recall that when $|R| < 1$ the eigenfrequencies of single oscillators vary continuously with R but do not match either the frequency of the modulation or the natural shifted frequency of the oscillator. Therefore, the individual synchronization to the external modulation plays no role and the phases of the oscillators are free to synchronize with one another through a synchronization to the phase of the mean.

Computer simulations whose results are shown in fig. 3.8 confirm the oscillatory instability, and the phase space points of individual oscillators shown in figure 3.9 corroborate this phase synchronisation. Although the solid and open circles again form separate groups, the entire ring of open and solid circles alternates between the positive quadrants and negative quadrants: all the oscillators are mutually synchronized.

In the next section we collect the results for the coupled system into a phase diagram indicating the regions of stability and instability of different types.

3.4 Phase Diagram

A convenient way to summarize various observations and characterize the instabilities systematically is by means of appropriate *phase diagrams* in which the stability boundaries are depicted as functions of the system parameters. Since there are many parameters in this model, the full diagram would involve a many-dimensional representation. We present the diagram in the two-dimensional space $(A, T_p/T_k)$ that characterizes the external modulation for a given set of oscillator parameters ω_k, k, and γ.

Figure 3.10 shows the phase diagram for the system parameters indicated in the caption. The colored regions denote unstable regimes, each color coding for a particular type of instability (regimes A to C); white regions correspond to the absorbing state (regime D).

Regime A :
The yellow region denotes parameter ranges where the individual oscillators are unstable but the mean amplitude for the coupled system is zero - "incoherent unstable oscillations". In this case the distinction between "single oscillators" and "individual oscillators" becomes moot, since the mean term in eq. (3.6) plays no role.

Regime B :
Blue regions - "saddle nodes" - denote monotonic divergence of the mean with one positive Λ and zero Ω. Green regions - "unstable nodes" - also denote monotonic instabilities but with two positive Λ's and zero Ω. Note that there may exist superpositions of the green (or blue) regions with the yellow ones, as already mentioned in the previous section.

Regime C :
Oscillatory instabilities of the mean with positive Λ and nonzero Ω are depicted in pink - "unstable spirals".

In our terminology for various instabilities we have loosely followed the usual conventions of nonlinear dynamics.

The phase diagram just described is quite rich and intricate. Instabilities cover even larger regions in parameter space, and do so with increasing intricacy, as the damping γ decreases. A typical phase diagram for low damping is shown in fig. 3.11.

It is also helpful to follow the behavior of the oscillator system across the various collective instability boundaries by considering the signs of Ω and Λ for the collective modes as one increases the modulation amplitude A (thus moving upward vertically along the phase diagram) for different fixed values of the modulation period T_p. Various associated bifurcation diagrams presenting Λ (solid lines) and Ω (dotted lines) as functions of A are shown in fig. 3.12, for oscillator parameters identical to those of fig. 3.10.

Consider first the period $T_p = 0.75\,T_k$, shown in panel (a). As A increases, Λ changes sign, becoming positive at $A_c = 1.14$, while Ω remains positive throughout. This represents a transition from a stable spiral to an unstable one (pink region in fig. 3.10).

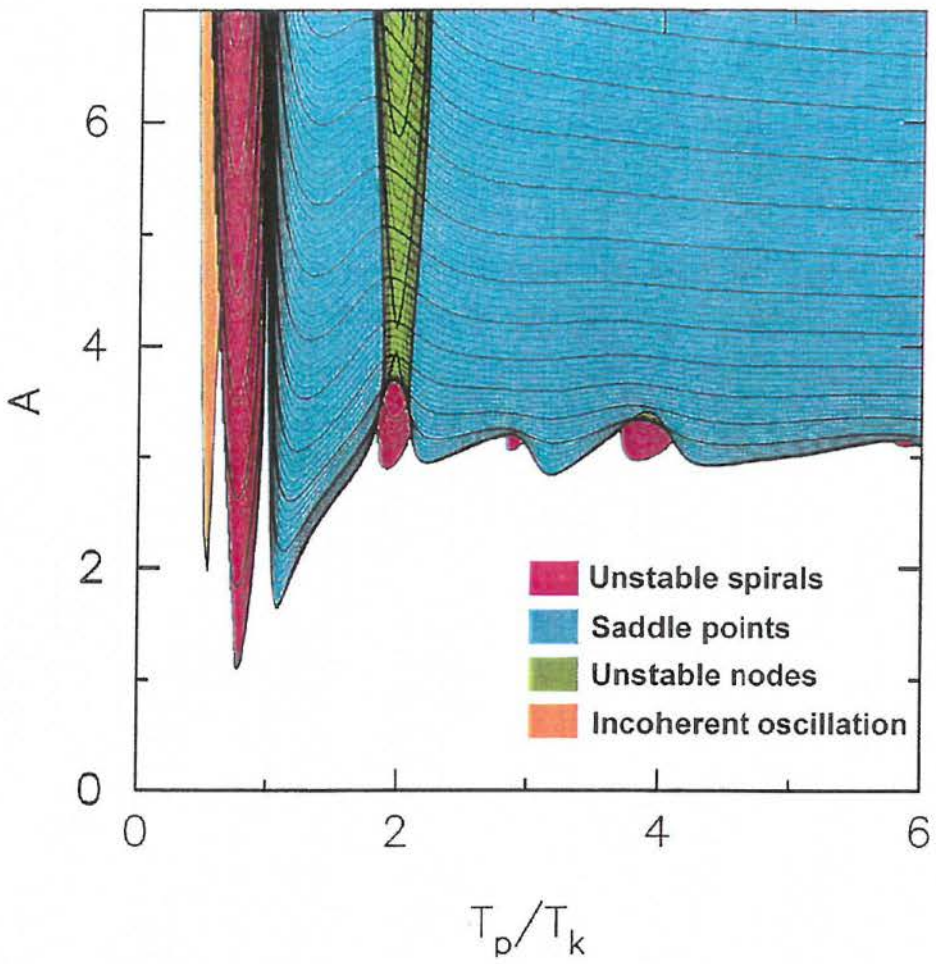

Figure 3.10: Phase diagram for the mean field model with oscillator parameters $\omega_0 = 0.4$, $k = 1.28$ and $\gamma = 0.16$. White regions denote stable regimes. The various instability regimes are color coded as indicated. The characteristic behavior in each instability regime is described in the text.

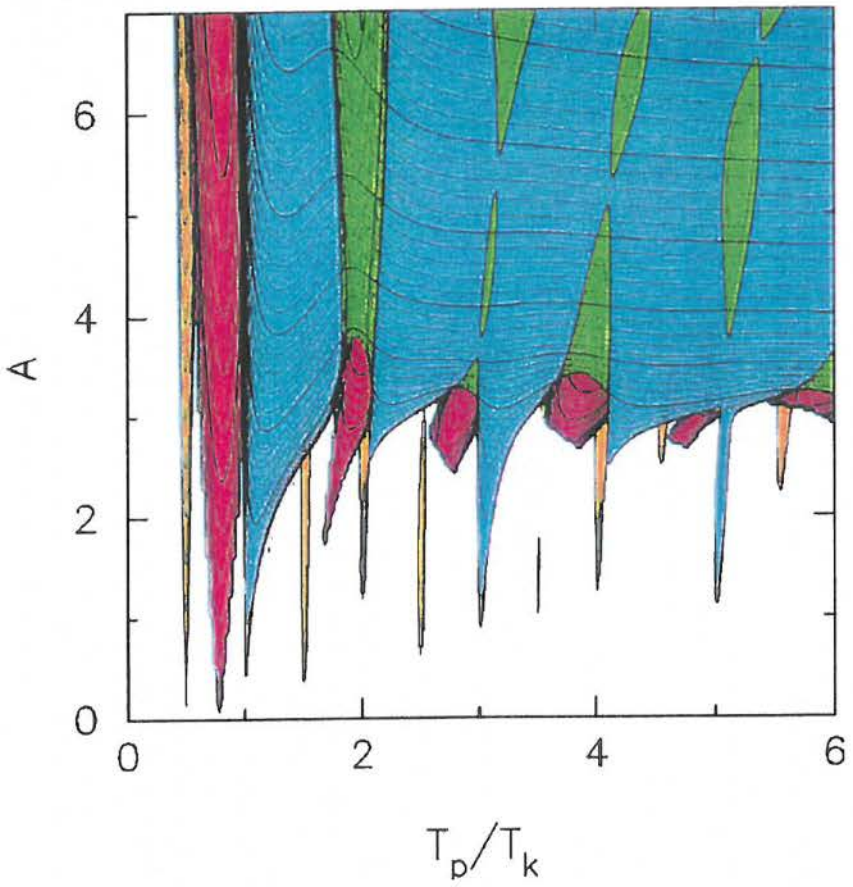

Figure 3.11: Phase diagram for the mean field model with oscillator parameters $\omega_0 = 0.4$, $k = 1.28$ and $\gamma = 0.01$.

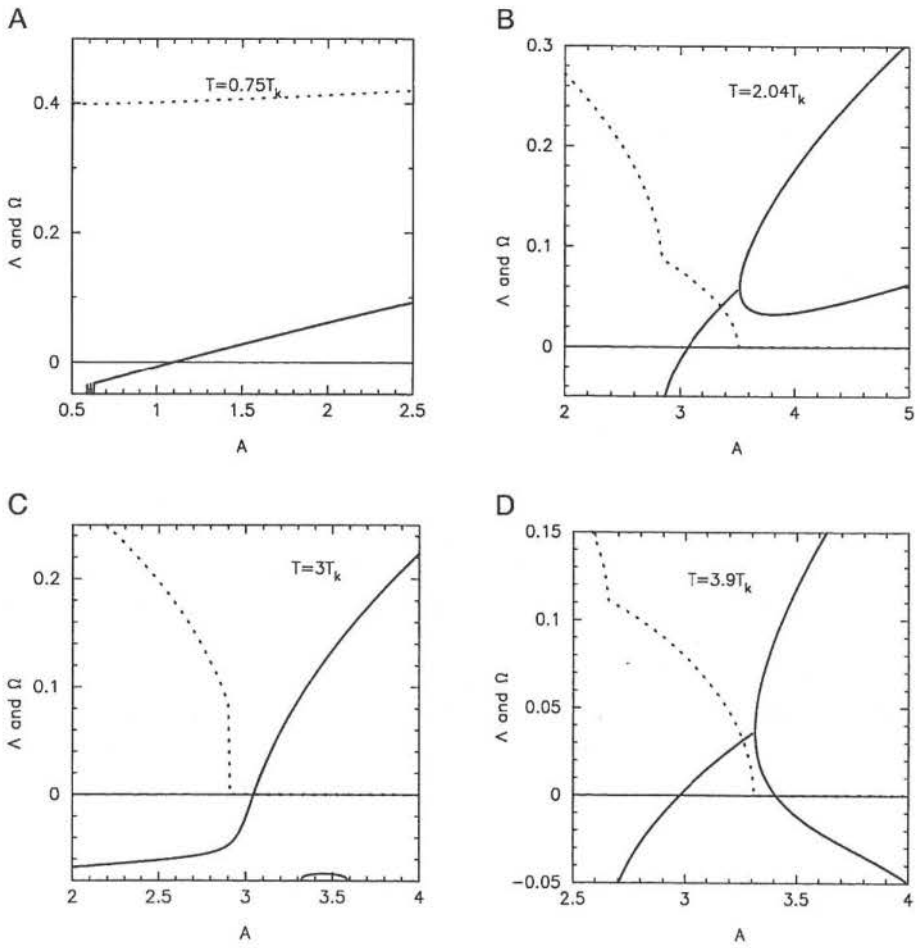

Figure 3.12: Bifurcation diagrams showing Λ (solid lines) and Ω (dotted lines) with changing modulation amplitude A for various values of the modulation period. Panel (a): $T_p/T_k = 0.75$; (b): $T_p/T_k = 2.0$; (c): $T_p/T_k = 3.0$; (d): $T_p/T_k = 3.9$. The behavior implied by these diagrams is discussed in detail in the text. Oscillator parameters are $\omega_0 = 0.4$, $k = 1.28$, and $\gamma = 0.16$.

Consider next the period $T_p = 2\,T_k$, shown in panel (b). Here Λ becomes positive at $A_c = 3.06$, while Ω remains positive. This therefore again marks a transition from a stable spiral to an unstable one (pink region). However, with a further increase in amplitude, Ω eventually goes to zero at $A_c' = 3.51$, where Λ bifurcates into two positive values (an unstable node, green region) via a saddle-node bifurcation. The oscillatory instability thus switches to a monotonic instability at this point.

A different transition pattern is seen when $T_p = 3\,T_k$, shown in panel (c). It begins with a stable spiral and switches to a stable node at $A_c = 2.91$. With a further increase in amplitude the system undergoes a transition to a saddle node (blue region) at $A_c' = 3.04$.

A more complex transition pattern is shown in panel (d), in which the character of the instability changes several times along the line $T_p = 3.9\,T_k$. As usual, at low amplitudes there is a stable spiral. At the point $A_c = 2.99$ the system moves into an unstable spiral (pink region). The unstable spiral becomes an unstable node (very small green region in the phase diagram) via a saddle-node bifurcation at $A_c' = 3.30$. A further transition to a saddle node (blue) occurs at $A_c'' = 3.4$.

In the next section we will investigate the appearance of these instabilities in two limiting cases, namely that of *negligible inertia* (particle mass $m \to 0$), the so-called overdamped limit; and the *adiabatic limit* $T_p \to \infty$ of an infinite modulation period.

3.5 Two Limiting Cases

3.5.1 The $m = 0$ Limit

An interesting limit is that of negligible inertia (particle mass $m \to 0$), for which eq. (3.2) becomes

$$\gamma \dot{x}_i + \omega_0^2 \left[1 + \xi_i(t)\right] x_i = -\frac{k}{N} \sum_{j=1}^{N} (x_i - x_j) \;, \tag{3.13}$$

with the mean field version

$$\gamma \dot{x} + \left\{\omega_0^2 \left[1 + \xi_\tau(t)\right] + k\right\} x = k \langle x \rangle \;. \tag{3.14}$$

This limit is realized for high friction and high natural frequencies of the oscillators, so that inertial effects are negligible compared to the friction and elastic force terms.

It is obvious that the phenomenon of individual parametric resonance disappears in this limit, as well as any oscillating collective instability. But the collective nonoscillatory ($\Omega = 0$) instabilities persist, and their frontier, defined simply by the condition $\Lambda = 0$, is given from eq.(3.9) by

$$\frac{4\,A^2\,k/\omega_0^2}{T_p\,[(1+k/\omega_0^2)^2 - A^2]^2}\left[\cosh\frac{AT_p}{2} - \cosh\frac{(1+k/\omega_0^2)T_p}{2}\right] = \left[1 - \frac{k/\omega_0^2(1+k/\omega_0^2)}{(1+k/\omega_0^2)^2 - A^2}\right]\sinh\frac{(1+k/\omega_0^2)T_p}{2}\,. \tag{3.15}$$

(In writing down this equation we have set $\gamma/\omega_0^2 = 1$ through a suitable time scaling.) The corresponding curves in the $(A, k/\omega_0^2)$ plane are represented in figure 3.13 for different values of the period T_p of the external modulation. These results are similar to those obtained in [2] for the case of a sinusoidal parametric perturbation instead of the piecewise-constant one used here. We remark that, in general, the transition is *re-entrant* with respect to the strength k of the coupling. This phenomenon, that has no equivalent in equilibrium phase transitions, has already been observed in Refs. [27] and [28], for an extended system subjected to multiplicative coloured noise.

3.5.2 The Adiabatic Limit

As we saw in the previous section, increased damping leads, in general, to greater stability: the stability boundaries "move up" in the phase diagram when γ is increased, indicating that a stronger modulation is needed to cause unstable behavior. Furthermore, the oscillatory instabilities eventually disappear with increasing modulation period T_p, leaving only the monotonic collective instabilities. However, it should be noted that the latter, for sufficiently large modulation period, are simply due to an inversion of the effective harmonic potential and hence not due to any special collective effects. That there might be an inversion can already be anticipated from the fact that at least one of the shifted frequencies in eq. (3.7) could become imaginary.

An analysis of the system for large T_p is fairly simple and instructive in

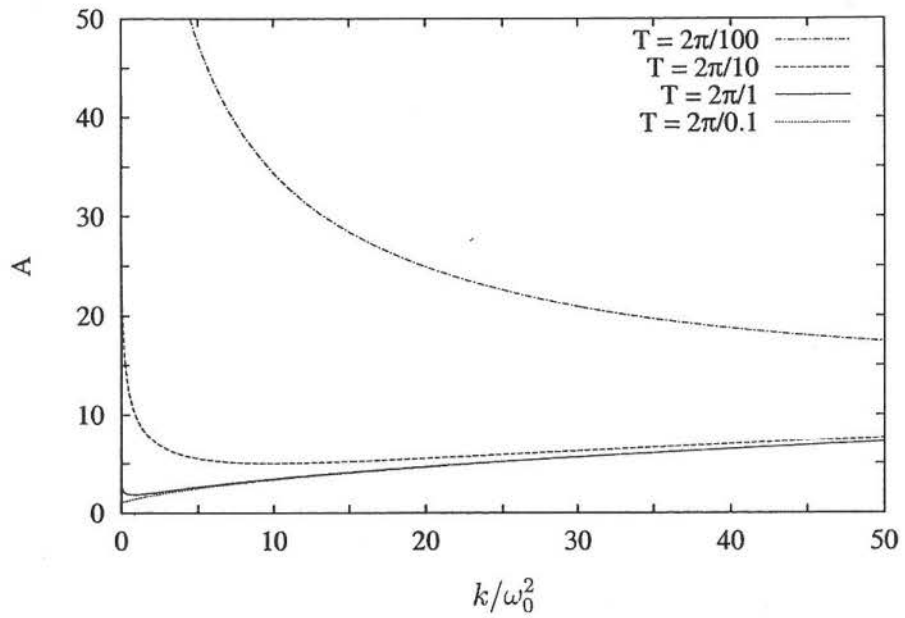

Figure 3.13: The borderlines in the parameter plane $(A,\ k/\omega_0^2)$ for the collective instability in the inertialess limit, for different values of the external period T_p.

elucidating the source of instabilities more explicitly. In the adiabatic limit $T_p \to \infty$ the single oscillator frequencies are frozen in time, half of them at the value $\tilde{\omega}_+$ and the other half at $\tilde{\omega}_-$, where

$$\tilde{\omega}_\pm = \omega_0 \sqrt{1 + \frac{k}{2\omega_0^2} \pm A} \ . \tag{3.16}$$

The mean field equations of motion are then simply

$$\begin{aligned} \langle \ddot{x} \rangle_+ + \gamma \langle \dot{x} \rangle_+ + \tilde{\omega}_+^2 \langle x \rangle_+ &= \frac{k}{2} \langle x \rangle_- \ , \\ \langle \ddot{x} \rangle_- + \gamma \langle \dot{x} \rangle_- + \tilde{\omega}_-^2 \langle x \rangle_- &= \frac{k}{2} \langle x \rangle_+ \ , \end{aligned} \tag{3.17}$$

where $\langle \cdots \rangle_\pm$ indicates an average over the oscillators with frequency $\tilde{\omega}_\pm$ respectively. This 4×4 system can be diagonalized analytically. The eigen-

modes of the coupled system are characterized by the complex frequencies

$$\Omega_{\pm}^{(1)} = i\frac{\gamma}{2} \pm \omega_0 \sqrt{1 + \frac{k}{2\omega_0^2} - \frac{\gamma^2}{4\omega_0^2} + \sqrt{A^2 + \left(\frac{k}{2\omega_0^2}\right)^2}}\,, \tag{3.18}$$

$$\Omega_{\pm}^{(2)} = i\frac{\gamma}{2} \pm \omega_0 \sqrt{1 + \frac{k}{2\omega_0^2} - \frac{\gamma^2}{4\omega_0^2} - \sqrt{A^2 + \left(\frac{k}{2\omega_0^2}\right)^2}}\,. \tag{3.19}$$

This case clearly illustrates the distinction between what we have called "single oscillator instabilities" and "collective instabilities". The former refers to the frequencies (3.16) while the latter refers to (3.18) and (3.19). While the single oscillators would remain stable until $A > A_s = 1 + k/2\omega_0^2$ (at which point $\tilde{\omega}_-$ becomes imaginary), the chain becomes destabilized when A reaches the value $A_c = \sqrt{1 + k/2\omega_0^2}$, where the imaginary part of $\Omega_-^{(2)}$ becomes negative. Note that the transition point is independent of γ. Beyond A_c the system is in a saddle-point/unstable-node instability region of non-oscillatory exponential growth; beyond A_s this is simply due to a potential inversion for the individual oscillators. In the phase diagrams in figs. 3.10 and 3.11 this translates to a stability boundary that settles at $A_c = 3$ as $T_p \to \infty$. In particular, the boundary $A_c = \sqrt{1 + k/\omega_0^2}$ remains valid in the inertia-less limit $m \to 0$, consistent with the early work of Van den Broeck and Kawai [27], and our discussion in the foregoing.

One concludes that the origin of the instabilities presented as narrow blue and pink tongues *in the low-A region* of figs. 3.10 and 3.11 is entirely different from the mechanism based on the temporarily inverted potential. Some more insight into the mechanism of these instabilities can be obtained using the simple model of two coupled parametric oscillators (the so-called parametric dimer), presented in the next section.

3.6 The Parametric Oscillator Dimer

3.6.1 The Dimer Model

Recent work [5] involves a model closely related to ours, namely, that of two coupled oscillators subject to parametric modulations with a phase difference

τ. The equations of motion for this system are just the $N = 2$ version of eq.(3.2) (again for unit mass $m = 1$),

$$\ddot{x}_1 = -\omega_0^2 \left[1 + \xi_1(t)\right] x_1 - \gamma \dot{x}_1 - \frac{k}{2}(x_1 - x_2) \ ,$$
$$\ddot{x}_2 = -\omega_0^2 \left[1 + \xi_2(t)\right] x_2 - \gamma \dot{x}_2 - \frac{k}{2}(x_2 - x_1) \ . \qquad (3.20)$$

The piecewise-constant periodic modulations of the two oscillators differ by a constant phase τ, so that we can write eq.(3.3) for this case as

$$\xi_1(t) = A \, \mathrm{sgn} \, \sin(\omega_p t) \ ,$$
$$\xi_1(t) = A \, \mathrm{sgn} \, \sin[\omega_p (t + \tau)] \ . \qquad (3.21)$$

We want to investigate whether the mean position $\langle x \rangle = (x_1 + x_2)/2$ reproduces the macroscopic behavior of the mean in the globally coupled model.

In the absence of parametric modulation ($A = 0$), one is left with coupled ordinary damped harmonic oscillators, whose total energy decays exponentially to zero. Note that in this case the dimer has two eigenmodes, the *symmetric* (or *mutually synchronized*) mode $x_1(t) = x_2(t)$, and the *antisymmetric* (or *mutually antisynchronized*) mode $x_1(t) = -x_2(t)$, with the former having a (slightly) lower proper energy.

When the parametric modulations are applied, energy is periodically pumped into the system, which may or may not lead to parametric resonance, i.e., to an infinite growth of the amplitude of the two oscillators. The above-mentioned symmetric and antisymmetric motions are, in general, no longer the eigenmodes of the dimer (except, of course, for $\tau = 0$). However, the motion is always a linear combination of these modes and, in particular, the behavior of the mean is reflected in the excitation of the symmetric mode by the parametric modulations.

A simple analysis, based on Floquet theory, was carried out in [5] in order to establish the boundaries of the parametric resonance for the dimer, as a function of the parameters A, $T_p = 2\pi/\omega_p$, ω_0, γ, k and τ. The simplifying feature (as in the case of the mean-field model) is that the piecewise constant parametric modulation leads to a piecewise linear system. One can then construct the Floquet operator explicitly by simply multiplying the piecewise linear evolution operators. Consequently, its eigenvalues $\{\lambda_i\}_{i=1,2,3,4}$

($|\lambda_1| \geq |\lambda_2| \geq |\lambda_3| \geq |\lambda_4|$) can be computed without any difficulty (although there is no simple analytic expression for them). Parametric instability occurs when $|\lambda_1| > 1$, and one can therefore directly get the implicit equation for the boundaries of the regions of instability. (See Appendix C for further details.)

One of the main conclusions is that the regions of parametric instability are sensitively dependent on the phase difference τ. Of particular interest is the behavior of the *anti-phased* dimer $\tau = T_p/2$. This particular case captures many of the features of the mean-field coupled system. This assertion is based on the comparison of the regions of parametric resonance (see [5]), as well as the bifurcation diagrams for the dimer that take into account the details of qualitatively different trajectories, as will be seen below.

3.6.2 Comparison with the Mean-Field Model

In order to characterize different types of parametric instability, and to facilitate comparison with the mean field results, we present bifurcation diagrams using the same color conventions as in the diagrams for the mean field model, figs. (3.10) and (3.11).

If Im $\lambda_1 \neq 0$, then clearly one has an oscillatory instability, represented by the pink regions. If Im $\lambda_1 = 0$, the instability can be either oscillatory or monotonic. Using the eigenvector corresponding to λ_1 as initial condition, we have determined whether or not $< x >$ crosses zero during a full period of the modulation. If it does, the point is assigned to a pink region. If it does not, the eigenvalue λ_2, that is second largest in magnitude, will determine whether the point belongs to a blue ($|\lambda_2| \leq 1$) or green ($|\lambda_2| > 1$) region. The pink, blue and green regions all arise from the instability of the symmetric mode.

The yellow region, on the other hand, requires the instability of the antisymmetric mode *and* the decay of the symmetric mode. However, such a purely antisynchronous solution is forbidden in the case $\tau = T_p/2$ [5], i.e., yellow regions cannot appear at all in the anti-phased dimer.

Results for relatively large damping ($\gamma/\omega_0 = 0.4$) are presented in the bifurcation diagram of fig. 3.14, which should be compared with fig. 3.10. The

similarity between the two figures is remarkable. Despite some extra green regions and the absence of the yellow tongue, one notices that the principal resonance regions of the dimer bifurcation diagram for $1/2 \lesssim T_p/T_k \lesssim 3/2$ fit the same region in the mean-field model almost exactly. The green regions connected to pink regions in the mean-field model are also well emulated by the dimer.

Figure 3.15 illustrates the bifurcation diagram for a small value of the damping, $\gamma/\omega_0 = 0.01$. Comparison with figure 3.11 shows that although the agreement between the two models is not as good as it is for higher values of γ/ω_0, the basic structure and similarities of the phase diagram and the bifurcation diagram are nonetheless preserved. The main differences are the complex pink patterns in the region $T_p/T_k \gtrsim 3$ of the dimer. Also, as in the high-γ case, the dimer has larger green regions than the mean field model, suggesting that the coupling in the latter plays a stronger role in stabilizing the system. But what is important is that, in spite of these differences, the principal resonance region $1/2 \lesssim T_p/T_k \lesssim 3/2$ again shows an almost perfect match.

In the dimer, the competition between two kinds of synchronization plays a key role in the destabilization of the system: on the one hand, synchronization between each oscillator and its modulation; on the other hand, synchronization between the two oscillators. This competition is essentially governed by the values of A and k. Larger values of A favor the former, while larger values of k favor the latter. When the coupling is weak, the energy difference between the symmetric and the antisymmetric modes is small and both can be excited. In this case, the individual oscillators are nearly independent and the stability diagram of the dimer is similar to that of a single oscillator. As the coupling strength increases, the energy of the antisymmetric oscillations increases until eventually only in-phase oscillations are energetically accessible. This mutually synchronized motion brings the system out of synchronization with the modulation. The stability diagram of the anti-phased dimer in the (T_p/T_k, k) plane shown in fig. 3.16 illustrates this explanation.

First consider $T_p/T_k \approx 0.5$, where a single oscillator is in the main para-

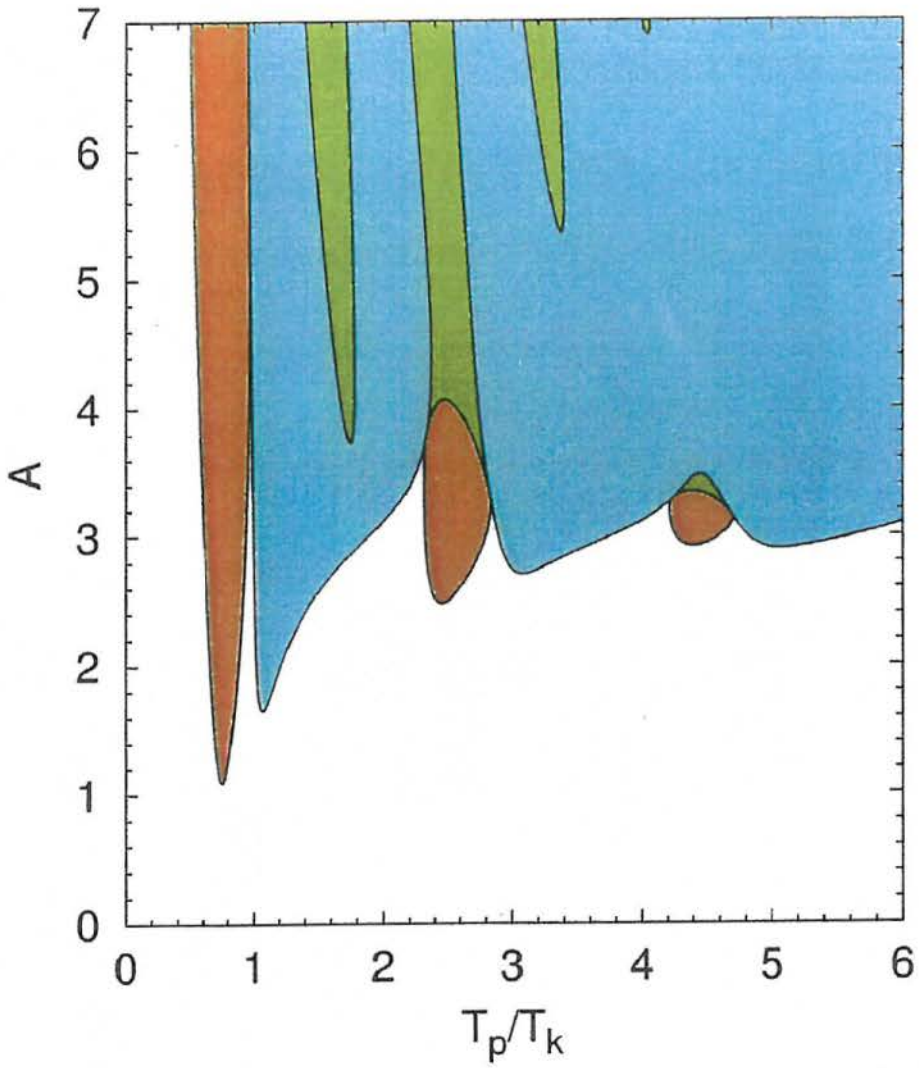

Figure 3.14: Bifurcation diagram for the anti-phased dimer with the same parameters as in fig. 3.10.

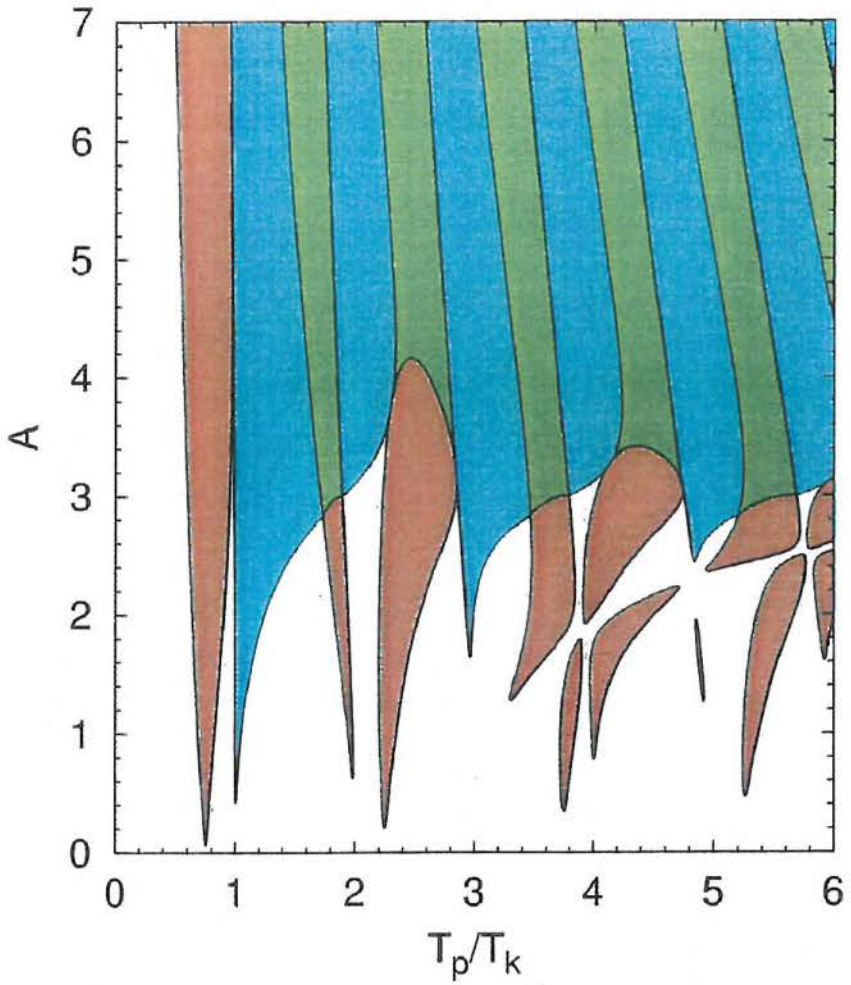

Figure 3.15: Phase diagram for the anti-phased dimer with the same parameters as in fig. 3.11.

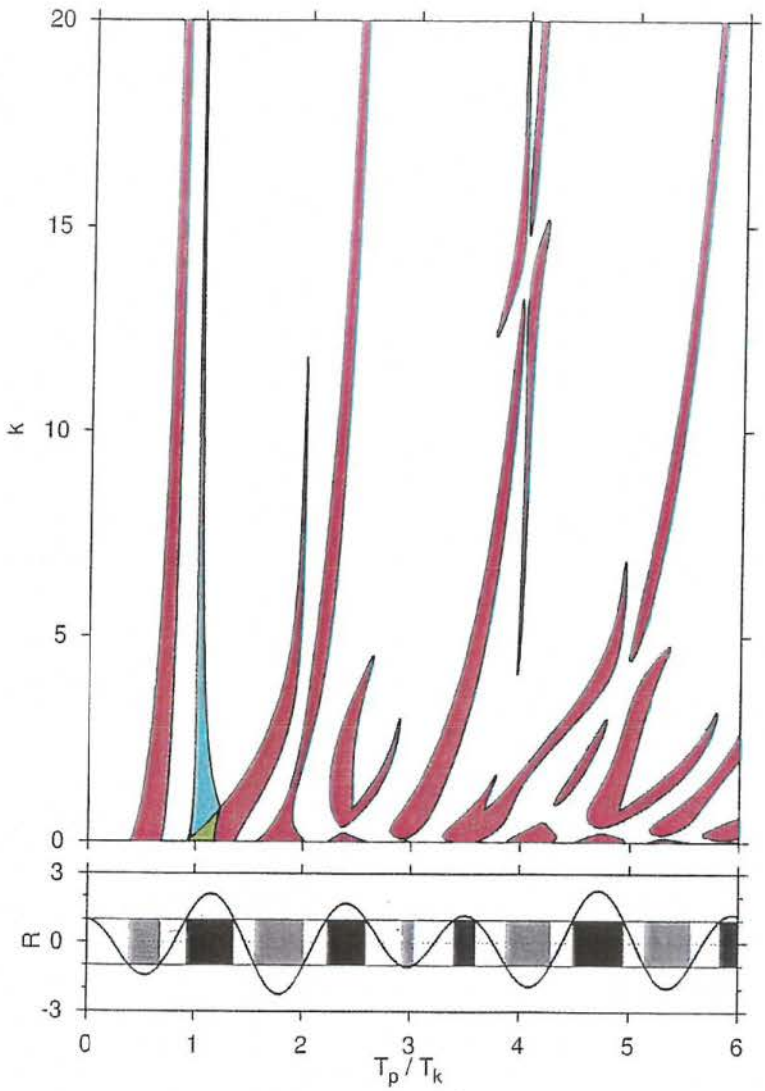

Figure 3.16: Upper panel: Bifurcation diagram for the anti-phased dimer in the $(T_p/T_k, k)$ plane for $A = 0.9$, $\gamma = 0.01$, and $\omega_0 = 0.4$, using the same color convention as in fig. 3.10. Lower panel: R [eq. (2.9)] as a function of T_p/T_k; light grey areas denote $R < -1$ and dark grey areas $R > 1$.

metric instability region [1]($R < -1$, the first light-grey region in the lower panel of fig. 3.16). For small k, the dimer is also unstable and still dominated by the antisymmetric mode (even though the symmetric mode cannot disappear, as mentioned above). However, as k increases, the excitation of the antisymmetric mode becomes more difficult and the symmetric mode becomes dominant, and the system is stabilized. When $0.5 \lesssim T_p/T_k \lesssim 1$, a single oscillator is stable ($|R| < 1$, between the dark- and light-grey regions). In this parameter region, individual oscillators do not have to be synchronous to the modulation, see fig. 2.2. They are free to become mutually synchronized and the system becomes unstable above a certain coupling strength. Since the symmetric mode dominates, this type of instability persists even for large k. Finally, when $T_p/T_k \approx 1$, the single oscillator is again in an unstable region ($R > 1$, the dark-grey region). Although the situation is similar to the first case, the individual oscillators now have a zero-frequency mode which is not subject to synchronization with the modulation. Therefore, the zero-frequency mode of the two oscillators can be mutually synchronized, which produces a monotonic growth of the mean.

The good agreement between the dimer and mean-field models is not merely a coincidence. Consider one particular test oscillator in the globally coupled system. Now define the set of its "associates" as made up of all the oscillators whose modulation phases lie within an interval $\pm T_p/4$ around its phase. The set of its "opponents" comprises all the other oscillators, whose average modulation phase is opposite to that of the test oscillator. When the oscillators are synchronized to the modulations, the associates are also mutually synchronized to one another, regardless of the coupling. When the coupling increases, there is a competition between two kinds of synchronization: synchronization between opponents and associates, and synchronization with their own modulations. This situation is similar to that of the anti-phased dimer, which helps explain the remarkable similarities between the instability diagrams of the dimer and mean-field models. Note that this description becomes *exact* in the quenched limit (see Subsection 3.5.2), the associates and opponents being represented, respectively, by $< x >_+$ and $< x >_-$. From this perspective, the choice $\tau = T_p/2$ for the dimer appears as a natural one, being not only a particularly symmetric case in the general dimer problem [5], but also the effective phase difference between the two groups.

[1]Recall that for small friction coefficients γ, the boundaries $|R| = 1$ and $|R| = R_c$ nearly coincide.

Chapter 4

Discussion and Conclusions

We have investigated the collective instabilities of a simple model of globally and harmonically mean-field coupled linear parametric oscillators, subjected to periodic piecewise linear perturbations of their frequencies. The initial phases of the individual perturbations are randomly and uniformly distributed in the interval between zero and T_p (the period of the external perturbation). Owing to its simplicity, this model can be completely solved analytically, as shown in Section 3.2. Therefore, one can study the collective behavior of the oscillators in various regimes determined by the values of the intrinsic parameters of the oscillators and by the characteristics of the parametric perturbation. We showed that collective instabilities occur in certain parameter regimes and presented phase diagrams as a function of the perturbation parameters, indicating detailed stability boundaries and the types of instability.

First, an analysis of the single oscillator (Section 2.2) enabled us to identify the modes that contribute to the oscillator's displacement. Their temporal behavior $\sim \exp(s_j t)$ is determined by the complex poles $s_j = \Lambda_j + i\Omega_j$ of the Laplace transform of the propagator. The structure of these poles is controlled by the so-called *resonance parameter* R, as given by eqs.(2.9), (2.12), and (2.13). As long as $|R|$ is less than a critical value $R_c\,(> 1)$, the oscillator is stable, i.e., all the poles have negative real parts. The borderline between stability and instability is given by the parametric resonance condition $|R| = R_c$. Another important borderline is given by $|R| = 1$. For $|R| < 1$, the Λ's are R-independent, while the Ω_j's are R-dependent; this means that the oscillating frequencies Ω_j of the modes bear no simple rela-

tion either to the proper frequency of the oscillators ω_0, or to the frequency of the parametric perturbation ω_p. For $|R| > 1$, the Λ's become R-dependent (and two-valued), while the Ω_j's are R-independent, and simply equal to a (half)integer multiple of the modulation frequency. An important feature of the poles is that (for a fixed value of R) all of them have the same real part $\Lambda_j = \Lambda$. This implies that they preserve their relative weights in the oscillator's behavior (as dictated by the initial conditions), i.e., there is no mode that dominates over all the others.

The situation becomes very different when such parametric oscillators are coupled, for instance, via a mean-field interaction. An immediate and rather trivial effect is a shift in the proper frequencies of the oscillators. But the most remarkable thing is that each mode of the single oscillator gives birth to a mode of the collective system, with modified Λ's and Ω's. For given values of the parameters, the Λ's are no longer the same for all the modes. Therefore, there appears the possibility of the asymptotic predominance of some modes that may become unstable ($\Lambda > 0$), while the other modes remain stable. Correspondingly, the collective instabilities are no longer those of the single oscillator. In particular, the $|R| = R_c$ boundary loses its significance, i.e., it no longer constitutes a frontier separating regions of stability and instability.

In addition to the familiar parametric instability of individual oscillators (regime A), two kinds of collective instabilities are identified (as well as the individual motions that underly them). In one of the instabilities, the mean amplitude diverges monotonically (regime B). In the other type of collective instability, the divergence is oscillatory (regime C). The frequencies of collective oscillatory instabilities, in general, bear no simple relation to the frequencies of the individual oscillators, or to the frequency of the perturbation.

Generally speaking, instabilities arise from phase synchronization, although not all phase synchronization leads to instability. There are two possible competing synchronization mechanisms: synchronization of individual oscillators with the external modulation ("modulation-synchronization"), and mutual synchronization between oscillators ("mutual synchronization"). In the absence of the external modulation, only mutual synchronization is possible. On the other hand, when the coupling is absent, a single oscillator satisfying the parametric resonance condition $|R| > R_c$ synchronizes with

the external modulation. In the presence of external modulations with random phases *and* coupling, even in a parameter regime where either mechanism by itself would lead to synchronization, it is not possible for both types of synchronization to occur simultaneously. As already mentioned, the collective behavior can therefore be discussed in terms of the two competing synchronization mechanisms.

Regime A :
Here $R < -R_c$, the individual uncoupled oscillators are parametrically unstable. When these oscillators are coupled, one can imagine one of two possible scenarios. If the coupling leads to mutual synchronization, the individual oscillators can no longer be synchronous with the external modulation and therefore the coupled system has been stabilized by the coupling. On the other hand, if the coupling does not lead to mutual synchronization, but instead there is modulation synchronization, then the oscillators may be individually unstable, but with $< x >= 0$. Our results indicate that the second scenario is the correct one for sufficiently small values of k, as shown in the yellow regions of "incoherent instability" in figs. 3.10 and 3.11. Modulation synchronization has won out. On the other hand, there is a coupling energy cost to the lack of mutual synchronization, which slows down the instability of individual oscillators relative to their uncoupled amplitude growth. For larger k's the first scenario takes over, and the yellow region disappears above a certain value of the coupling.

Regime B :
This is the parametric resonance regime $R > R_c$. The situation is in some ways similar to the previous case, but there is a major difference: there is now a mode, the "$j = 0$" mode, whose frequency is zero and which therefore cannot synchronize with the modulation, in contrast to the other modes. The amplitude of this mode can grow monotonically in either direction, and the coupling among the oscillators leads to a tendency for the zero-mode of all the individual oscillators to move in the same direction. Thus, while the growth rate of the $j \neq 0$ modes is reduced by coupling due to the lack of mutual synchronization, that of the $j = 0$ mode is enhanced because the coupling fosters mutual synchronization of this mode.

Regime C :
If the individual oscillators are not in regimes of parametric instability, and moreover $|R| < 1$, there is no synchronization to the modulation and the os-

cillators are free to synchronize with one another. Mutual synchronization is thus established and the mean $< x >$ becomes oscillatory with (practically) the same frequency as that of individual oscillators in the coupled system. The oscillatory mean drives the system into unstable states via the mean field coupling.

Regime D :
Both the individual oscillators and the mean go to the "absorbing" zero state.

As complete analytical results on the characteristics of the collective modes are available, one can construct the phase diagram in the space of the perturbation parameters (A, T_p/T_0), as discussed in Section 3.4.

An interesting fact is that many of the features of the behavior of this infinite system are already manifest in the behavior of the very simple system of just two coupled oscillators, with a difference $\tau = T_p/2$ between the phases of their perturbations. In the absence of external modulation, this dimer has two eigenmodes: symmetric or mutually synchronized (lower energy), and antisymmetric or mutually anti-synchronized (higher energy). In the presence of time-periodic piecewise linear modulations which are exactly out of phase, a competition ensues between these two modes (which are no longer normal modes). This competition is in many ways similar to the competition between modulation synchronization and mutual synchronization described for the globally coupled system, and here again it determines the stability of the dimer. When the coupling is weak, the energy difference between symmetric and antisymmetric modes is small and both can be excited. In this case, the individual oscillators are nearly independent and the stability diagram of the dimer is similar to that of a single oscillator. The synchronization of each oscillator with its modulation dominates the behavior, and instabilities thus represent unbounded excitation of the antisymmetric mode. With increasing coupling, the energy of the antisymmetric mode increases, until it is too high to be excited. Only the symmetric mode can be excited, i.e., the oscillators become mutually synchronized. The synchronization with the modulation is thus destroyed, and the associated parametric instability is suppressed. Although the similarity between the dimer and globally coupled model is remarkable, these two systems also exhibit various important differences. In the dimer model, mutual synchronization only involves two oscillators, of course; on the other

hand, in the global coupling model an oscillator must be synchronous with essentially all the others to create collective motion. Therefore, in the thermodynamic limit $N \to \infty$, the collective instability in the global coupled system is a genuine phase transition, whereas the instabilities in the dimer are simple bifurcations. Nevertheless, the stability boundaries and dynamics of the mean amplitudes in both cases show striking similarities.

There also exists a case that lies, in some sense, in between these two and that promises interesting new features: a one-dimensional chain of oscillators with nearest-neighbour coupling. When the phase of the modulations of the oscillators in the chain is chosen at random, there is a significant chance that both neighbours of any given oscillator have phases close to its phase. In this case, the oscillator in the middle can easily establish simultaneously both mutual synchronization with its neighbours and synchronization with its modulation. Therefore, locally this oscillator could become unstable. On the other hand, if the neighbours of a given oscillator are modulated with phases opposite to its own modulation phase, the oscillator may be stabilized. Therefore, the spatial pattern of the modulation phase is expected to play an important role, and the instability may become wavelength-dependent, suggesting spatial pattern formation. Of course, such patterns cannot be observed in either a dimer or a globally-coupled model.

We now turn to a discussion that is intended to show the *robustness* of the phenomena described. Although no simple analytical results can be obtained in the cases we briefly present below, numerical simulations offer a large spectrum of reliable information.

First, the same collective instabilities are possible when the global coupling is replaced by nearest-neighbour coupling on a $2D$ square lattice, for example. Of course, the phase diagram would look different - in the sense that the positions of the instability regions would be different. However, new phenomena might be observerd which are not possible in the mean-field case - such as, for example, the appearance of spatial regions with alternately high- and low-amplitude movements of the particles. A "global" synchronisation of the particles is much more difficult to achieve, as in the case of the $1D$ lattice briefly discussed above.

Second, other types of disorder in the phases of the perturbation can be

studied, for example other distributions of quenched phases with compact support, or quenched incommensurate phases, or phases with a random time evolution - e.g., a dichotomic Markov process. This case, as well as the corresponding white noise limit, has been studied in [40]. Also, the shape of the individual perturbations need not be a piecewise constant. In all these cases similar results are obtained.

Third, by analogy with other nonequilibrium phase transitions involving the instability of an absorbing state [41], the inclusion of nonlinear terms (for example, a $-x^3$ term in eq.(3.6)) will not modify the appearance or location of the instability - corresponding to unstable spirals, saddle nodes and unstable nodes, respectively - but will prevent the divergence of the fluctuations that would occur if the system had been a linear one. A genuine second-order nonequilibrium phase transition occurs, with $\langle x \rangle$ as the symmetry-breaking order parameter; its effective value grows continuously from zero as one leaves the absorbing state. An exact analytic treatment of the problem is impossible in these instances, but numerical simulations provide convincing evidence. See figure 4.1 for an example.

Finally, as we have shown, the monotonic growth of the mean can also appear in two limiting cases in which the individual parametric resonance dissapears. One of them is the limit of massless particles, while the other is that of "quenched disorder" $T_p \to \infty$ (for which half the oscillators - chosen at random - are excited with $\xi = \text{constant} = A$, and the other half with $\xi = -A$).

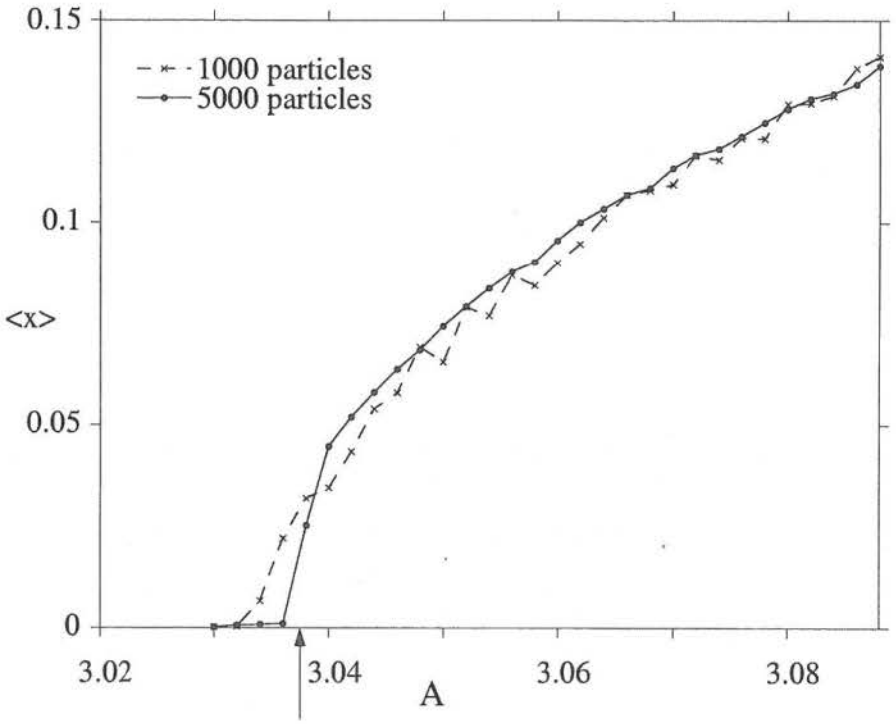

Figure 4.1: The order parameter $\langle x \rangle$ as a function of A for the parameter values $\omega_0 = 0.4$, $\gamma = 0.16$, $k = 1.28$ and $T_p = T_0$, obtained by numerical simulation of a globally coupled system with size $N = 1000$ (dashed line) and $N = 5000$ (full line). The arrow indicates the theoretical location of the phase transition, $A = 3.038$, cf. eq. (3.9). Each point represents the mean over the results of 20 runs.

Appendix A

Time Evolution of a Single Parametric Oscillator

We solve the equation of motion (2.5) using a standard Floquet method. The damping term can be eliminated by introducing a new variable y defined by

$$x(t) = e^{-\gamma t/2} y(t) \ , \tag{A.1}$$

so that eq. (2.5) becomes

$$\ddot{y} + \omega^2(t) y = 0 \ , \tag{A.2}$$

with the time-dependent frequency[1]

$$\omega^2(t) \equiv \omega_0^2[1 + \xi_\tau(t)] - \gamma^2/4 \ . \tag{A.3}$$

The solution of the undamped frequency-modulated oscillator (A.2) can be expressed in terms of the time-evolution operator $\mathbf{g}_\tau(t)$ from $t = 0$ up to time t, as

$$\begin{pmatrix} y(t) \\ \dot{y}(t) \end{pmatrix} = \mathbf{g}_\tau(t) \begin{pmatrix} y(0) \\ \dot{y}(0) \end{pmatrix} \ . \tag{A.4}$$

For a piecewise constant modulation such as (2.6), the explicit form of the time-evolution operator is known. Using its periodicity and composition property we note that, for $t = nT_p + u$,

$$\mathbf{g}_\tau(t) = \mathbf{g}_\tau(nT_p + u) = \mathbf{g}_\tau(u)\mathbf{g}_\tau(nT_p) = \mathbf{g}_\tau(u)\left[\mathbf{g}_\tau(T_p)\right]^n \ . \tag{A.5}$$

[1]Recall that the arbitrary phase τ can be set to zero here, but is retained explicitly in order to make the connection with the coupled system (Chapter 3) clearer.

It is thus sufficient to find $\mathbf{g}_\tau(t)$ for $t \in [0, T_p]$.
When the phase is $\tau \in [0, T_p/2]$, the frequency varies as

$$\omega(t) = \begin{cases} \omega_+ & \text{for } t \in \left[0, \frac{T_p}{2} - \tau\right) , \\ \omega_- & \text{for } t \in \left[\frac{T_p}{2} - \tau, T_p - \tau\right) , \\ \omega_+ & \text{for } t \in [T_p - \tau, T_p] , \end{cases} \tag{A.6}$$

while for $\tau \in [T_p/2, T_p)$,

$$\omega(t) = \begin{cases} \omega_- & \text{for } t \in [0, T_p - \tau) , \\ \omega_+ & \text{for } t \in \left[T_p - \tau, \frac{3T_p}{2} - \tau\right) , \\ \omega_- & \text{for } t \in \left[\frac{3T_p}{2} - \tau, T_p\right) , \end{cases} \tag{A.7}$$

where the frequencies $\omega_\pm$ are defined in eq. (2.10). During each constant-frequency time window, the system evolves according to the well known propagator of a simple harmonic oscillator of the appropriate frequency,

$$\mathbf{g}_\pm(t, t') = \begin{pmatrix} \cos[\omega_\pm(t - t')] & \frac{1}{\omega_\pm} \sin[\omega_\pm(t - t')] \\ -\omega_\pm \sin[\omega_\pm(t - t')] & \cos[\omega_\pm(t - t')] \end{pmatrix} . \tag{A.8}$$

The full operator $\mathbf{g}_\tau(t)$ can be expressed as a product of the $g_\pm$'s. For the case (A.6),

$$\mathbf{g}_\tau(t) = \begin{cases} \mathbf{g}_+(t, 0) \\ \qquad \text{for } t \in \left[0, \frac{T_p}{2} - \tau\right) , \\ \mathbf{g}_-\left(t, \frac{T_p}{2} - \tau\right) \mathbf{g}_+\left(\frac{T_p}{2} - \tau, 0\right) \\ \qquad \text{for } t \in \left[\frac{T_p}{2} - \tau, T_p - \tau\right) , \\ \mathbf{g}_+(t, T_p - \tau) \mathbf{g}_-\left(T_p - \tau, \frac{T_p}{2} - \tau\right) \mathbf{g}_+\left(\frac{T_p}{2} - \tau, 0\right) \\ \qquad \text{for } t \in [T_p - \tau, T_p) , \end{cases} \tag{A.9}$$

and for the case (A.7),

$$\mathbf{g}_\tau(t) = \begin{cases} \mathbf{g}_-(t,0) \\ \qquad \text{for } t \in [0, T_p - \tau) \,, \\ \mathbf{g}_+(t, T_p - \tau)\mathbf{g}_-(T_p - \tau, 0) \\ \qquad \text{for } t \in \left[T_p - \tau, \frac{3T_p}{2} - \tau\right) \,, \\ \mathbf{g}_-\left(t, \frac{3T_p}{2} - \tau\right) \mathbf{g}_+\left(\frac{3T_p}{2} - \tau, T_p - \tau\right) \mathbf{g}_-(T_p - \tau, 0) \\ \qquad \text{for } t \in \left[\frac{3T_p}{2} - \tau, T_p\right) \,. \end{cases} \tag{A.10}$$

These expressions can be simplifed further by using time-translation invariance, $\mathbf{g}_\pm(t+u, t'+u) = \mathbf{g}_\pm(t,t') = \mathbf{g}_\pm(t-t',0)$. Therefore one can put $\mathbf{g}_\pm(t,0) \equiv \mathbf{g}_\pm(t)$ with no loss of generality.

In particular, for $t = T_p$,

$$\mathbf{g}_\tau(T_p) = \mathbf{S}_\tau \mathbf{g}_0(T_p) \mathbf{S}_\tau^{-1} \tag{A.11}$$

where

$$\begin{aligned} &\mathbf{g}_0(T_p) \equiv \mathbf{g}_-\left(\frac{T_p}{2}\right)\mathbf{g}_+\left(\frac{T_p}{2}\right), \quad \mathbf{S}_\tau \equiv \mathbf{g}_+(\tau), && \text{for } \tau \in \left[0, \frac{T_p}{2}\right) \,, \\ &\mathbf{g}_0(T_p) \equiv \mathbf{g}_+\left(\frac{T_p}{2}\right)\mathbf{g}_-\left(\frac{T_p}{2}\right), \quad \mathbf{S}_\tau \equiv \mathbf{g}_-\left(\tau - \frac{T_p}{2}\right), && \text{for } \tau \in \left[\frac{T_p}{2}, T_p\right) \,. \end{aligned} \tag{A.12}$$

This allows us to conclude that the trace, determinant, and eigenvalues of $\mathbf{g}_\tau(T_p)$ do not depend on the phase τ.

Transforming back to the original variables, we finally obtain the time-evolution operator for $x(t)$ and $\dot{x}(t)$,

$$\mathbf{G}_\tau(t) = e^{-\gamma t/2}\mathbf{g}_\tau(t) \,, \tag{A.13}$$

i.e.,

$$\begin{pmatrix} x(t) \\ \dot{x}(t) + \frac{\gamma}{2}x(t) \end{pmatrix} = \mathbf{G}_\tau(t) \begin{pmatrix} x(0) \\ \dot{x}(0) + \frac{\gamma}{2}x(0) \end{pmatrix} \,. \tag{A.14}$$

A.1 Laplace Transform Method

The linear character of the problems suggests the use of Laplace transforms in order to get more information on the temporal evolution of the amplitude of the oscillator. We have

$$\begin{aligned}\tilde{x}(s) &= \int_0^\infty e^{-st}x(t)dt \\ &= [\tilde{\mathbf{G}}_\tau(s)]_{11}x(0) + [\tilde{\mathbf{G}}_\tau(s)]_{12}\left(\frac{\gamma}{2}x(0) + \dot{x}(0)\right), \end{aligned} \tag{A.15}$$

where $[\tilde{\mathbf{G}}_\tau(s)]_{ij}$ is a matrix element of the Laplace transform of the time-evolution operator. In general, if $\tilde{x}(s)$ has poles at $s_j = \Lambda_j + i\Omega_j$, with j running over some given set of values J, then

$$x(t) = \sum_{j\in J} c_j e^{\Lambda_j t}e^{i\Omega_j t}\ , \tag{A.16}$$

where the c_j's are constants determined (through the inverse Laplace transform) by the initial conditions,

$$c_j = 2\pi i \lim_{s\to s_j}(s-s_j)\left\{\left[\tilde{\mathbf{G}}_\tau(s)\right]_{11}x(0) + \left[\tilde{\mathbf{G}}_\tau(s)\right]_{12}\left(\frac{\gamma}{2}x(0)+\dot{x}(0)\right)\right\}\ . \tag{A.17}$$

We see from (A.15) that the poles of $\tilde{x}(s)$ are determined by the poles of $[\tilde{\mathbf{G}}_\tau(s)]_{11,12}$. With the help of eqs. (A.5), (A.11), and (A.13),

$$\begin{aligned}\tilde{\mathbf{G}}_\tau(s) &= \int_0^\infty e^{-st}\mathbf{G}_\tau(t)dt \\ &= \sum_{m=0}^{\infty}\left[e^{-sT_p}\mathbf{G}_\tau(T_p)\right]^m \int_0^{T_p} e^{-st}\mathbf{G}_\tau(t)dt \\ &= \left(\mathbf{I} - e^{-sT_p}\mathbf{G}_\tau(T_p)\right)^{-1}\int_0^{T_p} e^{-st}\mathbf{G}_\tau(t)dt \\ &= \frac{\frac{1}{2}e^{-\gamma T_p/2}\left[e^{(s+\gamma)T_p}\mathbf{I} - \mathbf{G}_\tau^{-1}(T_p)\right]}{\cosh\left[\left(s+\frac{\gamma}{2}\right)T_p\right] - R}\int_0^{T_p} e^{-st}\mathbf{G}_\tau(t)dt\ , \end{aligned} \tag{A.18}$$

where $\mathbf{I}$ is the 2×2 identity matrix and

$$\begin{aligned} R &= \frac{1}{2} e^{\gamma T_p/2} \ \mathrm{Tr}\ \mathbf{G}_0(T_p) = \frac{1}{2} \ \mathrm{Tr}\ \mathbf{g}_0(T) \\ &= \cos\left(\frac{\omega_+ T_p}{2}\right) \cos\left(\frac{\omega_- T_p}{2}\right) - \frac{\omega_+^2 + \omega_-^2}{2\omega_+\omega_-} \sin\left(\frac{\omega_+ T_p}{2}\right) \sin\left(\frac{\omega_- T_p}{2}\right) \end{aligned} \tag{A.19}$$

represents the *resonance parameter* [2]. It is directly seen that the poles s_j of $\tilde{x}(s)$ are given by the condition (2.11) in the main text, that corresponds to a zero denominator in the expression (A.18) for the Laplace transform of the evolution operator. We note that there is a countable infinity of such poles, i.e., $j \in Z$.

[2] The geometric series in eq.(A.18) converges provided

$$\| e^{-sT_p} \mathbf{G}_0(T_p) \| < 1 \ .$$

Appendix B

Time Evolution of the Mean in the Mean-Field Model

The mean field equation (3.6) can be rearranged as

$$\ddot{x} + \gamma\dot{x} + \{\omega_0^2[1 + \xi_\tau(t)] + k\}x = k\langle x\rangle \ , \tag{B.1}$$

which describes a single parametric oscillator of "shifted" proper frequency

$$\omega_k = \omega_0\sqrt{1 + \frac{k}{\omega_0^2}} \ , \tag{B.2}$$

driven by an effective force $k\langle x\rangle$. Therefore, it can be solved using the time-evolution operator (A.13) of a single oscillator, except that $\omega_\pm$ in eq. (2.10) must be replaced with the new shifted frequencies

$$\omega_\pm = \omega_0\sqrt{1 \pm A + \frac{k}{\omega_0^2} - \left(\frac{\gamma}{2\omega_0}\right)^2} \ . \tag{B.3}$$

The general solution of eq. (B.1) can be written as

$$\begin{aligned}\begin{pmatrix} x(t) \\ \dot{x}(t) + \frac{\gamma}{2}x(t) \end{pmatrix} &= \mathbf{G}_\tau(t)\begin{pmatrix} x(0) \\ \dot{x}(0) + \frac{\gamma}{2}x(0) \end{pmatrix} \\ &+ k\mathbf{G}_\tau(t)\int_0^t \mathbf{G}_\tau(t')^{-1}\begin{pmatrix} 0 \\ \langle x(t')\rangle \end{pmatrix} dt' \ . \end{aligned} \tag{B.4}$$

Taking the average of eq. (B.4) with respect to the random phase and the initial conditions, we obtain a self-consistent equation for the mean amplitude,

$$\begin{aligned}\langle x(t)\rangle &= \langle[\mathbf{G}_\tau(t)]_{11}\rangle\,\langle x(0)\rangle + \langle[\mathbf{G}_\tau(t)]_{12}\rangle\left(\frac{\gamma}{2}\,\langle x(0)\rangle + \langle\dot{x}(0)\rangle\right)\\ &+ k\int_0^t K(t-t')\,\langle x(t')\rangle\,dt' \ , \end{aligned} \tag{B.5}$$

where the kernel is defined by

$$K(t-t') = \left\langle\left[\mathbf{G}_\tau(t)\mathbf{G}_\tau^{-1}(t')\right]_{12}\right\rangle \ . \tag{B.6}$$

The kernel in (B.6) depends only on the time difference *strictly* because of the *uniform* distribution of the initial phases τ. One can solve the integral equation (B.5) using Laplace transforms. The solution in Laplace space is given by

$$\langle\tilde{x}(s)\rangle = \frac{\left\langle[\tilde{\mathbf{G}}_\tau(s)]_{11}\right\rangle\langle x(0)\rangle + \left\langle[\tilde{\mathbf{G}}_\tau(s)]_{12}\right\rangle(\gamma/2\,\langle x(0)\rangle + \langle\dot{x}(0)\rangle)}{1 - k\left\langle[\tilde{\mathbf{G}}_\tau(s)]_{12}\right\rangle} \ . \tag{B.7}$$

As already explained for the case of the single oscillator in Appendix A, the temporal evolution of the mean is determined by the poles of the corresponding Laplace transform, $\langle\tilde{x}(s)\rangle$. It is directly seen that the poles of the single oscillator with shifted frequency (that correspond to the poles of the Laplace transform of the evolution operator) are no longer poles for the Laplace transform of the mean, i.e., the modes of the single oscillator are no longer modes of the mean. Instead, equation (B.7) has a set of poles determined by the condition

$$\left\langle[\tilde{\mathbf{G}}_\tau(s)]_{12}\right\rangle = \frac{1}{k} \ , \tag{B.8}$$

and this set obviously differs from the set derived for a single parametric oscillator. A rather lengthy calculation allows us to find an explicit expression of this condition - namely, eq.(3.9).

Appendix C

The Parametric Oscillator Dimer

Rewriting equations (3.20) and (3.21) that specify the model, we have

$$\begin{aligned}\ddot{x}_1 &= -\omega_0^2\,[1+\xi_1(t)]\,x_1 - \gamma\dot{x}_1 - \frac{k}{2}(x_1 - x_2)\ ,\\ \ddot{x}_2 &= -\omega_0^2\,[1+\xi_2(t)]\,x_2 - \gamma\dot{x}_2 - \frac{k}{2}(x_2 - x_1)\ ,\end{aligned} \tag{C.1}$$

with

$$\begin{aligned}\xi_1(t) &= A\ \mathrm{sgn}\ \sin(\omega_p t)\ ,\\ \xi_1(t) &= A\ \mathrm{sgn}\ \sin[\omega_p(t+\tau)]\ .\end{aligned} \tag{C.2}$$

A simple rescaling of time to dimensionless units $t' = t\omega_0$ shows that these equations are governed by the dimensionless parameter combinations $r = \omega_0/\omega_p = T_p/T_0$, A, k/ω_0^2, γ/ω_0 and $\theta = \omega_p\tau$. Moreover, the behaviour of the system is invariant with respect to the transformation $\theta \to 2\pi - \theta$, since this just amounts to an exchange of the indices labelling the oscillators. Defining the four-dimensional vector in phase space

$$\mathbf{X}(t) = \begin{pmatrix} x_1 \\ \dot{x}_1 \\ x_2 \\ \dot{x}_2 \end{pmatrix}\ , \tag{C.3}$$

eqs.(C.1) can be written in the matrix form $\dot{\mathbf{X}}(t) = \mathbf{E}(t)\mathbf{X}(t)$, where the matrix $\mathbf{E}$ is periodic in time,

$$\mathbf{E}(t) = \mathbf{E}(t + T_p)\ . \tag{C.4}$$

Let $\mathbf{G}(t)$ denote the corresponding time-evolution operator, i.e.,

$$\mathbf{X}(t) = \mathbf{G}(t)\mathbf{X}(0) \; . \tag{C.5}$$

This obeys the differential equation

$$\dot{\mathbf{G}}(t) = \mathbf{E}(t)\,\mathbf{G}(t) \; , \tag{C.6}$$

with the initial condition

$$\mathbf{G}(0) = \mathbf{I} \; , \tag{C.7}$$

the 4×4 unit matrix. Owing to the periodicity of the matrix $\mathbf{E}$ one has

$$\mathbf{G}(t + nT_p) = \mathbf{G}(t)\,\mathbf{G}(nT_p) = \mathbf{G}(t)\;[\mathbf{G}(T_p)]^n \; . \tag{C.8}$$

This leads to the conclusion that the long-time behavior of the system is determined by the eigenvalues $\{\lambda_i\}_{i=1,2,3,4}$ of the *Floquet operator* $\mathbf{G}(T_p)$, which propagates the system in phase space during a full period T_p of the modulation. It is obvious that the system becomes unstable, i.e., a parametric resonance occurs, if $\max_j\{|\lambda_j|\} > 1$.

The simplifying feature of the piecewise linear perturbation used here is that, in a period T_p, the evolution operator is known for each time window of constant values of the two modulations. Therefore, the Floquet operator is the product of these known evolution operators.

For the sake of clarity, let us first analyse the frictionless case $\gamma = 0$. The interval T_p can be divided in four subintervals of constant values of the modulations ξ_1 and ξ_2, namely $(\xi_1,\, \xi_2) = (A,\, A)$, $(A,\, -A)$, $(-A,\, -A)$, $(-A,\, A)$ when $\tau \leq T_p/2$ and $(\xi_1,\, \xi_2) = (A,\, -A)$, $(A,\, A)$, $(-A,\, A)$, $(-A,\, -A)$ for $\tau \geq T_p/2$. For each such subinterval the propagator is known:

$$\mathbf{G}_{\xi_1,\xi_2}(t) = \frac{1}{P^2 - M^2} \times$$

$$\begin{pmatrix} -m_1c_p + p_1c_m & -m_1s_p + p_1s_m & k(-c_p + c_m) & k(-s_p + s_m) \\ m_1s_pP^2 - p_1s_mM^2 & -m_1c_p + p_1c_m & k(s_pP^2 - s_mM^2) & k(-c_p + c_m) \\ k(-c_p + c_m) & k(-s_p + s_m) & -m_2c_p + p_2c_m & -m_2s_p + p_2s_m \\ k(s_pP^2 - s_mM^2) & k(-c_p + c_m) & m_2s_pP^2 - p_2s_mM^2 & -m_2c_p + p_2c_m \end{pmatrix} . \tag{C.9}$$

$$P^2 = \frac{\omega_1^2 + \omega_2^2 + \sqrt{(\omega_1^2 - \omega_2^2)^2 + 4k^2}}{2} ,$$
$$M^2 = \frac{\omega_1^2 + \omega_2^2 - \sqrt{(\omega_1^2 - \omega_2^2)^2 + 4k^2}}{2} , \qquad \text{(C.10)}$$

where $\omega_{1,2}^2 = \omega_0^2(1 + \xi_{1,2}) + k$ are the constant frequencies corresponding to each time subinterval. Further,

$$\begin{aligned} c_p &= \cos(Pt) \; ; \quad s_p = P^{-1} \sin(Pt) \; ; \\ c_m &= \cos(Mt) \; ; \quad s_p = M^{-1} \sin(Mt) \; ; \\ m_{1,2} &= M^2 - \omega_{1,2}^2 \; ; \quad p_{1,2} = P^2 - \omega_{1,2}^2 \; . \end{aligned} \qquad \text{(C.11)}$$

Finally, the Floquet operator is given by

$$\mathbf{G}(T_p) = \mathbf{G}_{-+}(\tau)\ \mathbf{G}_{--}(T_p/2 - \tau)\ \mathbf{G}_{+-}(\tau)\ \mathbf{G}_{++}(T_p/2 - \tau) \qquad \text{(C.12)}$$

when $\tau \leq T_p/2$, and

$$\mathbf{G}(T_p) = \mathbf{G}_{--}(\tau - T_p/2)\ \mathbf{G}_{-+}(T_p - \tau)\ \mathbf{G}_{++}(\tau - T_p/2)\ \mathbf{G}_{+-}(T_p - \tau) \qquad \text{(C.13)}$$

for $\tau \geq T_p/2$.

As already explained, the stability properties of the coupled system are determined by the modulii of the four eigenvalues $\lambda_1, \ldots \lambda_4$ of the Floquet operator. Note that when $\tau = 0$ or $\tau = T_p/2$, the expression for $\mathbf{G}(T_p)$ reduces to the product of just two matrices.

The case when damping is also present can be dealt with as in the case of the single oscillator, i.e., by noting that if $\mathbf{X}(t)$ is a solution for $\gamma = 0$, then $\mathbf{Y}(t) = e^{-\gamma t/2}\tilde{\mathbf{X}}(t)$ is a solution for $\gamma \neq 0$, where $\tilde{\mathbf{X}}(t) = \mathbf{X}(t)|_{\omega_{1,2}^2 \to \omega_{1,2}^2 - \gamma^2/4}$.

A final remark: In the absence of damping, Liouville's theorem ensures that $\det \mathbf{G}(T_p) = \lambda_1\lambda_2\lambda_3\lambda_4 = 1$. In contrast with the single oscillator case, the condition $\lambda_j = \pm 1$ is not sufficient to determine the boundaries of the region of parametric resonance. For coupled oscillators, the eigenvalue with the largest magnitude can cross the unit circle $|\lambda_j| = 1$ and hence enter a region of instability (parametric resonance) in other directions in the complex plane. The roots of the fourth order characteristic polynomial of the Floquet operator must be found numerically to determine the instability boundaries. This is computationally quite feasible, since one has an analytic expression for the Floquet operator.

Bibliography

[1] See, e.g., Y. Kuramoto, *Chemical Oscillations, Waves and Turbulence*, Springer, Berlin (1984); Y. Kuramoto, Physica D **50**, 15 (1991); Y. Kuramoto and I. Nishikawa, J. Stat. Phys. **49**, 569 (1987); H. Daido, Prog. Theor. Phys. **77**, 622 (1987); H. Daido, Phys. Rev. Lett. **68**, 1073 (1992); S.H. Strogatz and R.E. Mirollo, Physica D **31**, 1143 (1988); S. H. Strogatz, C. M. Marcus, R. M. Westervelt, and R. E. Mirollo, Physica D **36**, 23 (1989); J. W. Swift, S. H. Strogatz, and K. Wiesenfeld, Physica D **55**, 239 (1992); S. H. Strogatz, R. E. Mirollo, and P. C. Matthews, Phys. Rev. Lett. **68**, 2730 (1992); K. Wiesenfeld and J. W. Swift, Phys. Rev. E **51**, 1020 (1995); K. Wiesenfeld, P. Colet and S. H. Strogatz, Phys. Rev. Lett. **76**, 404 (1996); S.H. Park and S. Kim, Phys. Rev. E **53**, 3425 (1996); K. Park, S. W. Rhee, and M. Y. Choi, Phys. Rev. E **57**, 5030 (1998); H. A. Tanaka, A. J. Lichtenberg, and S. Oishi, Phys. Rev. Lett. **78**, 2104 (1997); H. Hong, M. Y. Choi, J. Yi, and K. S. Soh, Phys. Rev. E **59**, 353 (1999).'

[2] I. Bena and C. Van den Broeck, Europhys. Lett. **48**, 498 (1999).

[3] I. Bena, R. Kawai, C. Van den Broeck, M. Copelli, and K. Lindenberg, submitted for publication.

[4] C. Van den Broeck and I. Bena, in *Stochastic Processes in Physics, Chemistry and Biology*, eds. J. A. Freund and T. Pöschel, Springer Verlag, Berlin (2000).

[5] M. Copelli and K. Lindenberg, submitted for publication, cond-mat/0008022.

[6] L. D. Landau and E. M. Lifshitz, *Mechanics*, Pergamon Press, Oxford (1969); V. I. Arnold, *Equations Différentielles Ordinaires*, Editions Mir, Moscou (1974).

[7] I. Zlatev, G. Huey, and P. J. Steinhardt, Phys. Rev. D **57**, 2152 (1998); S. Mukhoyama, Phys. Rev. D **57**, 6191 (1998).

[8] M. Chiba and M. Tosa, MNRAS **244**, 714 (1990); K. M. Kuzanyan and D. D. Sokoloff, Astrophys. & Space Sci. **208**, 245 (1993); D. Moss, Astron. Astrophys. **308**, 381 (1996).

[9] P. M. Gresho and R. L. Sani, J. Fluid Mech. **40**, 783 (1970); G. Ahlers, P. C. Hohenberg, and M. Lucke, Phys. Rev. A **32**, 3493 (1985); A. A. Wheeler, G. B. McFadden, B. T. Murray, and S. R. Coriell, Phys. Fluids A **3**, 2847 (1991); R. Clever, G. Schubert, and F. H. Busse, Phys. Fluids A **5**, 2430 (1993); B. V. Saunders, B. T. Murray, G. B. McFadden, S. R. Coriell, and A. A. Wheeler, Phys. Fluids A **4**, 1176 (1992); M. Faraday, Philos. Trans. Roy. Soc. (London) **52**, 319 (1831); J. W. Miles, J. Fluid Mech. **148**, 451 (1984); S. T. Milner, J. Fluid Mech. **225**, 81 (1991).

[10] H. Suhl, J. Phys. Chem. Solids **1**, 209 (1957); R. W. Damon, in *Magnetism*, eds. G. T. Rado and H. Suhl, Academic Press, New York (1963), Vol. **I**, p. 551; V. S. L'vov, *Wave Turbulence under Parametric Excitation*, Springer, Berlin (1994).

[11] A. H. Nayfeh and D. T. Mook, *Nonlinear Oscillations*, Wiley Interscience, New York (1979), pp. 295-300; S. Riyopoulos, J. Plasma Phys. **46**, 473 (1991); Phys. Rev. Lett. **68**, 3303 (1992).

[12] F. M. Penning, Physica (Utrecht) **3**, 873 (1936); H. G. Dehmelt, Adv. At. Mol. Phys. **3**, 53 (1967); M. Calvo, Phys. Rev. B **55**, 10571 (1997); I. A. Aronov, O. N. Barnets, and M. O. Osmanov, Phys. Lett. A **146**, 141 (1990); J. M. Galpin, Y. Fautrelle, and A. D. Sneyd, J. Fluid Mech. **239**, 409 (1992).

[13] For a review on optical parametric oscillators see the special issue of J. Opt. Soc. Am. B **4**, No. 10 (1987).

[14] C. L. Liao and B. W. Huang, J. Sound & Vibr. **180**, 47 (1995); A. Argento, J. Sound & Vibr. **182**, 595 (1995); S. Natsiavas, J. of Sound & Vibr. **184**, 93 (1995).

[15] N. I. Markevich and E. E. Selkov, J. Theor. Biol. **140**, 27 (1989); L. A. Blumenfeld, Biofizika **38**, 129 (1993) (in Russian); J. P. Blanchard,

C. F. Blackman, and D. E. House, Bioelectromagnetics **16**, 274 (1995); M. Schienbein and H. Gruler, Phys. Rev. E **56**, 7116 (1997).

[16] K. Lindenberg, V. Seshadri, and B. J. West, Phys. Rev. A **22**, 2171 (1980); N. G. van Kampen, *Stochastic Processes in Physics and Chemistry*, North Holland, Amsterdam (1981), pp. 382, 387 and 393; A. Abdullaev, S. Darmanyan, and M. Djumaev, Phys. Lett. A**141**, 423 (1989); P. S. Landa and A. A. Zaikin, Phys. Rev. E **54**, 3535 (1996); P. S. Landa, A. A. Zaikin, M. G. Rosemblum, and J. Kurths, Phys. Rev. E **56**, 1465 (1997).

[17] R. M. Mazo, J. Stat. Phys. **24**, 39 (1981); M. Gitterman, R.J. Schrager, and G.H. Weiss, Phys Lett. A**142**, 84 (1989); C. Zerbe, P. Jung, and P. Hänggi, Phys. Rev. E **49**, 3626 (1994).

[18] J. Tan and G. Gabrielse, Phys. Rev. Lett. **67**, 3090 (1991).

[19] P. Coullet and K. Emilsson, Physica D **61**, 119 (1992); V. Petrov, Q. Ouyang, and H. L. Swinney, Nature **388**, 655 (1997).

[20] A. H. Nayfeh and D. T. Mook, *Nonlinear Oscillations*, Wiley, New York (1979).

[21] B. Denardo, B. Galvin, A. Greenfield, A. Larraza, S. Putterman, and W. Wright, Phys. Rev. Lett. **68**, 1730 (1992).

[22] A. S. Mikhailov, Phys. Rep. **184**, 308 (1989); L. Schimansky-Geier and Ch. Zulicke, Z. Phys. B **82**, 157 (1991); J. Garcia-Ojalvo, A. Hernandez-Machado, and J. M. Sancho, Phys. Rev. Lett. **71**, 1542 (1993); L. Raimrez-Piscina, A. Hernandez-Machado, and J. M. Sancho, Phys. Rev. B **48**, 119 (1993); C. Van den Broeck, J. M. R. Parrondo, J. Armero, and A. Hernandez-Machado, Phys. Rev. E **49**, 2639 (1994); C. Van den Broeck, J. M. R. Parrondo, and R. Toral, Phys. Rev. Lett. **73**, 3395 (1994); A. S. Pikovski, K. Rateitschak, and J. Kurths, Z. Phys. B **95**, 541 (1994); A. Becker and L. Kramer, Phys. Rev. Lett. **73**, 2618 (1995); J. M. R. Parrondo, C. Van den Broeck, J. Buceta, and J. de la Rubia, Physica A **224**, 153 (1996); J. Garcia-Ojalvo, J. M. R. Parrondo, J. M. Sancho, and C. Van den Broeck, Phys. Rev. E **54**, 6918 (1996); G. Grinstein, M. A. Munoz, and T. Yuhai, Phys. Rev. Lett. **76**, 4376 (1996); J.-H. Li and Z.-Q. Huang, Phys. Rev. E **53**, 3315 (1996); C. Van den Broeck, J. M. R. Parrondo, R. Toral, and R. Kawai, Phys.

Rev. E **55**, 4084 (1997); S. Kim, S. H. Park, Ch. Doering, and C.S. Ryu, Phys. Lett. A **224**, 147 (1997); R. Muller, K. Lippert, A. Kuhnel, and U. Behn, Phys. Rev. E **56**, 2658 (1997).

[23] J. Garcia-Ojalvo and J. M. Sancho, *Noise in Spatially Extended Systems*, Springer, Berlin (1999).

[24] C. W. Meyer, G. Ahlers, and D. S. Canell, Phys. Rev. A **44**, 2514 (1991).

[25] See, e.g., T. Vicsek, in *Proceedings of the Workshop on Surface Disordering: Growth, Roughening, and Phase Transitions*, Proceedings of the Les Houches Summer School of Theoretical Physics, Les Houches, 1992, eds. R. Jullien, J. Kertesz, P. Meakin and D. E. Wolf, Nova Science, Commack, New York (1992); A. L. Barabasi and H. E. Stanley, *Fractal Concepts in Surface Growth*, Cambridge University Press, Cambridge (1995).

[26] J. Martin-Regalado, S. Balle, and N. B. Abraham, IEEE J. Quantum Electron. **32**, 257 (1996).

[27] C. Van den Broeck and R. Kawai, Phys. Rev. E **57**, 3866 (1998).

[28] C. Van den Broeck, J. M. R. Parrondo, R. Toral, and R. Kawai, Phys. Rev. E **55**, 4084 (1997).

[29] J. R. Sanmartin, Am. J. Phys. **52**, 937 (1984).

[30] http://monet.physiks.unibas.ch/{}sim elmer/pendulum/vpend.htm

[31] D. H. Towne, *Wave Phenomena*, Dover, New York (1967).

[32] H. Casimir, Proc. Kon. Ned. Akad. Wetensch. B **51**, 793 (1948).

[33] S. K. Lamoreaux, Phys. Rev. Lett. **78**, 5 (1996).

[34] J. Y. Ji, H. H. Jung, J. W. Park, and K. S. Soh, Phys. Rev. A **56**, 4440 (1997).

[35] E. I. Butikov, in *Computing in Science & Engineering*, May-June, 76 (1999) (for a review of the elementary theory of parametric resonance); A. P. Muñunzuri, M. G. Gesteira, V. P. Muñunzuri, V. I. Krinski, and V. P. Villar, Phys. Rev. E **50**, 4258 (1994); J. M. Galpin, Y. Fautrelle,

and A. D. Sneyd, J. Fluid Mech. **239**, 409 (1992); M. Calvo, Phys. Rev. B **55**, 10571 (1997); N. V. Fomin, O. L. Shalaev, and D. V. Shantsev, J. Appl. Phys. **81**, 8091 (1997); I. Zlatev, G. Huey, and P. Steinhardt, Phys. Rev. E **57**, 2152 (1998).

[36] See, e.g., W. Magnus and S. Winkler, *Hill's Equation*, eds. L. Bers, R. Courant and J. J. Stoker, Interscience, New York (1966).

[37] C. Kittel, *Introduction to Solid State Physics*, Wiley, New York (1997), Ch. 7.

[38] M. Remoissenet, *Waves Called Solitons*, Springer, Berlin (1999).

[39] S. Alexander, J. Bernasconi, W. R. Schneider, and R. Orbach, Rev. Mod. Phys. **53**, 175 (1981).

[40] B. Cleuren, Master's Thesis, Limburgs Universitair Centrum, Belgium (1999) (unpublished).

[41] A. Becker and L. Kramer, Phys. Rev. Lett. **73**, 955 (1994); G. Grinstein, M. A. Munoz, and T. Yuhai, Phys. Rev. Lett. **76**, 4376 (1996).

Part II

Hydrodynamic Fluctuations in Kolmogorov Flow

Chapter 1

Introduction

Fluids under various nonequilibrium constraints (temperature gradients, shears, etc.) may develop very rich modes of behavior, that often lead to the formation of complex nonequilibrium structures [1] and can culminate in turbulence-like manifestations. These esentially nonlinear phenomena have attracted a lot of interest in the last few decades. Correspondingly, a central issue in nonequilibrium statistical physics is the role of fluctuations in the onset of hydrodynamical instabilities that lead to the appearance of new flow patterns. Various approaches have been established [2, 3], and taken together they have enabled us to get a deep insight in the (fluctuating) behavior of nonequilibrium fluids and to draw some general conclusions.

One of the most important conclusions from the nonequilibrium statistical mechanics of fluids is the fact that in nonequilibrium stationary states, long-ranged spatial and temporal correlations of the relevant hydrodynamic variables are *always* present, even far away from any hydrodynamic instability or critical point. This is in contradiction with the classical picture of Bogoliubov [4] and Uhlenbeck [5], that suggests that dynamic correlations of the molecules interacting via short-range forces should also be short-ranged. Preliminary evidence that the dynamic correlations may become long-ranged in fluids occurs near an *equilibrium* critical point, where the thermal conductivity diverges. As the critical molecular fluctuations extend over distances much larger than the intermolecular distances, they can be treated using the formalism of some form of *generalized hydrodynamics.* Critical phenomena can then be explained by a theory of *hydrodynamic mode coupling* [7]. Subsequent developments have revealed that dynamic correlations may become

long-ranged even far away from criticality: a second breakdown of the classical picture appeared with the attempts to extend the Boltzmann equation to moderately dense gases [8]. The transport coefficients were formally represented as virial expansions; but the coefficients of these expansions (that contain cluster integrals involving the interaction of 2, 3, 4, ... molecules) can be shown to diverge. This can be attributed to the existence of long-distance molecular correlations (namely, to an increased frequency of the occurrence of so-called "ring collisions", i.e., sequences of n collisions among n molecules, $n \geq 3$; this is connected to the fact that in a moderately dense fluid the mean free time/path is almost of the same order as the interaction time/radius). A suitable "resummation" procedure allows one to express the coefficients of the virial expansion in terms of hydrodynamic modes and to show that the nonanalytic (logarithmic) behaviour of the transport coefficients in terms of particle density can be again interpreted as resulting from hydrodynamic mode couplings.

Attention turns now to the *nonequilibrium* regimes. At a fundamental level, kinetic theories (and, more generally, for fluids of arbitrary densities, nonequilibrium ensemble methods [9]) are able to account for the generic long-range behaviour of nonequilibrium correlation functions. Through a suitable coarse-graining procedure (using a Zwanzig-type projection operator), one can obtain "hydrodynamic" equations for the unequal- and equal-time corelation functions of the microscopic densities of mass, momentum and energy. The nonequilibrium constraints imposed on the system are found to lead to couplings of these "hydrodynamic modes" (between themselves and/or to the external fields), that are similar to those that are responsible for the anomalous behaviour of the transport coefficients of a fluid in equilibrium near its critical point. These couplings are therefore connected to the long-range behaviour of the correlations. In the same spirit (but with a slightly different technique), Procaccia and co-workers [10] started from the Liouville equation and constructed an ensemble distribution function for the stationary nonequilibrium state, in terms of which both equal- and unequal-time correlation functions can be computed. Both these procedures [9, 10] allow one to calculate the dynamic form factor $S_{\mathbf{q}}(\omega)$ (see Appendix A), and to analyse the effect of long-range density fluctuations on light scattering.

Another approach is the extension of the time correlation function method of linear response (the Green-Kubo formalism) to the description of nonlinear transport in systems far from equilibrium. The most clear results are

those obtained in the case of a fluid under shear. Here again, mode-coupling effects lead to a nonanalytic dependence on the shear rate of both the pressure and of the self-diffusion coefficient. This is related to a long-time tail in the velocity autocorrelation function [11].

But the most frequently-used theoretical approach for the study of the fluctuations is the *Landau-Lifshitz fluctuating hydrodynamics* [12], mainly because of its simplicity as compared to the more fundamental approaches mentioned above. Fluctuating hydrodynamics is a phenomenological, Langevin-type stochastic formulation of standard fluid mechanics. It is based on two fundamental hypotheses. First, the fluid is considered as a continuous medium, in which each infinitesimal volume element is itself taken to contain a very large number of constituent particles. Second, the assumption of local equilibrium: at each instant, every volume element of the fluid is in equilibrium with its surroundings and thermodynamics is locally valid. If one neglects the internal degrees of freedom of the molecules, then the state of the fluid is described mathematically by the momentum density field and the fields of two thermodynamic quantities supplemented by a suitable equation of state - for example, the mass and total energy densities. Then the standard hydrodynamic equations are nothing but the conservation equations for these quantities, with the generic form

$$\frac{\partial h(\mathbf{r}, t)}{\partial t} = -\boldsymbol{\nabla} \cdot [h\mathbf{v} + \mathbf{D}_h] \ , \tag{1.1}$$

$h(\mathbf{r}, t)$ representing the density of a generic hydrodynamic variable, and $\mathbf{v}$ the velocity field. The non-convective (i.e., the *dissipative*) part of the variable's flow density $\mathbf{D}_h$ is expressed through the *closure relation*. For the momentum flow, it is given by Newton's law (eventually in the Navier-Stokes form) for the dissipative part of the pressure tensor; and for the total energy flow, by Fourier's law for the heat flux.

Spontaneous fluctuations of hydrodynamic variables are then introduced into these transport equations by adding random components to the dissipative parts of the pressure and heat fluxes. Since these fluxes are not conserved quantities, the correlations of the random terms are expected to be short-ranged and short-lived, so that on a hydrodynamic scale they are assumed to be delta-correlated. Their strengths are not arbitrary; rather, in view of the *local equilibrium assumption*, they are chosen to yield the correct equilibrium thermodynamic fluctuations in agreement with the fluctuation-

dissipation relations.

For a $3D$ fluid, the basic equations of the fluctuating hydrodynamic formalism, in the field variables $\rho(\mathbf{r}, t)$, $\mathbf{v}(\mathbf{r}, t)$ and $T(\mathbf{r}, t)$, read

$$\begin{aligned}
&\frac{\partial \rho}{\partial t} + \boldsymbol{\nabla} \cdot (\rho \mathbf{v}) = 0 \,, \\
&\rho \frac{\partial \mathbf{v}}{\partial t} = -\rho(\mathbf{v} \cdot \boldsymbol{\nabla})\mathbf{v} - \boldsymbol{\nabla} p + \eta \Delta \mathbf{v} + \left(\zeta + \frac{\eta}{3}\right) \boldsymbol{\nabla}(\boldsymbol{\nabla} \cdot \mathbf{v}) + \mathbf{F}_{ext} - \boldsymbol{\nabla} \cdot \mathbf{S} \,, \\
&\rho c_v \frac{\partial T}{\partial t} = -\rho c_v (\mathbf{v} \cdot \boldsymbol{\nabla}) T - \beta T \boldsymbol{\nabla} \cdot \mathbf{v} + \boldsymbol{\nabla} \cdot (\kappa \boldsymbol{\nabla} T) - \boldsymbol{\nabla} \cdot \mathbf{q} \,. \qquad (1.2)
\end{aligned}$$

Here, besides the usual notations [1], $\mathbf{F}_{ext}$ refers to the density of an applied external force field, $\mathbf{S}$ is the fluctuating part of the pressure tensor, and $\mathbf{q}$ is the fluctuating part of the heat flow. These stochastic variables are Gaussian white noises with zero mean,

$$\begin{aligned}
\langle S_{ik}(\mathbf{r}\,, t) \rangle &= 0 \,, \\
\langle g_i(\mathbf{r}, t) \rangle &= 0 \,, \qquad (1.3)
\end{aligned}$$

and variances (for a $3D$ fluid) given by

$$\begin{aligned}
&\langle S_{ij}(\mathbf{r}, t) S_{kl}(\mathbf{r}', t') \rangle = \\
&= \frac{2\, k_B T}{\rho} \left[\eta \left(\delta_{ik}\delta_{jl} + \delta_{il}\delta_{jk} \right) + \left(\zeta - \frac{\eta}{3} \right) \delta_{ij}\delta_{kl} \right] \delta(\mathbf{r} - \mathbf{r}')\, \delta(t - t') \,, \\
&\langle g_i(\mathbf{r}, t) g_k(\mathbf{r}', t') \rangle = 2\, \kappa\, k_B T\, \delta_{ik}\, \delta(\mathbf{r} - \mathbf{r}')\, \delta(t - t') \,, \\
&\langle S_{ij}(\mathbf{r}, t) g_k(\mathbf{r}', t') \rangle = 0 \qquad (1.4)
\end{aligned}$$

(T and, in general, η, ζ, κ as well, are space and time dependent.)

Fluctuating hydrodynamics has been used by various authors to study the statistical properties of simple fluids subject to nonequilibrium constraints, such as a temperature gradient (e.g., near a Rayleigh-Bénard convective threshold) [13] or shear [14]. Long-range correlations of the fluctuating hydrodynamic variables result in a simple, direct manner, and are reflected, in particular, in the structure of the dynamic form factor. The principal

[1] ρ is the mass density, $\mathbf{v}$ the velocity, p the hydrostatic pressure, η and ζ the shear and bulk viscosity coefficients in the Navier-Stokes expression for the viscous pressure tensor, c_v the isochoric specific heat, $\beta = (\partial p / \partial T)_\rho$, T the temperature and κ the thermal conductivity coefficient in the Fourier expression for the heat flow.

difficulty of the method comes from the problem of incorporating boundary conditions. It is a remarkable and non-trivial fact that fluctuating hydrodynamics and ensemble-like theories give identical results, especially if one recalls that the ensemble method has to resort to mode-coupling theory to compute equal-time correlations functions, while these correlations follow directly from the Langevin assumption in the equations of fluctuating hydrodynamics. The connection between these methods and the deep source of their agreement are discussed in detail by Kirkpatrick and co-workers [9].

Recent light scattering results (see Appendix A), obtained for systems under a temperature gradient, have shown quantitative agreement with theoretical predictions [15]. Quantitative agreement has also been demonstrated with results based on particle simulations, for systems under a temperature gradient [16, 17], under shear [18], and near the convective Rayleigh-Bénard instability [19]. We note that computer simulations can in principle be extended to highly nonequilibrium regimes that are difficult to attain in light scattering experiments.

All these results corroborate the fact that the Landau-Lifschitz fluctuating hydrodynamics is a robust, reliable framework to study nonequilibrium fluctuations.

On the other hand, macroscopic studies of sub-sonic hydrodynamical instabilities are usually based on the *incompressibility* assumption. This choice is partly due to the fact that even in the absence of noise the mathematical analysis of convective instabilities arising in *compressible* fluids proves to be quite involved [20, 21]. The difficulty of assigning appropriate boundary conditions also plays a role. However, as was first pointed out by Zaitsev and Shliomis [22], *the incompressibility assumption is essentially inconsistent with the very foundations of the fluctuating hydrodynamics formalism*, since it imposes fictitious correlations between the velocity components of the fluid. Indeed, it is easy to see that the idea of simultaneous fluctuations at different points of an incompressible fluid has no physical meaning at all, since the signal propagation velocity in such a medium is infinitely large: the incompressibility condition $\boldsymbol{\nabla} \cdot \mathbf{v} = 0$ implies that the velocity fluctuations are correlated in the entire volume of the fluid.

From another point of view, the compressibility of the fluid mostly affects *fast* sound modes, whereas the dynamics of the system near an instability

threshold is governed by *slow* dissipative modes, and these two time-scales are well separated in a fluid. We may thus expect that the behavior of a fluid evolving near a subsonic instability threshold is practically unaffected by its compressibility. This intuitive argument has been used by many authors who have considered fluctuating incompressible hydrodynamic equations, or even the corresponding normal form amplitude equations themselves[2], to which random noise terms are added [23]. In these approaches, the characteristics of the noise terms cannot be related to equilibrium statistical properties of the fluid, and thus remain arbitrary. A more satisfactory approach would be to start with the full compressible fluctuating hydrodynamic equations. Reducing these equations to a final normal form amplitude equation near the instability would lead directly to the explicit form of the associated noise terms consistent with such requirements as the fluctuation-dissipation theorem. Such a procedure, however, proves to be quite difficult mainly because of the boundary conditions. To the best of our knowledge, the only attempt in this direction has been made by Schmitz and Cohen [20] for the case of the Bénard instability. Concentrating on the behavior of a small layer in the bulk, these authors have succeeded in deriving the linearized *fluctuating* equations close to the convective instability. Whether this technique can be generalized to derive the corresponding normal form amplitude equation for the case of the Bénard instability is not clear at the present time.

One way to overcome this conceptual difficulty is to look for idealized models which, in spite of their extreme simplicity, can nevertheless lead to hydrodynamical instabilities analogous to those observed in real systems. A complete analysis of such a simple model will then allow us to draw some general conclusions that may be applied to more complicated systems as well.

This part of the present thesis is devoted to the study of such a model proposed some fifty years ago by Kolmogorov [3]. This is a two-dimensional flow resulting from a static forcing that is periodic in one of the two spatial coordinates. The basic flow essentially follows the applied force field, as long as the intensity of the latter is sufficiently small. However, if the applied force is progressively increased, this laminar flow becomes unstable and gives rise, through an initial bifurcation, to rotating convective patterns. A succession of bifurcations of increasing complexity leads finally to a turbu-

[2]These are usually postulated on the basis of the symmetries present in the system.
[3]See [24] for a description and an experimental realization.

lent behavior, with a specific underlying mechanism of energy transfer (the so-called "Kolmogorov-Kraichnan inverse energy cascade" [25]). The richness of this so-called *Kolmogorov flow*, combined with its simplicity, has attracted a great deal of both theoretical and numerical work. Meshalkin and Sinai [26] analysed the appearance of the first instability using a continued-fraction technique, with a suitable truncation procedure; some of the results were found independently by Green [27], who also predicted the possibility of secondary instabilities. Lorenz [28] seems have been the first to study the nonlinear regime resulting from the first instability and to evoke the possibility of a turbulence-like behaviour. Nepomniaschichii [29] and later Sivashinsky [30] went further into the nonlinear analysis and succeeded in reducing the nonlinear evolution to a description in terms of a Kuramoto-Sivashinsky equation, which is known to possess chaotic solutions. Finally, She [31] carried out a numerical analysis of the successive bifurcations that lead to turbulence, and of the energetics in the turbulent regime. Particle simulations, based on lattice-Boltzmann [32] or lattice-gas automata [33], have been used to study the statistical properties of the flow in the high Reynolds number regime [31, 34, 35, 36]. The basic aim of most of these works is the study of the mechanisms that lead to turbulence. All these theoretical studies have concentrated on the case of an *incompressible* fluid.

We take a different approach. Taking advantage of the simplicity of this flow, we make a complete comparative analysis of the compressible and incompressible cases, from equilibrium up to the vicinity of the first instability threshold that leads to rotating convective patterns. Both the linear (near-equilibrium) and nonlinear (near-instability) regimes are investigated. Fluctuations are accounted for in the framework of the Landau-Lifshitz formalism. This allows us to draw some general conclusions on the role of compressibility, as well as that of fluctuations in the onset of the hydrodynamic instabilities. All the theoretical deductions are supported by numerical simulations of the underlying equations of fluctuating hydrodynamics. Particle simulations are also discussed.

The next chapter is devoted to the study of the linear regime before the onset of the first instability leading to convective rolls [37]. We start with a description of Kolmogorov flow, and review some well known aspects of its macroscopic behavior. As will be seen, the *periodic boundary conditions* associated with this model permit a detailed analysis of the linearized fluctuating hydrodynamic equations to be made, and, consequently, of the the

fluctuation spectrum as well. Long-range correlations of the velocity fluctuations are obtained. In particular, we are able to show that in the long-time limit the flow behaves basically as if the fluid were incompressible, regardless of the value of the Reynolds number. The situation is different for the short-time behavior. We establish that here the incompressibility assumption leads to an incorrect form of the static correlation functions (in agreement with the prediction of Zaitsev and Shliomis [22]), except near the instability threshold, where our results strongly suggest that the incompressibility assumption again becomes valid. On the other hand, the linearized fluctuating hydrodynamic equations are clearly not valid close to, and beyond, the instability threshold. Although extensive numerical simulations have basically confirmed our predictions, a satisfactory answer to this important problem requires a full nonlinear analysis of the fluctuating Kolmogorov flow.

This is done in Chapter 3 (see also [38]). First, a nonlinear analysis is carried out for an incompressible fluid. The normal form amplitude equation is derived, and the explicit forms of the stationary stream function and the associated velocity field just above the instability are constructed. The subsequent section is devoted to the analysis of a compressible fluid. We first set up a perturbative technique based on a natural small parameter present in the system: namely, the ratio of the time scales of viscous dissipative modes and sound modes. This technique allows us to identify the relevant normal modes of the system, as well as the couplings between them, resulting in the relevant critical dynamics. It is then shown that the behaviour of the system is basically the same as that derived for an incompressible fluid, at least close to the instability threshold. We then focus on the statistical properties of the flow and show that, close to the instability, the stochastic dynamics of the system is governed by a set of two nonlinear coupled Langevin equations in Fourier space. Here again, the equivalence with the incompressible case is established. The theoretical predictions are confirmed by numerical simulations of the nonlinear fluctuating hydrodynamic equations.

Chapter 4 is devoted to an analysis of particle simulations of Kolmogorov flow [39]. It is shown that a spurious diffusion of the center of mass in the phase space corrupts the statistical properties of the flow. The analytical expression for the corresponding diffusion coefficient is derived. Although this effect is shown to be unimportant in practice in a macroscopic system,

it dramatically affects particle simulations of all types: molecular dynamics, Bird algorithm, and lattice-particle simulations. One has therefore to take it into account appropriately.

The final chapter is devoted to concluding remarks.

Chapter 2

The Linear Regime

2.1 Kolmogorov Flow

Consider a two-dimensional isothermal flow in a rectangular box oriented along the coordinate axes: $0 \leq x \leq L_x, 0 \leq y \leq L_y$. Periodic boundary conditions are assumed in both directions and the flow is maintained through an external force field of the form

$$\mathbf{F}_{ext} = F_0 \sin(2\pi n y/L_y)\,\mathbf{1}_x\,, \tag{2.1}$$

where $\mathbf{1}_x$ is the unit vector in the x-direction. This model represents the so-called *Kolmogorov flow*, and it belongs to the wider class of two-dimensional (potentially) negative eddy viscosity flows [40]. It is entirely characterized through the strength F_0 of the force field, the parameter n, which controls the wave number of the forcing, and the aspect ratio a_r, defined as

$$a_r = L_x/L_y\,. \tag{2.2}$$

In the following, we will concentrate mainly on the case $n = 1$.

According to the Landau-Lifshitz theory, the fluctuating hydrodynamic equations for this model read

$$\frac{\partial \rho}{\partial t} = -\boldsymbol{\nabla} \cdot (\rho\,\mathbf{v}) \tag{2.3}$$

and

$$\rho \frac{\partial \mathbf{v}}{\partial t} = -\rho\,(\mathbf{v}\cdot\boldsymbol{\nabla})\,\mathbf{v} - \boldsymbol{\nabla} p - \boldsymbol{\nabla}\cdot\boldsymbol{\sigma} + \mathbf{F}_{ext}\,, \tag{2.4}$$

where ρ is the mass density, p the hydrostatic pressure and $\boldsymbol{\sigma}$ the *two-dimensional* fluctuating stress tensor:

$$\sigma_{ij} = -\eta \left(\frac{\partial v_i}{\partial x_j} + \frac{\partial v_j}{\partial x_i} - \delta_{ij} \boldsymbol{\nabla} \cdot \mathbf{v} \right) - \zeta \delta_{i,j} \boldsymbol{\nabla} \cdot \mathbf{v} + S_{ij} . \qquad (2.5)$$

$\mathbf{S}$ is a random tensor whose elements $\{S_{ij}\}$ are Gaussian white noises with zero mean and covariances given by:

$$\begin{aligned} \langle S_{ij}(\mathbf{r},t)\, S_{k\ell}(\mathbf{r}',t') \rangle &= 2k_B T_0\, \delta(t-t')\, \delta(\mathbf{r}-\mathbf{r}') \left[\eta(\delta_{ik}\delta_{j\ell} + \delta_{i\ell}\delta_{jk}) \right. \\ &\quad \left. + (\zeta - \eta)\delta_{ij}\delta_{k\ell} \right] , \end{aligned} \qquad (2.6)$$

where T_0 stands for the (uniform) temperature. For simplicity, we shall assume that the shear and bulk viscosity coefficients, η and ζ, are *state independent*, i.e., that they are constant.

One more remark in the context of fluctuations: When imposing a force field, one has to keep in mind that both in microscopic simulations and in real systems, the fluid is made out of individual particles. Hence what one can impose is not a bulk force, but rather an acceleration field acting on the particles. Since the density of particles is fluctuating, we conclude that the external field in the momentum equation (2.4) is also a fluctuating quantity:

$$\mathbf{F}_{ext} = \rho(x,y)\, a_0 \sin(2\pi n\, y/L_y)\, \mathbf{1}_x, \qquad (2.7)$$

where a_0 is the amplitude of the imposed acceleration field. This is an interesting problem in its own right, and will be discussed in detail in Chapter 4. For the present we need to note that this effect is only important for particle simulations of the flow, i.e., for systems involving a rather small number of particles (as compared, say, to Avogadro's number). On a macroscopic scale, this effect is completely negligible. Therefore, in this chapter and in the next one, we will consider F_0 as a *constant, non-fluctuating quantity.*

Let us now focus on the *deterministic behavior.* It can be checked easily that in the stationary state the pressure and the density are uniform in space ($p_{st} = p_0$, $\rho_{st} = \rho_0$), whereas the velocity profile basically follows the external force field,

$$\begin{aligned} \mathbf{v}_{st} &= u_0 \sin(2\pi\, y/L_y)\, \mathbf{1}_x , \\ u_0 &= \frac{F_0\, L_y^2}{4\pi^2 \eta} . \end{aligned} \qquad (2.8)$$

For sufficiently small F_0, this stationary flow is stable. As we increase F_0, however, the flow becomes unstable giving rise to rotating convective patterns. Other instabilities of increasing complexity may occur for larger values of F_0, culminating in a chaotic behavior similar to what is observed in turbulent flows [28, 31, 35]. In this thesis we shall limit ourselves to the analysis of the system near its first instability.

We have yet to supplement the momentum conservation equation (2.4) with an equation of state relating the pressure to the density (recall that the system is isothermal). In this section we shall simply assume that the flow is incompressible, i.e.,

$$\boldsymbol{\nabla} \cdot \mathbf{v} = \frac{\partial u}{\partial x} + \frac{\partial v}{\partial y} = 0\,, \tag{2.9}$$

where u and v represent the x and y components of the velocity, respectively. Relation (2.9) implies a uniform density ρ_0 throughout the system for all time, if this is initially the case. It also implies the existence of a scalar function $\psi(x,\, y,\, t)$, known as the *stream function*, defined by the relations

$$u = \frac{\partial \psi}{\partial y}\,, \quad v = -\frac{\partial \psi}{\partial x}\,. \tag{2.10}$$

Scaling length by L_y, velocity by u_0 and time by L_y/u_0, the dimensionless equation for the stream function reads

$$\begin{aligned} \frac{\partial(\nabla^2 \psi)}{\partial t} = & - \frac{\partial \psi}{\partial y}\frac{\partial(\nabla^2 \psi)}{\partial x} + \frac{\partial \psi}{\partial x}\frac{\partial(\nabla^2 \psi)}{\partial y} + R^{-1}\,\nabla^2(\nabla^2 \psi) \\ & + 8\,\pi^3\,R^{-1}\cos(2\,\pi\,y)\,, \end{aligned} \tag{2.11}$$

where R is the *Reynolds number*,

$$R = \frac{\rho_0\, u_0\, L_y}{\eta}\,, \tag{2.12}$$

a measure of the "distance" from equilibrium. The stationary solution of (2.11) reads

$$\psi_{st} = -\frac{1}{2\,\pi}\cos(2\,\pi\,y)\,. \tag{2.13}$$

Setting $\psi = \psi_{st} + \delta\psi$, and linearizing (2.11) around ψ_{st}, one gets

$$\begin{aligned} \frac{\partial(\nabla^2 \delta\psi)}{\partial t} = & - \sin(2\,\pi\,y)\frac{\partial(\nabla^2 \delta\psi)}{\partial x} - 4\,\pi^2 \sin(2\,\pi\,y)\frac{\partial\, \delta\psi}{\partial x} \\ & + R^{-1}\,\nabla^2(\nabla^2 \delta\psi)\,. \end{aligned} \tag{2.14}$$

As the boundary conditions are periodic, $\delta\psi(x,y,t)$ can be expanded in Fourier series

$$\delta\psi(x,\,y,\,t) = \sum_{k_x,\,k_y\,=\,-\,\infty}^{\infty} \exp\left(-\,2\,\pi\,i\,k_y\,y\right)\,\exp\left(-\,2\,\pi\,i\,k_x\,x/a_r\right)\,\delta\psi_{k_x,\,k_y}(t)\,,$$

$$\delta\psi_{k_x,\,k_y}(t) = \int_0^1 dy\,\exp\left(2\,\pi\,i\,k_y\,y\right)\frac{1}{a_r}\int_0^{a_r} dx\,\exp\left(2\,\pi\,i\,k_x\,x/a_r\right)\,\delta\psi(x,\,y,\,t)\,.$$

(2.15)

Equation (2.14) can then be transformed to :

$$\begin{aligned}\frac{\partial\delta\psi_{k_x,\,k_y}}{\partial t} = \quad & -4\,\pi^2\,R^{-1}\,(\tilde{k}_x^2 + {k_y}^2)\delta\psi_{k_x,\,k_y} \\ & +\pi\,\tilde{k}_x\,\left[\delta\psi_{k_x,\,k_y\,+\,1} - \delta\psi_{k_x,\,k_y\,-\,1}\right] \\ & +2\,\pi\,\frac{\tilde{k}_x\,k_y}{\tilde{k}_x^2 + {k_y}^2}\,\left[\delta\psi_{k_x,\,k_y\,+\,1} + \delta\psi_{k_x,\,k_y\,-\,1}\right]\,, \qquad (2.16)\end{aligned}$$

where we have set

$$\tilde{k}_x = k_x/a_r\,. \qquad (2.17)$$

In its general form, the analysis of this equation is quite difficult [26]. On the other hand, if ψ_{st} is stable, then in the long-time (hydrodynamic) limit, the evolution of the system will be governed mainly by the long-wavelength modes. Accordingly, we start our analysis by considering only the modes $k_y = 0\,,\pm 1$, i.e., we assume that $\delta\psi(k_x\,,k_y\,t) \approx 0$ for $|k_y| \geq 2$ [27]. This is the so-called *three-mode approximation* and its validity and limits are verified through comparisons with the appropriate computer simulations and calculations from near equilibrium up to the vicinity of the instability threshold, as will become clear subsequently.

The infinite set of coupled eqs.(2.16) is therefore truncated (for each fixed k_x) to a set of just three equations. Defining the vector

$$\boldsymbol{\delta\psi}_{k_x} \equiv \begin{pmatrix} \delta\psi_{k_x,\,0} \\ \delta\psi_{k_x,\,1} \\ \delta\psi_{k_x,\,-1} \end{pmatrix}\,, \qquad (2.18)$$

this set can be written in the following matrix form :

$$\frac{\partial \delta\psi_{k_x}(t)}{\partial t} = \mathbf{A}(k_x) \cdot \delta\psi_{k_x}(t)\,, \tag{2.19}$$

with

$$\mathbf{A}(k_x) =$$

$$\begin{pmatrix} -4\pi^2 R^{-1}\tilde{k}_x^2 & \pi\tilde{k}_x & -\pi\tilde{k}_x \\ \pi\tilde{k}_x(1-\tilde{k}_x^2)/(1+\tilde{k}_x^2) & -4\pi^2 R^{-1}(1+\tilde{k}_x^2) & 0 \\ -\pi\tilde{k}_x(1-\tilde{k}_x^2)/(1+\tilde{k}_x^2) & 0 & -4\pi^2 R^{-1}(1+\tilde{k}_x^2) \end{pmatrix}. \tag{2.20}$$

We note that the matrix $\mathbf{A}(k_x)$ is diagonal for $k_x = 0$, so that the solution of eq. (2.19) reduces to:

$$\delta\psi_{0,1}(t) \sim \delta\psi_{0,-1}(t) \sim \exp(-4\pi^2 R^{-1}\, t). \tag{2.21}$$

Further, by the definition of the stream function (eq. (2.10)), $\psi_{0,0}(t) = 0$ for all t. We thus concentrate on the case $k_x \neq 0$, looking for a similarity transformation $\mathbf{T}(k_x)\cdot\mathbf{A}(k_x)\cdot\mathbf{T}^{-1}(k_x)$ which diagonalizes the matrix $\mathbf{A}(k_x)$. After some algebra, one finds

$$\mathbf{T}(k_x) = \begin{pmatrix} [\lambda_1(k_x)-\lambda_3(k_x)]/\pi\tilde{k}_x & 1 & -1 \\ [\lambda_2(k_x)-\lambda_3(k_x)]/\pi\tilde{k}_x & 1 & -1 \\ 0 & 1 & 1 \end{pmatrix}, \tag{2.22}$$

as well as

$$\mathbf{T}^{-1}(k_x) =$$

$$\begin{pmatrix} \pi\tilde{k}_x/(\lambda_1-\lambda_2) & \pi\tilde{k}_x/(\lambda_2-\lambda_1) & 0 \\ (\lambda_2-\lambda_3)/[2(\lambda_2-\lambda_1)] & (\lambda_1-\lambda_3)/[2(\lambda_1-\lambda_2)] & 1/2 \\ (\lambda_2-\lambda_3)/[2(\lambda_1-\lambda_2)] & (\lambda_3-\lambda_1)/[2(\lambda_1-\lambda_2)] & 1/2 \end{pmatrix}. \tag{2.23}$$

Here $\{\lambda_i(k_x)\}_{i=1,2,3}$ are the eigenvalues of $\mathbf{A}(k_x)$, given by

$$\lambda_1(k_x) = -2\pi^2 R^{-1}(1 + 2\tilde{k}_x^2) + \pi\sqrt{2\tilde{k}_x^2(1-\tilde{k}_x^2)/(1+\tilde{k}_x^2) + 4\pi^2 R^{-2}},$$

$$\lambda_2(k_x) = -2\pi^2 R^{-1}(1 + 2\tilde{k}_x^2) - \pi\sqrt{2\tilde{k}_x^2(1-\tilde{k}_x^2)/(1+\tilde{k}_x^2) + 4\pi^2 R^{-2}},$$

$$\lambda_3(k_x) = -4\pi^2 R^{-1}(1 + \tilde{k}_x^2). \tag{2.24}$$

Equation (2.19) then becomes

$$\frac{\partial \delta\phi_i(k_x, t)}{\partial t} = \lambda_i(k_x)\,\delta\phi_i(k_x, t) \quad (i = 1, 2, 3), \tag{2.25}$$

where

$$\boldsymbol{\delta\phi}(k_x) = \mathbf{T}(k_x) \cdot \boldsymbol{\delta\psi}_{k_x}. \tag{2.26}$$

It follows from (2.24) that $\lambda_2(k_x)$ and $\lambda_3(k_x)$ are always negative, whereas there exists a critical value of the Reynolds number

$$R_c(k_x) = 2\sqrt{2}\pi \frac{1+\tilde{k}_x^2}{\sqrt{1-\tilde{k}_x^2}} \qquad (0 < \tilde{k}_x^2 < 1) \tag{2.27}$$

for which $\lambda_1(k_x)$ vanishes, thus indicating the limit of stability of the corresponding mode [41]. Clearly $R_c(k_x)$ is an increasing function of $|k_x|$, so that the first modes to become unstable correspond to $|k_x| = 1$, provided the aspect ratio $a_r > 1$. As $a_r \to 1$, $R_c \to \infty$, indicating that no instability can develop for perturbations of the same spatial periodicity as the applied force [42]. In the following, we shall therefore concentrate mainly on the case $a_r > 1$. For $a_r = 2$, relation (2.27) predicts a critical Reynolds number $R_c \approx 12.8255$. Analytical calculations can still be handled (using Maple or Mathematica symbolic programs) when the modes $k_y = \pm 2$ are taken into account as well, and lead to

$$R_c^{(5)}(k_x) = R_c(k_x)\left[1 + \frac{\tilde{k}_x^4(\tilde{k}_x^2+3)}{2(\tilde{k}_x^2+4)^2(\tilde{k}_x^2-1)}\right]^{-1/2} \qquad (0 < \tilde{k}_x^2 < 1). \tag{2.28}$$

For $a_r = 2$, one finds a critical Reynolds number $R_c^{(5)} \approx 12.8738$, so that the discrepancy remains below 0.4%. Numerical evaluation of R_c performed with a total amount of 103 modes shows no further significant discrepancy. This is an indication that one can rely reasonably well on a *three-mode approximation* (that is $\delta\psi_{k_x,k_y}(t) \approx 0$ for $|k_y| \geq 2$), at least as long as R is close to R_c. As will be shown in the next chapter, this approximation leads to the correct velocity field beyond the instability. We shall use this approximation below to study the statistical properties of the system. Among other results, this will also allow us to decide whether or not the three-mode approximation applies for near-equilibrium situations as well.

2.2 Hydrodynamic Fluctuations

To study the spectra of the fluctuations, we first linearize the hydrodynamic equations (2.3) and (2.4) around the stationary state. Setting $\rho = \rho_0 + \delta\rho$, $p = p_0 + \delta p$ and $\mathbf{v} = \mathbf{v}_{st} + \delta\mathbf{v}$, and following Landau and Lifshitz [12], the fluctuating hydrodynamic equations read

$$\frac{\partial\,\delta\rho}{\partial t} = -\rho_0\left(\frac{\partial\,\delta u}{\partial x} + \frac{\partial\,\delta v}{\partial y}\right) - u_0\,\sin\left(2\,\pi\,y/L_y\right)\frac{\partial\,\delta\rho}{\partial x}\,, \tag{2.29}$$

$$\rho_0\,\frac{\partial\,\delta\mathbf{v}}{\partial\,t} = -\rho_0\left(\mathbf{v}_{st}\cdot\boldsymbol{\nabla}\right)\delta\mathbf{v} - \rho_0\left(\delta\mathbf{v}\cdot\boldsymbol{\nabla}\right)\mathbf{v}_{st} - \boldsymbol{\nabla}\,\delta p - \boldsymbol{\nabla}\cdot\delta\boldsymbol{\sigma}\,. \tag{2.30}$$

$\delta\boldsymbol{\sigma}$ is the two-dimensional linearized fluctuating stress tensor,

$$\delta\sigma_{ij} = -\eta\left(\frac{\partial\,\delta v_i}{\partial\,x_j} + \frac{\partial\,\delta v_j}{\partial\,x_i} - \delta_{ij}\,\boldsymbol{\nabla}\cdot\delta\mathbf{v}\right) - \zeta\,\delta_{ij}\,\boldsymbol{\nabla}\cdot\delta\mathbf{v} + S_{ij}\,. \tag{2.31}$$

We have yet to specify the equation of state. Since the fluid is compressible and isothermal, we simply set

$$\delta p = c_s^2\,\delta\rho\,, \tag{2.32}$$

where c_s is the isothermal speed of sound. Scaling lengths by L_y, time by L_y/c_s, $\delta\rho$ by ρ_0 and $\delta\mathbf{v}$ by the speed of sound, the dimensionless fluctuating equations in Fourier space are

$$\begin{aligned}\frac{\partial\,\delta\rho_{k_x,k_y}(t)}{\partial t} &= 2\,\pi\,i\left(\tilde{k}_x\,\delta u_{k_x,k_y} + k_y\,\delta v_{k_x,k_y}\right)\\ &+ \varepsilon\,R\,\pi\,\tilde{k}_x\left(\delta\rho_{k_x,k_y+1} - \delta\rho_{k_x,k_y-1}\right),\end{aligned} \tag{2.33}$$

$$
\begin{aligned}
\frac{\partial \delta u_{k_x,k_y}(t)}{\partial t} = & - \pi\,\varepsilon\,R(\delta v_{k_x,k_y+1} + \delta v_{k_x,k_y-1}) \\
& + \pi\,\varepsilon\,R\,\tilde{k}_x\,(\delta u_{k_x,k_y+1} - \delta u_{k_x,k_y-1}) \\
& - 4\,\pi^2\,\varepsilon(\tilde{k}_x^2 + k_y^2)\,\delta u_{k_x,k_y} \\
& - 4\,\pi^2\,\alpha\,\varepsilon\,\tilde{k}_x(\tilde{k}_x\,\delta u_{k_x,k_y} + k_y\,\delta v_{k_x,k_y}) \\
& + 2\,\pi\,i\,\tilde{k}_x\,\delta\rho_{k_x,k_y} + F_{k_x,k_y}(t)\,, \qquad (2.34)
\end{aligned}
$$

$$
\begin{aligned}
\frac{\partial \delta v_{k_x,k_y}(t)}{\partial t} = & \quad \pi\,\varepsilon\,R\,\tilde{k}_x\,(\delta v_{k_x,k_y+1} - \delta v_{k_x,k_y-1}) \\
& - 4\,\pi^2\,\varepsilon(\tilde{k}_x^2 + k_y^2)\,\delta v_{k_x,k_y} \\
& - 4\,\pi^2\,\alpha\,\varepsilon\,k_y\,(\tilde{k}_x\,\delta u_{k_x,k_y} + k_y\,\delta v_{k_x,k_y}) \\
& + 2\,\pi\,i\,k_y\,\delta\rho_{k_x,k_y} + G_{k_x,k_y}(t)\,, \qquad (2.35)
\end{aligned}
$$

where

$$
\alpha = \zeta/\eta \qquad (2.36)
$$

and

$$
\varepsilon = \frac{\eta}{\rho_0 c_s\,L_y}\,. \qquad (2.37)
$$

The functions F_{k_x,k_y} and G_{k_x,k_y} are Fourier components of the noise terms ; their covariances follow directly from eqs.(2.6),

$$
\begin{aligned}
\left\langle F_{k_x,k_y}(t)\,F_{k'_x,k'_y}(t')\right\rangle &= 8\pi^2\varepsilon\,\mathcal{A}\,[(\alpha+1)\,\tilde{k}_x^2 + k_y^2]\,\delta_{\mathbf{k}+\mathbf{k}',0}\,\delta(t-t')\,, \\
\left\langle F_{k_x,k_y}(t)\,G_{k'_x,k'_y}(t')\right\rangle &= 8\pi^2\varepsilon\,\mathcal{A}\,\alpha\,\tilde{k}_x\,k_y\,\delta_{\mathbf{k}+\mathbf{k}',0}\,\delta(t-t')\,, \\
\left\langle G_{k_x,k_y}(t)\,G_{k'_x,k'_y}(t')\right\rangle &= 8\pi^2\varepsilon\,\mathcal{A}\,[\tilde{k}_x^2 + (\alpha+1)\,k_y^2]\,\delta_{\mathbf{k}+\mathbf{k}',0}\,\delta(t-t')\,, \qquad (2.38)
\end{aligned}
$$

where $\mathbf{k} \equiv (k_x/a_r,\ k_y)$ and

$$
\mathcal{A} = \frac{k_B\,T_0}{M\,{c_s}^2}\,, \qquad (2.39)
$$

$M = a_r \rho_0 {L_y}^2$ being the total mass of the system.

The analysis of the Langevin equations above can be simplified greatly by observing that the quantity ε must remain small if one wishes to remain within the limit of validity of the hydrodynamic regime [43]. Further, as already mentioned, we limit ourselves to strictly *subsonic flows*, so that $\varepsilon R = u_0/c_s << 1$. We thus have at our disposal a natural small parameter which, however, has to be used with care since the solution of the Langevin equations (2.33) - (2.35) proves to be singular in the limit $\varepsilon \to 0$. Moreover, it turns out that the behavior of the system is qualitatively independent of the value of the bulk viscosity coefficient and so (to avoid cumbersome notation) we simply set $\alpha = 0$ (recall that $\alpha = \zeta/\eta$). Even then the calculations are lengthy and tedious; therefore we concentrate here mainly on the final results, giving only a brief sketch of the intermediate steps.

We pay particular attention to two quantities. First, the dynamic structure factor or scattering function (see Appendix A), defined as the space-time Fourier transform of the density autocorrelation function:

$$S_{\mathbf{k}}(\omega) = \int_{-\infty}^{+\infty} dt \, \exp(i\,\omega t) \, \langle \delta\rho_{\mathbf{k}}(t) \, \delta\rho_{-\mathbf{k}}(0) \rangle \ , \tag{2.40}$$

$$\langle \delta\rho_{\mathbf{k}}(t) \, \delta\rho_{-\mathbf{k}}(0) \rangle = \frac{1}{S^2} \int\int d\mathbf{r} \, d\mathbf{r}' \, \exp\left\{ 2\pi i \, \mathbf{k} \cdot (\mathbf{r} - \mathbf{r}') \right\} \, \left\langle \delta\rho(\mathbf{r}, t) \, \delta\rho(\mathbf{r}', 0) \right\rangle \ , \tag{2.41}$$

where the integrals extend over the surface $S = a_r \times 1$ of the system. Next, the space-time Fourier transform of the velocity autocorrelation function, defined in a similar fashion:

$$W_{\mathbf{k}}(\omega) = \int_{-\infty}^{+\infty} dt \, \exp(i\,\omega t) \, \langle \delta\mathbf{v}_{\mathbf{k}}(t) \cdot \delta\mathbf{v}_{-\mathbf{k}}(0) \rangle \ , \tag{2.42}$$

as well as its static (equal-time) counterpart,

$$\langle \delta\mathbf{v}_{\mathbf{k}} \cdot \delta\mathbf{v}_{-\mathbf{k}} \rangle = \frac{1}{2\,\pi} \int_{-\infty}^{+\infty} d\omega \, W_{\mathbf{k}}(\omega) \ . \tag{2.43}$$

Analytic calculations can be done in two "extreme" situations: either in the vicinity of equilibrium (through a perturbative technique to be presented

below), or in the vicinity of the instability point (where we will use the three-mode approximation presented in the previous section). In both situations, the calculations[1] are extremely lengthy. However, as they do not present any conceptual difficulty, we omit the details here.

First of all, it is found that the behavior of the scattering function is essentially the same in both the extreme cases. Namely, *to dominant order in* ε, $S_{\mathbf{k}}(\omega)$ *is not affected by the nonequilibrium constraints*, i.e., it maintains its equilibrium form,

$$S_{\mathbf{k}}(\omega) = \frac{32\,\varepsilon\,\mathcal{A}\,k^4\,\pi^4}{(\omega^2 - 4\,k^2\,\pi^2)^2 + 16\,\varepsilon^2\,\omega^2\,k^4\,\pi^4}\,\left[1 + O(\varepsilon^2 R^2)\right]\,, \qquad (2.44)$$

where $k^2 = (\tilde{k}_x^2 + k_y^2)$. We note that the scattering function exhibits only sound mode peaks (Brillouin lines). The absence of a purely dissipative mode around $\omega \approx 0$ (the Rayleigh line) is directly related to the fact that Kolmogorov flow is *strictly isothermal*. Indeed, this means not only a constant temperature throughout the system, but also infinite thermal conductivity, i.e., $\Lambda_T \to \infty$ (Appendix A), which leads to an instantaneous decay of any entropy fluctuations. Therefore, the scattering function does not contain much information about the nonequilibrium constraints imposed on the system - except the fact that they do not affect the sound modes.

On the other hand, the velocity autocorrelation function $W_{\mathbf{k}}(\omega)$ does exhibit a purely dissipative viscous regime around $\omega \approx 0$, together with a "sound regime" located around $\omega \approx \pm 2\pi|\mathbf{k}|$. Here again we find that, to leading order in ε, the sound regime is not affected by the nonequilibrium constraints and behaves very much like the scattering function,

$$W_{\mathbf{k}}(\omega \approx \pm 2\pi|\mathbf{k}|) = \frac{8\,\varepsilon\,\mathcal{A}\,k^4\,\pi^2\omega^2}{(\omega^2 - 4\,k^2\,\pi^2)^2 + 16\,\varepsilon^2\,\omega^2\,k^4\,\pi^4}\,. \qquad (2.45)$$

The part of the autocorrelation function that corresponds to the viscous regime $\omega \approx 0$ (i.e., that corresponds to the long-time behavior of the system) is strongly dependent on R, and is therefore a source of information on the nonequilibrium state of the system. In the following we will therefore concentrate mainly on the spectrum of the velocity fluctuations.

[1] These were done using a combination of Maple symbolic calculus and FORTRAN 77 numeric calculus.

We first consider the *near-equilibrium* situations, limiting ourselves to relatively small values of the Reynolds number R. In this case the Langevin equations (2.33)-(2.35) can be solved perturbatively by expanding the hydrodynamic variables around their equilibrium values:

$$\delta\rho = \delta\rho_{eq} + \mu\,\delta\rho_1 + \mu^2\,\delta\rho_2 + \ldots \tag{2.46}$$

$$\delta\mathbf{v} = \delta\mathbf{v}_{eq} + \mu\,\delta\mathbf{v}_1 + \mu^2\,\delta\mathbf{v}_2 + \ldots \tag{2.47}$$

where the parameter μ is defined as $\mu \equiv R/2\pi$. After some lengthy algebra, one gets for the static correlation function

$$\langle \delta\mathbf{v}_{\mathbf{k}} \cdot \delta\mathbf{v}_{-\mathbf{k}} \rangle \; - \; \langle \delta\mathbf{v}_{\mathbf{k}} \cdot \delta\mathbf{v}_{-\mathbf{k}} \rangle_{eq} \; =$$

$$\left(\frac{R}{2\pi}\right)^2 \frac{\mathcal{A}\left(10 + 2\,\tilde{k}_x^6 + 5\,\tilde{k}_x^4 + \tilde{k}_x^2\right)}{2\left(\tilde{k}_x^2+4\right)\left(2\,\tilde{k}_x^2+5\right)\left(2\,\tilde{k}_x^2+1\right)\left(\tilde{k}_x^2+1\right)^2}\left[1 + O(\varepsilon^2,\,(R/2\pi)^2)\right], \tag{2.48}$$

where

$$\langle \delta\mathbf{v}_{\mathbf{k}} \cdot \delta\mathbf{v}_{-\mathbf{k}} \rangle_{eq} \; = \; 2\mathcal{A} \tag{2.49}$$

is the equilibrium contribution. To simplify the presentation, we have considered the case $k_y = 1$.

To check the validity of this result, we have solved numerically the Langevin equations (2.33)-(2.35). The traditional procedure consists of simulating the corresponding stochastic processes and using the hydrodynamical sample paths (time series) so obtained to construct the various correlation functions. This procedure is quite simple to set up, but requires very long runs in order to get reliable statistics in nonlinear problems. Alternatively, one can directly solve the equations governing the evolution of the correlation functions, that are obtained easily from the underlying Langevin equations [44]. The principle of this procedure - the so-called *direct method* of integration of the linear Langevin equations - is described in Appendix A. It is, of course, an exact method, and quite fast computationally, but it is limited to linear problems. We have used both techniques. The former was used to simulate the full nonlinear hydrodynamic equations (2.3) and (2.4) with a noisy stress

tensor, in real space. The space of an $L_x \times L_y$ cell is discretized in both x and y directions, and the values of the fluctuating variables in the nodes of this grid allow us to calculate the corresponding Fourier transforms, and to construct the corresponding correlation functions. In the long-time limit, one can obtain the values of the static correlation functions. The second method was used to study the statistical properties of the linear Langevin equations (2.33)-(2.35), with a cut-off beyond the first forty-one k_y modes (i.e., setting $\delta\rho_{k_x,k_y}(t) = \delta\mathbf{v}_{k_x,k_y}(t) \approx 0$ for $|k_y| \geq 21$).

In figure 2.2 we have presented the static velocity autocorrelation function, as given by the relation (2.48), together with the corresponding numerical solution obtained using the second of the two computational techniques described above. As may be seen, quantitative agreement is demonstrated for $R \leq 4$ but discrepancies gradually appear as we consider larger values of the Reynolds number. This is to be expected since the validity of the relation (2.48) can only be guaranteed for *small* values of the Reynolds number.

It is also instructive to study the properties of the static correlation function in real space, $\langle \delta\mathbf{v}(\mathbf{r}) \cdot \delta\mathbf{v}(0) \rangle$. This can be obtained by summing the product $\langle \delta\mathbf{v}_{\mathbf{k}} \cdot \delta\mathbf{v}_{-\mathbf{k}} \rangle \exp[2\pi i(x\,k_x + y\,k_y)]$ over $(k_x,\, k_y)$. Analytical calculations, however, prove to be extremely difficult to handle for the general case. We therefore limit ourselves to a special case where only one of the wavenumbers is summed over, the other being held fixed. Specifically, we set $k_y = 0$ to obtain:

$$\langle \delta\mathbf{v}_{k_x} \cdot \delta\mathbf{v}_{-k_x} \rangle - 2\mathcal{A} = \left(\frac{R}{2\pi}\right)^2 \frac{\mathcal{A}}{2\left(\tilde{k}_x^2 + 1\right)\left(1 + 2\,\tilde{k}_x^2\right)} \left[1 + O(\varepsilon^2,\, (R/2\pi)^2)\right]. \tag{2.50}$$

Note that setting $k_y = 0$ is equivalent to taking the spatial average over the y direction (cf. eq. (2.41)), so that relation (2.50) holds only for $k_x \neq 0$. In fact, $\delta\mathbf{v}_{0,0}(t) \equiv 0$, since the linear momentum of the center of mass is a conserved quantity. With this restriction, the summation can be performed in a straightforward manner to give

$$\begin{aligned} \langle \delta\mathbf{v}(x) \cdot \delta\mathbf{v}(0) \rangle \;-\; 2\mathcal{A}\,[\delta(x) - a_r] \;=\; \\ \frac{\mathcal{A}\,R^2\,a_r}{8\,\pi} \left\{ \sqrt{2}\,\frac{\cosh[\sqrt{2}\,\pi\,(x - a_r/2)]}{\sinh(\pi\,a_r/\sqrt{2})} \;-\; \frac{\cosh[2\,\pi\,(x - a_r/2)]}{\sinh(\pi\,a_r)} - \frac{1}{\pi\,a_r} \right\}, \end{aligned} \tag{2.51}$$

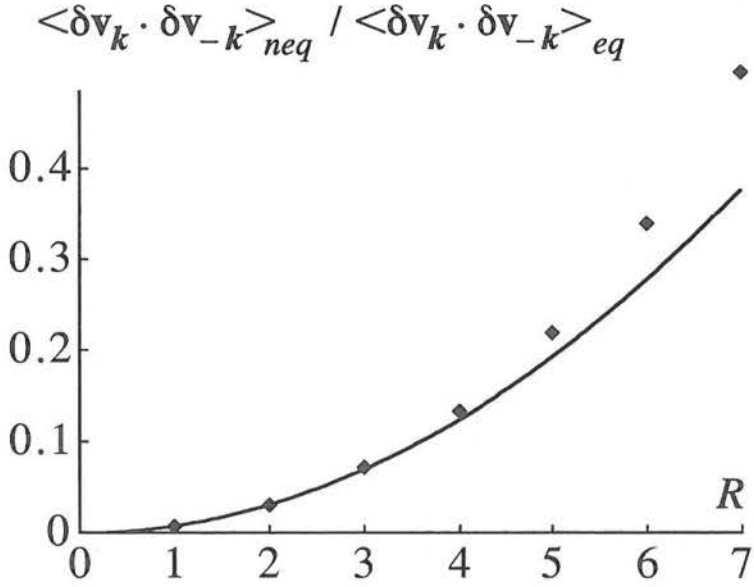

Figure 2.1: Fourier transform of the nonequilibrium part of the static velocity autocorrelation function, normalized by the corresponding equilibrium part, as a function of the Reynolds number. The solid curve represents the theoretical prediction, as given by eq. (2.48), whereas the diamonds correspond to results obtained by numerical simulation of the linear Langevin equations (2.33)-(2.35). The parameters are $a_r = 2$, $\varepsilon = 10^{-2}$, $\mathcal{A} = 10^{-3}/256$ (defined by eq. (2.39)), $k_y = 1, k_x = 1$ (i.e., $\tilde{k}_x = 1/2$). The estimated statistical errors are less than 4%.

where the second term on the left-hand side is the equilibrium contribution [45] (the stationary fluctuations around equilibrium, in accordance with standard linear response theory, are δ-correlated in space). Note the presence of a constant term in both the equilibrium and nonequilibrium (right-hand side) parts, which ensures the conservation of linear momentum. The nonequilibrium contribution to $\langle \delta\mathbf{v}(x) \cdot \delta\mathbf{v}(0) \rangle$ exhibits *long-range correlations* since the correlation length is clearly of the order of the size of the system. This is shown in figure 2.2 for $R = 3$, where quantitative agreement with numerical results is observed. The existence of long-range correlations is generic for fluids under shear constraints and have been predicted by several authors [11, 45], and confirmed by both microscopic [18] and lattice-gas automata simulations [36]. On the other hand, experimental evidence has so far only been reported for fluids under a temperature gradient, where quantitative agreement with fluctuating hydrodynamics has been demonstrated [15].

Let us now consider the *far from equilibrium* case. As pointed out in the last section, for R close to R_c one can expect the three-mode approximation (that is, $\delta\rho_{k_x,k_y}(t)$ and $\delta\mathbf{v}_{k_x,k_y}(t)$ are ≈ 0 for $|k_y| \geq 2$) to be reasonably reliable. As a consequence, eqs. (2.33)-(2.35) reduce to a system of nine coupled linear Langevin equations for each fixed k_x which, for consistency, must be limited to $|k_x| \leq \max\{a_r, 2\}$. The calculations can nevertheless be done, leading to the following expression for the static velocity autocorrelation function:

$$\langle \delta\mathbf{v}_{\mathbf{k}} \cdot \delta\mathbf{v}_{-\mathbf{k}} \rangle - 2\mathcal{A} = \frac{\mathcal{A}\, R^2}{2\,(R_c^2 - R^2)\left(1 + 2\,\tilde{k}_x^2\right)} \left[1 + O(\varepsilon^2\, R^2)\right] \ , \qquad (2.52)$$

where the second term on the left-hand side is the equilibrium contribution, $R_c(k_x = 1)$ is given by eq. (2.27), and $k_y = 1$. The nonequilibrium part diverges as $R \to R_c$, but then, of course, the linearized Langevin equations cease to be valid. Note also that a development of (2.52) in powers of $R/2\pi$ for small values of $R/2\pi$ does not lead to (2.48). This shows that the three-mode approximation, while appropriate for the description of the system in the vicinity of its first instability, i.e., for R close to R_c, *ceases to be valid near equilibrium*, i.e., for small values of R.

In figure 2.3 we have depicted the result (2.52) for increasing values of R, together with the numerical solution of the linear Langevin equations

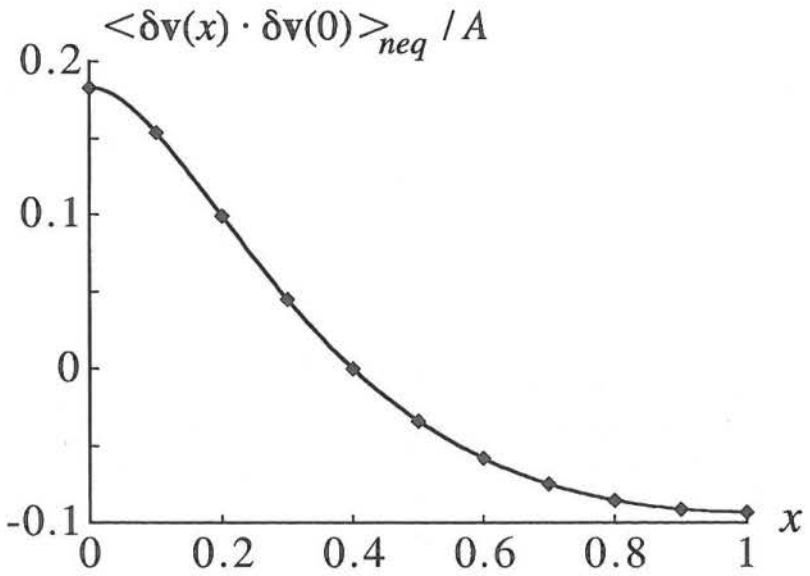

Figure 2.2: Nonequilibrium part of the static velocity autocorrelation function, normalized by $\mathcal{A}$, as a function of the spatial coordinate x. The solid curve represents the theoretical prediction, as given by eq. (2.51), whereas the diamonds correspond to results obtained by numerical simulation of the linear Langevin equations (2.33) - (2.35). The Reynolds number is set to $R = 3$ and the other parameters are as given in the caption of figure 2.2.

(2.30), as well as the results obtained by simulation of the full nonlinear hydrodynamic equations (2.3), (2.4) with a noisy stress tensor. Quantitative agreement is observed for values of R up to 12, but significant discrepancies start to show up as $R \to R_c \approx 12.87$ where the linearized theory leads to a diverging correlation function (cf. eq. (2.52)). This is not the case for the correlation function obtained using the full nonlinear equations, which seems to exhibit a maximum around R_c. It should however be noted that, owing to the slowing down of the relaxation of the "critical" Fourier modes, statistical errors are quite important for R close to R_c (about 15% for the last four data points), so that no definitive conclusion can be drawn at this stage. The analysis of the statistical properties of the nonlinear regime is relegated to Chapter 3.

2.3 Validity of the Incompressibility Assumption

As already mentioned, the macroscopic studies of subsonic hydrodynamical instabilities are based on the *incompressibility assumption* which is fundamentally inconsistent with the very foundations of the fluctuating hydrodynamics formalism [22]. For instance, using the time Fourier transform of eqs.(2.33)-(2.35) and (2.38), it is easy to show that, at equilibrium ($R = 0$), one has

$$\frac{U_{\mathbf{k}}(\omega)_{eq}}{V_{\mathbf{k}}(\omega)_{eq}} = \frac{\left(\omega^2 - 4\pi^2 k_y^2\right)^2 + 16\,\pi^4\,\tilde{k}_x^2 k_y^2}{\left(\omega^2 - 4\pi^2 \tilde{k}_x^2\right)^2 + 16\,\pi^4\,\tilde{k}_x^2 k_y^2}\left[1 + O(\varepsilon^2)\right] , \tag{2.53}$$

where $U_{\mathbf{k}}(\omega)$ and $V_{\mathbf{k}}(\omega)$ are the space-time Fourier transforms of $\langle\, \delta u(\mathbf{r},t)\delta u(\mathbf{r}',0)\,\rangle$ and $\langle\, \delta v(\mathbf{r},t)\delta v(\mathbf{r}',0)\,\rangle$ respectively. On the other hand, the incompressibility assumption, eq. (2.9), implies

$$U_{\mathbf{k}}(\omega)_{inc} \,/\, V_{\mathbf{k}}(\omega)_{inc} = k_y^2 \,/\, \tilde{k}_x^2 , \tag{2.54}$$

where the subscript "*inc*" refers to incompressible fluids. It is seen that, except near the origin $\omega \approx 0$ (i.e., in the long-time limit), this result is clearly in contradiction with the correct equilibrium form, eq. (2.53). In particular, the equilibrium static autocorrelations are independent of the wave vector,

$$\langle \delta u_{\mathbf{k}}\, \delta u_{-\mathbf{k}} \rangle_{eq} = \langle \delta v_{\mathbf{k}}\, \delta v_{-\mathbf{k}} \rangle_{eq} = \mathcal{A} , \tag{2.55}$$

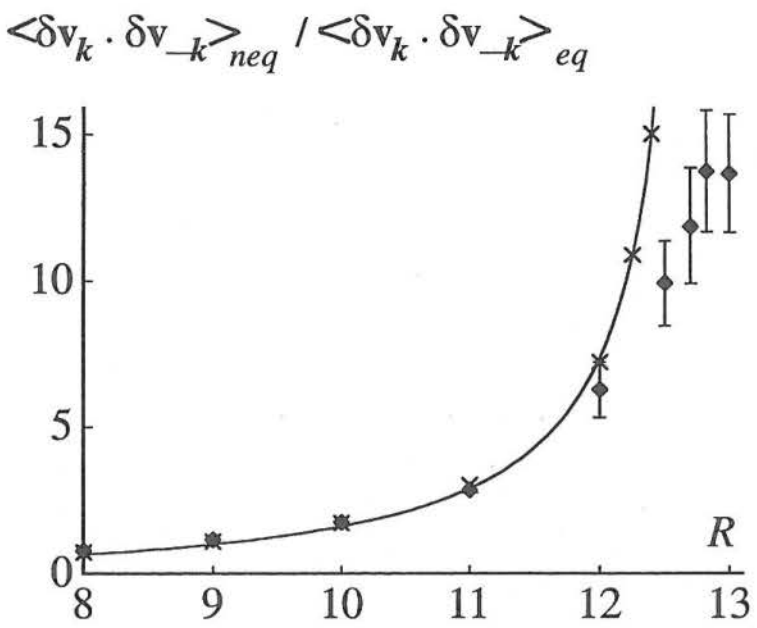

Figure 2.3: Fourier transform of the nonequilibrium part of the static velocity autocorrelation function, normalized by the corresponding equilibrium part, as a function of the Reynolds number. The solid curve represents the prediction based on the three-mode approximation, eq. (2.52), while crosses and diamonds correspond to numerical results obtained respectively by the simulation of linear and nonlinear Langevin equations, eqs. (2.30), (2.3) and (2.4). The parameters are as given in the caption of figure 2.2. The estimated statistical errors are about 15% for the last four data points.

whereas relation (2.54) leads to

$$\langle \delta u_{\mathbf{k}}\, \delta u_{-\mathbf{k}} \rangle_{inc} \,/\, \langle \delta v_{\mathbf{k}}\, \delta v_{-\mathbf{k}} \rangle_{inc} = \frac{k_y^2}{\tilde{k}_x^2} \,. \tag{2.56}$$

The situation is somewhat different for the *nonequilibrium* case. As we have shown in the previous section, to leading order in ε, both the scattering function and the sound regime of the velocity autocorrelation function assume their equilibrium forms, regardless of the value of the Reynolds number. The nonequilibrium constraints thus mainly affect the behavior of the fluid near the origin $\omega \approx 0$, i.e., the viscous regime. This result has an interesting consequence. It suggests that, as far as the nonequilibrium properties of the fluid are concerned, one may rely on the incompressibility assumption, eq. (2.9), since the compressibility of the fluid affects mainly the sound modes, which are well separated from the purely viscous modes, as long as ε is small. Rather complicated analytical calculations confirm the above arguments and lead to the following relation:

$$\frac{U_{\mathbf{k}}(\omega) - U_{\mathbf{k}}(\omega)_{eq}}{V_{\mathbf{k}}(\omega) - V_{\mathbf{k}}(\omega)_{eq}} = \frac{k_y^2}{\tilde{k}_x^2} \left[1 + O(\varepsilon^2 R^2)\right] \,. \tag{2.57}$$

Here both the numerator and the denominator on the left-hand side turn out to have Lorentzian shapes, sharply peaked around the origin (with a width of the order of ε), since the sound regime cancels out. Nevertheless, because of the presence of the equilibrium contributions, the relation (2.57) is still in contradiction with the incompressibility condition, eq. (2.54). There exist, however, two different situations where this objection can be ruled out:

(i) Near the origin, $\omega \approx 0$, where the fluid satisfies the incompressibility condition already at equilibrium, i.e., $U_{\mathbf{k}}(\omega)_{eq}\, \tilde{k}_x^2 \approx V_{\mathbf{k}}(\omega)_{eq}\, k_y^2$. Obviously, this situation concerns only the long-time behavior of the fluid. For instance, the static correlation functions, obtained from (2.57), obey

$$\frac{\langle \delta u_{\mathbf{k}}\, \delta u_{-\mathbf{k}} \rangle - \mathcal{A}}{\langle \delta v_{\mathbf{k}}\, \delta v_{-\mathbf{k}} \rangle - \mathcal{A}} = \frac{k_y^2}{\tilde{k}_x^2} \left[1 + O(\varepsilon^2 R^2)\right] \,, \tag{2.58}$$

which contradicts the incompressibility condition (2.54).

(ii) A more interesting situation concerns the behavior of the fluid near the instability, where it can be shown that in the limit $R \to R_c$ both the static and dynamic velocity correlation functions behave as $O\left[\left(R_c^2 - R^2\right)^{-1}\right]$,

cf. eq.(2.52). In other words, for R sufficiently close to R_c, equilibrium contributions become negligible, so that the fluid basically behaves as an incompressible one.

It should however be borne in mind that this appealing conclusion is based on the linearized Langevin equations (2.33)-(2.35) which are not valid near the convective instability. The study of the statistical properties of the system in the critical regime requires a nonlinear analysis of the fluctuating equations, which will be reported in the next chapter. Instead, here we resort to numerical analysis. More specifically, we have simulated the full nonlinear fluctuating hydrodynamic equations to obtain the ratio of the x and y components of the static velocity autocorrelation function for several values of the Reynolds number. The results are depicted in fig. 2.4 for $k_x = k_y = 1$, $a_r = 2$ (so that the expected value of this ratio for an incompressible fluid is 4). This is precisely what we observe, but only for values of $R \gtrsim 12.8$ (recall that $R_c \approx 12.87$), a domain which lies beyond the range of validity of the linearized hydrodynamic equations.

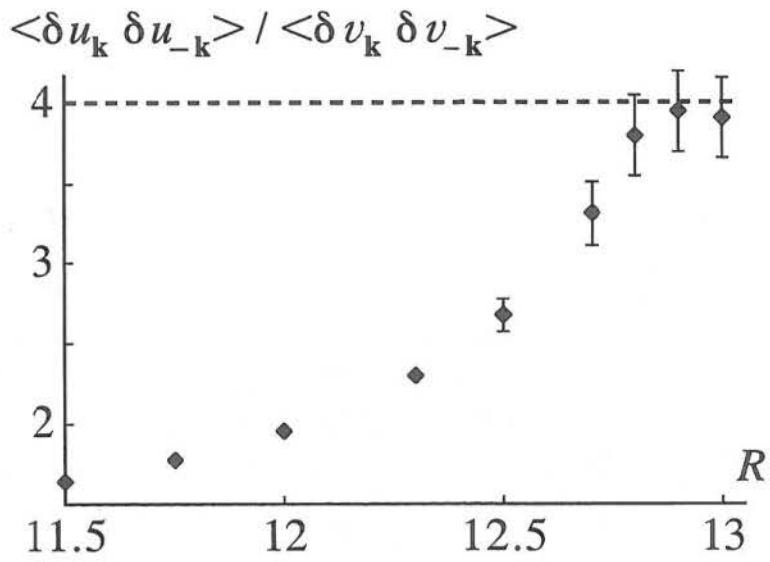

Figure 2.4: Ratio of x and y component of the velocity autocorrelation function in Fourier space, as a function of the Reynolds number. The parameters are $a_r = 2$, $\varepsilon = 10^{-2}$, $\mathcal{A} = 10^{-6}$ (defined by eq.(2.39)), $k_y = 1$, $k_x = 1$ (i.e., $\tilde{k}_x = 1/2$). The dashed line represents the expected ratio for an incompressible fluid, while the diamonds correspond to results obtained by the simulation of the full nonlinear Langevin equations, eqs. (2.3) and (2.4). The estimated statistical errors do not exceed 8%.

Chapter 3

The Nonlinear Regime

3.1 Incompressible Kolmogorov Flow in the Vicinity of the Instability

As was seen in the preceding chapter, the laminar flow (2.8) becomes unstable for a certain value R_c (eq. (2.27)) of the Reynolds number; above this threshold, rotating convective patterns emerge. In the vicinity of this threshold linear analysis fails, and one has to take into account the nonlinear effects that are present in the system. The study of the nonlinear equations that govern the evolution of a dynamical system is, in general, an extremely difficult task. It gets simplified in the vicinity of a bifurcation point; indeed, in this situation (as explained in Appendix B, see also [46, 47]), the system evolves in a restricted phase space, the *center manifold*, its dynamics then being determined by the *slow variables* (all the other *fast variables* following this evolution adiabatically). In the concrete case of Kolmogorov flow, there are two more elements that contribute to simplify the nonlinear analysis: (i) periodic boundary conditions, that enable the use of the Fourier transform formalism; (ii) the three-mode approximation (described in the previous chapter), that reduces the number of the relevant dynamical variables to the modes with $|k_y| = 0,\ 1$ (and, consistently, with $|k_x| < \max\{a_r, 2\}$).

To start with, let us consider the *incompressible deterministic* flow. As we saw in section 2.1, the incompressible system is completely described by the stream function $\psi(x, y, t)$ (eq. (2.10)), whose laminar stationary profile is given by (2.13) (we use the dimensionless variables introduced in

Section 2.1). The nonlinear evolution equation for $\delta\psi = \psi - \psi_{st}$ reads

$$\begin{aligned}\frac{\partial(\nabla^2\delta\psi)}{\partial t} = & - \sin(2\pi y)\frac{\partial(\nabla^2\delta\psi)}{\partial x} - 4\pi^2\sin(2\pi y)\frac{\partial\delta\psi}{\partial x} \\ & + R^{-1}\nabla^2(\nabla^2\delta\psi) - \frac{\partial\delta\psi}{\partial y}\frac{\partial(\nabla^2\delta\psi)}{\partial x} + \frac{\partial\delta\psi}{\partial x}\frac{\partial(\nabla^2\delta\psi)}{\partial y}\,.\end{aligned} \tag{3.1}$$

As in the linear case, we take the Fourier transform of this equation,

$$\begin{aligned}\frac{\partial\delta\psi_{k_x,k_y}}{\partial t} = & -4\pi^2 R^{-1}(\tilde{k}_x^2 + {k_y}^2)\delta\psi_{k_x,k_y} \\ & +\pi\tilde{k}_x\left[\delta\psi_{k_x,k_y+1} - \delta\psi_{k_x,k_y-1}\right] \\ & +2\pi\frac{\tilde{k}_x k_y}{\tilde{k}_x^2 + {k_y}^2}\left[\delta\psi_{k_x,k_y+1} + \delta\psi_{k_x,k_y-1}\right] \\ & - \frac{4\pi^2}{\tilde{k}_x^2 + k_y^2}\sum_{k'_x,k'_y=-\infty}^{\infty}(\tilde{k}_x k'_y - \tilde{k}'_x k_y)(\tilde{k'}_x^2 + {k'}_y^2)\delta\psi_{k'_x,k'_y}\delta\psi_{k_x-k'_x,k_y-k'_y}.\end{aligned} \tag{3.2}$$

We proceed to an initial truncation of this infinite set of coupled equations, by using the *three-mode approximation*, i.e., we assume that $\delta\psi_{k_x,k_y} \approx 0$ for $|k_y| \geq 2$. Then, using the transformations $\mathbf{T}(k_x)$ and its inverse, $\mathbf{T}^{-1}(k_x)$ (eqs.(2.22),(2.1)), one can express the truncated set of equations in terms of the normal modes $\delta\phi_i(k_x, t)$ $(i = 1, 2, 3)$ [1] as

$$\frac{\partial\delta\phi_i(k_x, t)}{\partial t} = \lambda_i(k_x)\,\delta\phi_i(k_x, t) + \Phi_i(k_x, t) \quad (i = 1, 2, 3) \tag{3.3}$$

[1]Note that, in view of the relations $\delta\psi_{-k_x,-k_y} = \delta\psi^*_{k_x,k_y}$ (where * denotes the complex conjugate), the modes $\delta\phi_i(-k_x, t)$ and $\delta\phi_i(k_x, t)$ are related according to

$$\begin{aligned}\delta\phi_1(-k_x, t) &= -\delta\phi_1^*(k_x, t)\,, \\ \delta\phi_2(-k_x, t) &= -\delta\phi_2^*(k_x, t)\,, \\ \delta\phi_3(-k_x, t) &= +\delta\phi_3^*(k_x, t)\,.\end{aligned}$$

where the $\Phi_i(k_x,\, t)$'s are infinite sums (with respect to k'_x) of second-order polynomials of the type $\delta\phi_p(k'_x,\, t)\delta\phi_l(k_x - k'_x,\, t)$ $(p, l = 1, 2, 3)$. Consistent with the three-mode approximation for k_y, one can now proceed to a truncation of (3.3) to modes with $|k_x| < \max\{a_r,\, 2\}$. But the system can be simplified further by taking into account the following: Close to the bifurcation point $R \approx R_c$, the mode $\delta\phi_1(k_x = 1)$ and its complex-conjugate $\delta\phi_1^*(k_x = 1)$ exhibit a *critical slowing down* since $\lambda_1(k_x = 1) \approx 0$. *All the other modes* represent the *fast modes* (in the terminology of the method of adiabatic elimination of variables, see Appendix B). On the slow time scale $t \sim O\left[\lambda_1(k_x = 1)^{-1}\right]$, they can then be considered as stationary, their time dependence arising mainly through $\delta\phi_1(k_x = 1,\, t)$ and its complex conjugate. Indeed, setting $\partial\delta\phi_1(k_x = 0,\, t)/\partial t \approx \partial\delta\phi_1(k_x \geq 2,\, t)/\partial t \approx \approx \partial\delta\phi_2(k_x,\, t)/\partial t \approx \partial\delta\phi_3(k_x,\, t)/\partial t \approx 0$, one can express the fast modes in terms of the slow mode, $\delta\phi_1(k_x = 1,\, t)$ and its complex-conjugate $\delta\phi_1{}^*(k_x = 1,\, t)$. If we now insert the expressions thus obtained for the fast modes into the evolution equations of the slow modes, we obtain a closed nonlinear equation for the latter. In practice, however, such a calculation is only possible close to the the bifurcation point, where the amplitude of $\delta\phi_1(k_x = 1,\, t)$ is supposed to approach zero as $R \to R_c$. In fact, there exist other types of transitions, such as the one arising in the Van der Pol equation, where the amplitude of the solution above the instability does not vanish as one approaches the critical point [48]. Detailed analysis shows that this is not the case here (i.e., $|\delta\phi_1(k_x = 1,\, t)| \to 0$ as $R \to R_c$), so that we can limit ourselves to *lowest* orders in $|\delta\phi_1(k_x = 1,\, t)|$.

Correspondingly, the infinite set (3.3) reduces finally to [2]

$$\begin{aligned}
\frac{\partial\delta\phi_1(k_x = 1,\, t)}{\partial t} &= \lambda_1(k_x = 1)\delta\phi_1(k_x = 1,\, t) \\
&- \alpha_1\left[\delta\phi_3(k_x = 0,\, t) + \delta\phi_3(k_x = 0,\, t)\right]\delta\phi_1(k_x = 1,\, t) \\
&- \beta_1\,\delta\phi_3(k_x = 2,\, t)\,\delta\phi_1^*(k_x = 1,\, t)\ ,
\end{aligned}$$

$$\begin{aligned}
\frac{\partial\delta\phi_3(k_x = 0,\, t)}{\partial t} &= \lambda_3(k_x = 0)\delta\phi_3(k_x = 0,\, t) \\
&+ \alpha_2\,\delta\phi_1(k_x = 1,\, t)\delta\phi_1^*(k_x = 1,\, t) \approx 0
\end{aligned}$$

[2] For uniformity, we use the notations

$$\delta\phi_3(k_x = 0,\, t) \equiv \delta\psi_{k_x=0,\, k_y=1} \qquad \text{and} \qquad \lambda_3(k_x = 0) \equiv -4\pi^2 R^{-1}\ .$$

$$\frac{\partial \delta\phi_3(k_x=2,\,t)}{\partial t} = \lambda_3(k_x=2)\delta\phi_3(k_x=2,\,t) - \beta_2\,\delta\phi_1^2(k_x=1,\,t) \approx 0\ ,$$

(3.4)

and their complex conjugates. These equations are valid up to terms of order $|\delta\phi_1(k_x=1,\,t)|^5$. Here the α's and β's are given, to leading order in $|R/R_c - 1|$, by

$$\begin{aligned}
\alpha_1 &= \frac{4\sqrt{2}\pi^2\sqrt{a_r^2-1}}{a_r(a_r^2+2)}\ ,\\
\beta_1 &= \frac{4\sqrt{2}\pi^2(a_r^2-3)}{a_r(a_r^2+2)\sqrt{a_r^2-1}}\ ,\\
\alpha_2 &= \frac{2\sqrt{2}\pi^2(a_r^2+1)}{a_r\sqrt{a_r^2-1}(a_r^2+2)^2)}\ ,\\
\beta_2 &= \frac{2\sqrt{2}\pi^2 a_r(a_r^2+1)}{(a_r^2+4)(a_r^2+2)^2\sqrt{a_r^2-1}}\ .
\end{aligned}$$

(3.5)

Finally, one obtains the so-called *normal form* or *amplitude equation* for the slow mode,

$$\begin{aligned}
\frac{\partial \delta\phi_1(k_x=1,\,t)}{\partial t} &= \lambda\,\delta\phi_1(k_x=1,\,t)\\
&\quad -\gamma|\delta\phi_1(k_x=1,\,t)|^2\,\delta\phi_1(k_x=1,\,t)\,\left[1 + O(|\delta\phi_1(k_x=1,\,t)|^2)\right]\ ,
\end{aligned}$$

(3.6)

where

$$\lambda \equiv \lambda_1(k_x=1) = \frac{4\pi^2}{R_c}\,\frac{a_r^2+1}{a_r^2(a_r^2+2)}\left(1 - \frac{R_c^2}{R^2}\right) + O\left(|R/R_c - 1|^2\right)\ ,$$

(3.7)

and γ is a positive constant which, to leading order in $|R/R_c - 1|$, is given by

$$\gamma = 8\sqrt{2}\,\pi^3\,\frac{(a_r^6 + 17\,a_r^4 + 16\,a_r^2 - 32)\,(a_r^2+1)^2}{a_r^3\,(a_r^2-1)^{3/2}\,(a_r^2+2)^3\,(a_r^2+4)^2}\ . \qquad (3.8)$$

Above the bifurcation point $R > R_c$ ($\lambda > 0$), the amplitude equation (3.6) admits two stable stationary solutions, corresponding to the rotation sense of the streamlines of the fluid:

$$\delta\phi_1(k_x = 1)^{\pm} = \pm\sqrt{\frac{\lambda}{\gamma}}\exp(i\,\theta_0)\,, \tag{3.9}$$

where θ_0 is a constant whose value depends on the initial conditions. The fact that the stationary solution still depends on the initial conditions simply reflects the Galilean invariance in the x-direction which results from the periodic boundary conditions imposed on the system. Using relation (3.9), one can compute the explicit form of the fast modes for $k_x = 0, \pm 1, \pm 2$. Applying the inverse transform $\mathbf{T}^{-1}(k_x)$ (eq. (2.1)) to the vector $\delta\boldsymbol{\phi}^{\pm}(k_x) = (\delta\phi_1^{\pm}, \delta\phi_2^{\pm}, \delta\phi_3^{\pm})$ and taking its inverse Fourier transform, one gets the explicit expression for the stream function in real space. To $O(R/R_c - 1)$, we obtain

$$\begin{aligned}
\psi_{st}^{\pm}(x,\,y) \;=\; & -\frac{1}{2\,\pi}\cos(2\,\pi\,y) \pm \frac{R_c\,a_r}{2\,\pi\,(a_r^2+2)}\,|\delta\phi_1|\left[\cos(2\pi x/a_r - \theta_0)\right. \\
& \left. -\frac{4\,\pi}{a_r\,R_c}\sin\left(2\pi x/a_r - \theta_0\right)\sin(2\pi y)\right] \\
& + \frac{R_c^2}{2\,\pi\,(a_r^2+2)^2}\,|\delta\phi_1|^2\left[1 - \right. \\
& \left. -\frac{a_r^4}{(a_r^2+4)^2}\cos\left(4\pi x/a_r - 2\theta_0\right)\right]\cos(2\pi y)
\end{aligned} \tag{3.10}$$

where we have set $|\delta\phi_1| \equiv |\delta\phi_1(k_x = 1)^{\pm}|$. Using relations (2.10), the velocity profiles can now be obtained in a straightforward manner. We find

$$\begin{aligned}
u_{st}^{\pm}(x,\,y) \;=\; & \sin(2\pi y) \mp \frac{4\,\pi}{(a_r^2+2)}\,|\delta\phi_1|\,\sin\left(2\pi x/a_r - \theta_0\right)\cos(2\pi y) \\
& - \frac{R_c(k_x=1)^2}{(a_r^2+2)^2}\,|\delta\phi_1|^2\left[1 - \right. \\
& \left. -\frac{a_r^4}{(a_r^2+4)^2}\cos\left(4\pi x/a_r - 2\theta_0\right)\right]\sin(2\pi y)\,.
\end{aligned} \tag{3.11}$$

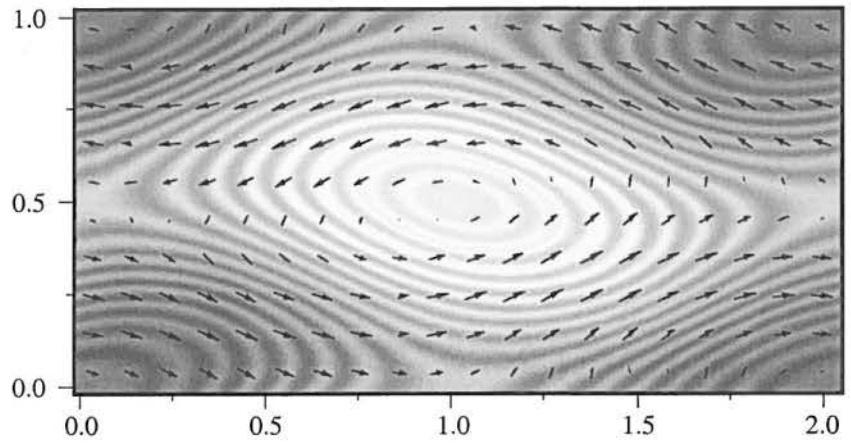

Figure 3.1: Density plot of the stream function, eq. (3.10), for $R = 15$, $a_r = 2$ and $\theta_0 = 0$. For the sake of clarity, a vector plot of the velocity field is also included.

$$v_{st}^{\pm}(x,\, y) = \pm \frac{R_c(k_x = 1)}{(a_r^2 + 2)} \, |\delta\phi_1(k_x = 1)| \, \Bigg[\sin\left(2\pi x/a_r - \theta_0\right) + \frac{4\,\pi}{a_r \, R_c(k_x = 1)} \cos\left(2\pi x/a_r - \theta_0\right) \sin(2\pi y) \Bigg] - \frac{2\, R_c^2 \, a_r^3}{(a_r^2 + 2)^2 \, (a_r^2 + 4)^2} |\delta\phi_1(k_x = 1)|^2 \, \sin\left(4\pi x/a_r - 2\theta_0\right) \cos(2\pi y) \, . \tag{3.12}$$

A density plot of the stream function (3.10) is given in figure 3.1 for $R = 15$, $a_r = 2$ and $\theta_0 = 0$ where, for the sake of clarity, a vector plot of the velocity field is also included. We note that the flow has an ABC-like topology [49], with closed streamlines (eddies), open ones and separatrices between them.

We recall that the above results rest on the three-mode approximation. To check the validity of this basic assumption, we have solved numerically the incompressible nonlinear hydrodynamic equations for $a_r = 2$, using standard techniques [50]. Figure 3.2 compares contour plots of the stream function

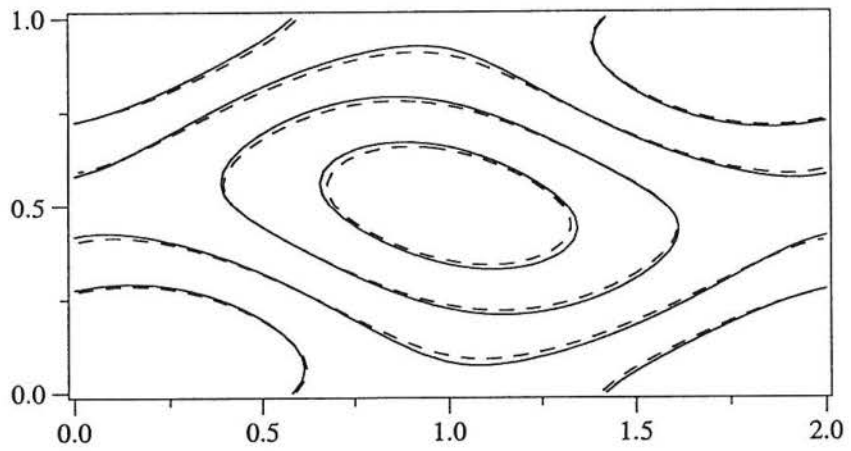

Figure 3.2: Stationary state contour plot of the stream function for $R = 15$, $a_r = 2$ and $\theta_0 = 0$. The full and dashed lines correspond to the theoretical prediction (eq. (3.10)) and numerical results, respectively. The discrepancy is less than 5%.

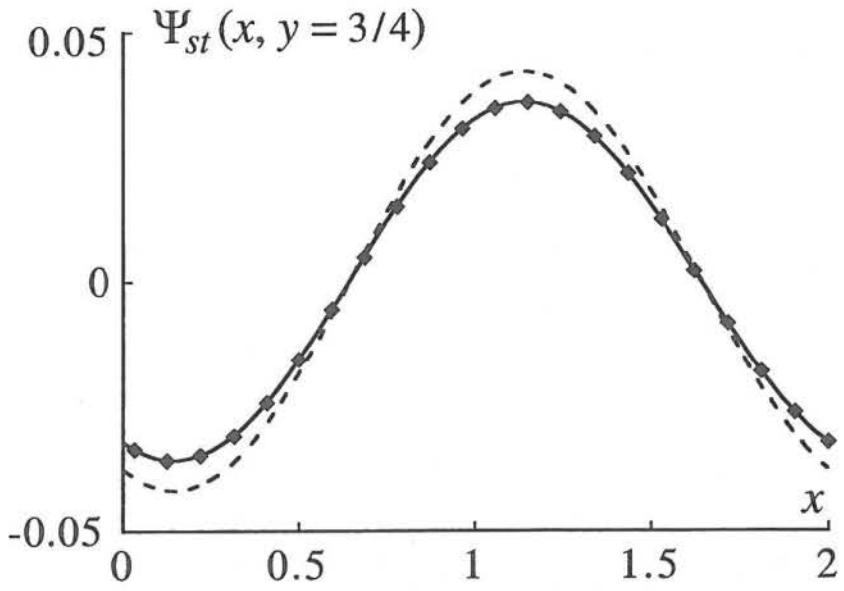

Figure 3.3: Horizontal profile of the stationary state stream function, with $y = 3/4$, as a function of the coordinate x for $R = 13$, $a_r = 2$ and $\theta_0 = 0$. The full and dashed lines represent theoretical predictions obtained by using an estimation of the critical Reynolds number based on five-mode (eq. (2.28)) and three-mode (eq. (2.27)) approximations, respectively. The diamonds correspond to numerical results.

thus obtained with its corresponding theoretical counterpart, eq. (3.10), for $R = 15$. Given the relatively large distance from the critical point ($R/R_c - 1 \approx 17\%$), the agreement is much better than expected, the discrepancy remaining below 5%. Surprisingly, the agreement does not improve as we consider smaller values of the Reynolds number. This is shown in figure 3.3, where both the numerical and theoretical horizontal profiles of the stream function (at a fixed value of the vertical coordinate, $y = 3/4$) are depicted for a value of the Reynolds number $R = 13$. The discrepancy now exceeds 10%. To understand the origin of this unexpected behavior, we note that the value of the critical Reynolds number that we have used to evaluate the stream function (eq. (3.10)) is based on the three-mode approximation (eq.(2.27)). As shown before, the accuracy of the value of R_c in the latter is about 0.4%, which is acceptable so long as the distance from the critical point ($R/R_c - 1$) remains much larger than 0.4%. But when $R = 13$, the distance from the critical point is about 1%, which is of the same order as the accuracy of R_c. This explains the relatively larger discrepancy observed in figure 3.3. To overcome this difficulty, one has to compute a more accurate value of the critical Reynolds number, based for instance on the five-mode approximation. As is well known [47], this correction concerns only the value of R_c, and in no way compromises the validity of the amplitude equation (3.6) and its corresponding solution, eq.(3.10). This is illustrated in figure 3.3, where excellent agreement with the numerical result is obtained if we use $R_c^{(5)}(k_x = 1)$ as the critical Reynolds number. For smaller values of R, one can numerically compute the value of R_c to the accuracy required and use it as an input in the amplitude equation (3.6).

So far, we have limited ourselves to the analysis of the deterministic equations, i.e., we have neglected possible noise terms. In principle, there is no difficulty in taking into account the noise contributions as well, except that the amplitudes of the field variables $(\delta\phi_1, \delta\phi_2, \delta\phi_3)$ are now directly related to the amplitude $\mathcal{B}$ of the noise, which is typically a small parameter. The relevant fast variables are $O(\mathcal{B}^{1/2})$, whereas the slow variables $\delta\phi_1(k_x = 1, t)$, $\delta\phi_1^*(k_x = 1, t)$ are $O(\mathcal{B}^{1/4})$. Keeping this in mind, one can repeat all the calculations above in the presence of noise. A detailed discussion of the stochastic adiabatic elimination of the fast variables is given in

Appendix B, following [48]. To leading order in $|\delta\phi_1(k_x = 1,\, t)|$, one finds

$$\begin{aligned}
\frac{\partial \delta\phi_1(k_x = 1,\, t)}{\partial t} &= \lambda\, \delta\phi_1(k_x = 1,\, t) \\
&- \gamma\, |\delta\phi_1(k_x = 1,\, t)|^2\, \delta\phi_1(k_x = 1,\, t) + \xi(t)\,, \\
\\
\frac{\partial \delta\phi_1^*(k_x = 1,\, t)}{\partial t} &= \lambda\, \delta\phi_1^*(k_x = 1,\, t) \\
&- \gamma\, |\delta\phi_1(k_x = 1,\, t)|^2\, \delta\phi_1^*(k_x = 1,\, t) + \xi^*(t)\,.
\end{aligned} \tag{3.13}$$

The functions $\xi(t)$ and its complex-conjugate $\xi^*(t)$ are Gaussian white noises with zero means and correlations given by

$$\begin{aligned}
\langle \xi(t)\, \xi(t') \rangle &= 0\,, \\
\langle \xi(t)\, \xi^*(t') \rangle &= \mathcal{B}\, \delta(t - t')\,,
\end{aligned} \tag{3.14}$$

where

$$\mathcal{B} = \frac{4\, k_B\, T_0\, a_r^2}{M\, u_0^2\, R} \Big[1 + O\left(|R/R_c - 1|\right) \Big]\,, \tag{3.15}$$

and M is the total mass of the system,

$$M = a_r \rho_0 L_y^2\,. \tag{3.16}$$

The results derived in this section are based explicitly on the incompressibility assumption. However, as discussed in the Introduction, this assumption is inconsistent with the very foundations of the fluctuating hydrodynamic formalism. On the other hand, we have presented in the previous chapter (Section 2.3) numerical evidence that in the vicinity of the bifurcation point the system behaves basically as an incompressible fluid. We therefore expect that the Langevin equation (3.13) should remain valid for R sufficiently close to R_c. We shall clarify this important issue in the next section.

3.2 Nonlinear Fluctuations in Compressible Flow

Let us now consider the compressible hydrodynamic equations (2.3)-(2.5) for which we need to specify an equation of state. Since the system is isothermal, we simply set

$$p = c_s^2 \rho \,, \tag{3.17}$$

where c_s is the isothermal speed of sound. As in the previous section, we start with the linearized (fluctuating) hydrodynamic equations around the reference state $\{\rho_0, \mathbf{v}_{st}\}$, where $\mathbf{v}_{st}$ is given by eq.(2.8). Setting

$$\begin{aligned} \rho &= \rho_0 + \delta\rho \,, \\ \mathbf{v} &= \mathbf{v}_{st} + \delta\mathbf{v} \,, \end{aligned} \tag{3.18}$$

and scaling lengths by L_y, time by L_y/c_s, $\delta\rho$ by ρ_0 and $\delta\mathbf{v}$ by the speed of sound c_s, one obtains the dimensionless linear fluctuating equations (2.33)-(2.35) in Fourier space (Section 2.2). We recall that R is the Reynolds number (defined in eq.(2.12)),

$$\varepsilon = \frac{\eta}{\rho_0 \, c_s \, L_y} \,, \tag{3.19}$$

and

$$\alpha = \zeta/\eta \,. \tag{3.20}$$

The functions F_{k_x,k_y} and G_{k_x,k_y} are Fourier components of the noise terms, with covariances given by eqs.(2.38) and (2.39).

For the sake of clarity, we first focus on the *deterministic behavior*, i.e., we drop for the moment the noise contributions in the evolution equations (2.33)-(2.35). Furthermore, we shall limit ourselves to the three-mode approximation, i.e., we shall neglect the modes with $|k_y| \geq 2$, for the very same reasons that we have discussed for the incompressible case. With these assumptions, eqs.(2.33)-(2.35) reduce to a system of nine coupled equations. It can then be checked that the change of variables

$$\begin{aligned} \delta\rho_{k_x}^{\pm}(t) &= \delta\rho_{k_x,1}(t) \pm \delta\rho_{k_x,-1}(t) \\ \delta u_{k_x}^{\pm}(t) &= \delta u_{k_x,1}(t) \pm \delta u_{k_x,-1}(t) \\ \delta v_{k_x}^{\pm}(t) &= \delta v_{k_x,1}(t) \pm \delta v_{k_x,-1}(t) \end{aligned} \tag{3.21}$$

leads to a partial diagonalization of the evolution equations, i.e., the equations for the variables $\{\delta\rho_{k_x,0},\ \delta\rho^-_{k_x},\ \delta u_{k_x,0},\ \delta u^-_{k_x},\ \delta v^+_{k_x}\}$ decouple from the rest. Furthermore, their associated eigenvalues turn out to remain strictly negative, regardless of the value of the Reynolds number R, so that they are not relevant for the onset of the convective instability. We therefore focus on the remaining four variables $\left\{\delta\rho^+_{k_x},\ \delta u^+_{k_x},\ \delta v^-_{k_x},\ \delta v_{k_x,0}\right\}$. Defining the vector

$$\delta\mathbf{h}_{k_x}(t) \equiv \begin{pmatrix} \delta\rho^+_{k_x} \\ \delta u^+_{k_x} \\ \delta v^-_{k_x} \\ \delta v_{k_x,0} \end{pmatrix}, \tag{3.22}$$

one readily finds

$$\frac{\partial}{\partial t}\delta\mathbf{h}_{k_x}(t) \;=\; \mathbf{C}(k_x)\cdot\delta\mathbf{h}_{k_x}(t)\,, \tag{3.23}$$

where the matrix $\mathbf{C}(k_x)$ is given by

$$\mathbf{C}(k_x) \;=$$

$$\begin{pmatrix} 0 & 2\pi i\tilde{k}_x & 2\pi i & 0 \\ 2\pi i\tilde{k}_x & -4\pi^2\varepsilon(1+\alpha\tilde{k}_x^2+\tilde{k}_x^2) & -4\pi^2\varepsilon\alpha\tilde{k}_x & -2\pi\varepsilon R \\ 2\pi i & -4\pi^2\varepsilon\alpha\tilde{k}_x & -4\pi^2\varepsilon(1+\alpha+\tilde{k}_x^2) & -2\pi\varepsilon\tilde{k}_x R \\ 0 & 0 & \pi\varepsilon\tilde{k}_x R & -4\pi^2\varepsilon\tilde{k}_x^2 \end{pmatrix}. \tag{3.24}$$

The analysis can be simplified to some extent by recalling that the parameter ε is small within the limits of validity of the hydrodynamic regime [43]. Furthermore, we only consider strictly sub-sonic flows, so that we restrict the analysis to a parameter domain where

$$\varepsilon \ll 1 \quad \text{and} \quad \varepsilon R = u_0/c_s \ll 1. \tag{3.25}$$

Accordingly, we evaluate the eigenvalues of the matrix $\mathbf{C}(k_x)$ perturbatively,

$$\tilde{\lambda}(k_x) \;=\; \tilde{\lambda}^{(0)}(k_x) \;+\; \varepsilon\,\tilde{\lambda}^{(1)}(k_x) \;+\; \ldots \tag{3.26}$$

After some algebra, one finds, to $O(\varepsilon^2)$,

$$\tilde{\lambda}_1(k_x) = \varepsilon \left[-2\,\pi^2(1 + 2\tilde{k}_x^2) + \pi \sqrt{4\,\pi^2 + 2\,R^2\,\tilde{k_x}^2\,(1 - \tilde{k}_x^2)/(1 + \tilde{k}_x^2)} \right] ,$$

$$\tilde{\lambda}_2(k_x) = \varepsilon \left[-2\,\pi^2(1 + 2\tilde{k}_x^2) - \pi \sqrt{4\,\pi^2 + 2\,R^2\,\tilde{k_x}^2\,(1 - \tilde{k}_x^2)/(1 + \tilde{k}_x^2)} \right] ,$$

$$\begin{aligned} \tilde{\lambda}_3(k_x) = &\quad 2\,\pi\,i \sqrt{1 + \tilde{k}_x^2} - 2\,\pi^2(\alpha + 1)\,\varepsilon(1 + \tilde{k}_x^2) , \\ \tilde{\lambda}_4(k_x) = &\quad -2\,\pi\,i \sqrt{1 + \tilde{k}_x^2} - 2\,\pi^2(\alpha + 1)\,\varepsilon(1 + \tilde{k}_x^2) . \end{aligned} \tag{3.27}$$

The eigenvalues $\tilde{\lambda}_1(k_x)$ and $\tilde{\lambda}_2(k_x)$ correspond to dissipative viscous modes, while $\tilde{\lambda}_3(k_x)$ and $\tilde{\lambda}_4(k_x)$ are related to the propagation of damped sound waves. It can then easily be checked that the real parts of $\tilde{\lambda}_2(k_x)$, $\tilde{\lambda}_3(k_x)$ and $\tilde{\lambda}_4(k_x)$ are always negative, whereas there exists a critical value of the Reynolds number, given by

$$R_c(k_x) = 2\sqrt{2}\,\pi \frac{1 + \tilde{k}_x^2}{\sqrt{1 - \tilde{k}_x^2}} \quad (0 < \tilde{k}_x^2 < 1) , \tag{3.28}$$

for which $\tilde{\lambda}_1(k_x)$ vanishes. This yields the limit of stability of the corresponding mode.

Remarkably, the above expression of the critical Reynolds number is identical to the one obtained in the incompressible case, cf. eq.(2.27). In fact, detailed analysis shows that the relation (3.28) is exact, i.e., it is independent of ε, at least within the framework of the three-mode approximation. On the other hand, if the modes $k_y = \pm 2$ are taken into account as well, a lengthy calculation (using Maple) leads to

$$R_c^{(5)}(k_x) = R_c(k_x) \left[1 + \frac{\tilde{k}_x^4\,(\tilde{k}_x^2 + 3)}{2\,(\tilde{k}_x^2 + 4)^2\,(\tilde{k}_x^2 - 1)} \right]^{-1/2} + O\left((u_0/c_s)^2\right) \quad (0 < \tilde{k}_x^2 < 1) . \tag{3.29}$$

This is again equivalent to the corresponding result obtained for the incompressible case (eq. (2.28)), the correction being $O(\varepsilon^2)$. In particular, the

first mode to become unstable corresponds to $|k_x| = 1$, provided $a_r > 1$.

We note that the matrix $\mathbf{C}$ is singular for $k_x = 0$, when one of its eigenvectors vanishes. This is the mode $\delta v_{0,0}$, which is identically zero because of linear momentum conservation. Accordingly, in what follows we shall concentrate on the case $k_x \neq 0$, looking for a similarity transformation $\mathbf{S}(k_x)\mathbf{C}(k_x)\mathbf{S}^{-1}(k_x)$ which diagonalizes the matrix $\mathbf{C}(k_x)$. For consistency, here again we perform the calculations perturbatively, i.e., we expand $\mathbf{S}(k_x)$ in powers of ε:

$$\mathbf{S}(k_x) = \mathbf{S_0}(k_x) + \varepsilon\,\mathbf{S_1}(k_x) + \ldots \tag{3.30}$$

Note that this method constitutes an alternative to the multiple time scale perturbation theory [51] that was generalized by Schmitz and Cohen [20] in order to study the Bénard instability in a compressible fluid.

Since the explicit form of the eigenvalues is known up to $O(\varepsilon^2)$, we only need to evaluate $\mathbf{S}(k_x)$ (and its inverse $\mathbf{S}^{-1}(k_x)$) up to the same order. Despite this simplification, the general expression of $\mathbf{S}(k_x)$ is quite involved:

$$\mathbf{S}(k_x) =$$

$$\begin{pmatrix} \dfrac{\varepsilon(2\pi+W)}{4\pi\tilde{k}_x(1+\tilde{k}_x^2)} & \dfrac{i}{2\pi(1+\tilde{k}_x^2)} & -\dfrac{\tilde{k}_x}{2\pi(1+\tilde{k}_x^2)} & -\dfrac{i(2\pi+W)}{2\pi R\tilde{k}_x^2} \\ \dfrac{\varepsilon(2\pi-W)}{4\pi\tilde{k}_x(1+\tilde{k}_x^2)} & \dfrac{i}{2\pi(1+\tilde{k}_x^2)} & -\dfrac{\tilde{k}_x}{2\pi(1+\tilde{k}_x^2)} & -\dfrac{i(2\pi-W)}{2\pi R\tilde{k}_x^2} \\ -2\pi i V & -2\pi i\tilde{k}_x & -2\pi i & \dfrac{4\pi\varepsilon R\tilde{k}_x}{\sqrt{1+\tilde{k}_x^2}} \\ 2\pi i U & -2\pi i\tilde{k}_x & -2\pi i & -\dfrac{4\pi\varepsilon R\tilde{k}_x}{\sqrt{1+\tilde{k}_x^2}} \end{pmatrix} . \tag{3.31}$$

Its inverse, also to $O(\varepsilon^2)$, is given by

$$\mathbf{S}^{-1}(k_x) =$$

$$\begin{pmatrix} \frac{2\pi\varepsilon R^2\tilde{k}_x^3}{W(1+\tilde{k}_x^2)} & -\frac{2\pi\varepsilon R^2\tilde{k}_x^3}{W(1+\tilde{k}_x^2)} & \frac{i}{4\pi\sqrt{1+\tilde{k}_x^2}} & -\frac{i}{4\pi\sqrt{1+\tilde{k}_x^2}} \\ \frac{i\pi(2\pi-W)}{W} & -\frac{i\pi(2\pi+W)}{W} & \frac{i\tilde{k}_x U}{4\pi(1+\tilde{k}_x^2)^{3/2}} & \frac{ik_x V}{4\pi(1+\tilde{k}_x^2)^{3/2}} \\ -\frac{i\pi\tilde{k}_x(2\pi-W)}{W} & \frac{i\pi\tilde{k}_x(2\pi+W)}{W} & \frac{iU}{4\pi(1+\tilde{k}_x^2)^{3/2}} & \frac{iV}{4\pi(1+\tilde{k}_x^2)^{3/2}} \\ \frac{i\pi R\tilde{k}_x^2}{W} & -\frac{i\pi R\tilde{k}_x^2}{W} & \frac{\varepsilon R\tilde{k}_x}{8\pi(1+\tilde{k}_x^2)^{3/2}} & -\frac{\varepsilon R\tilde{k}_x}{8\pi(1+\tilde{k}_x^2)^{3/2}} \end{pmatrix} . \tag{3.32}$$

Here

$$\begin{aligned} U &= \sqrt{1+\tilde{k}_x^2} + i\pi\varepsilon(\alpha+1)(1+\tilde{k}_x^2) , \\ V &= \sqrt{1+\tilde{k}_x^2} - i\pi\varepsilon(\alpha+1)(1+\tilde{k}_x^2) , \end{aligned}$$

and

$$W = \sqrt{4\pi^2 + 2\tilde{k}_x^2 \frac{1-\tilde{k}_x^2}{1+\tilde{k}_x^2} R^2} \quad . \tag{3.33}$$

We are interested in the nonlinear evolution equation near the instability threshold. The calculations follow exactly the same steps as in the incompressible case (Section 3.1). But, of course, they are even more involved and lengthy than in the previous instance. We will only give a brief sketch of the intermediate steps. We start by taking the Fourier transform of the fluctuating hydrodynamic equations (2.3)-(2.5). Using the change of variables (3.18) and (3.21), we derive the nonlinear fluctuating equations for $\delta\mathbf{h}_{k_x}$. We then apply the transformation $\mathbf{S}(k_x)$ to the latter, obtaining an infinite set of coupled nonlinear equations for the variables $\left(\delta\tilde{\phi}_1(k_x), \delta\phi_2(\tilde{k}_x), \delta\phi_3(\tilde{k}_x), \delta\phi_4(\tilde{k}_x)\right) \equiv \delta\tilde{\boldsymbol{\phi}}_{k_x}(t) = \mathbf{S}(k_x) \cdot \delta\mathbf{h}_{k_x}$. Close to the bifurcation point $R \approx R_c$, the modes $\delta\tilde{\phi}_1(k_x = 1)$ and its complex conjugate exhibit a critical slowing down, since $\tilde{\lambda}_1(k_x = 1) \approx 0$. We can therefore proceed to an adiabatic elimination of the other fast modes $\delta\phi_1(k_x \neq \pm 1)$, $\delta\tilde{\phi}_2, \delta\tilde{\phi}_3$, and $\delta\tilde{\phi}_4$, limiting ourselves to leading order in $|\delta\tilde{\phi}_1(k_x = 1)|$ (see the paragraph preceding eq. (3.13)). The final result is a set of two coupled Langevin equations for the slow mode $\delta\tilde{\phi}_1(k_x = 1, t)$ and its complex

conjugate $\delta\tilde{\phi}_1^*(k_x = 1,\, t)$:

$$\begin{aligned}
\frac{\partial \delta\tilde{\phi}_1(k_x = 1,\, t)}{\partial t} &= \tilde{\lambda}\, \delta\tilde{\phi}_1(k_x = 1,\, t) \\
&- \tilde{\gamma} |\delta\tilde{\phi}_1(k_x = 1,\, t)|^2\, \delta\tilde{\phi}_1(k_x = 1,\, t) + \tilde{\xi}(t) \\
\frac{\partial \delta\tilde{\phi}_1^*(k_x = 1,\, t)}{\partial t} &= \tilde{\lambda} \delta\tilde{\phi}_1^*(k_x = 1,\, t) \\
&- \tilde{\gamma} |\delta\tilde{\phi}_1(k_x = 1,\, t)|^2\, \delta\tilde{\phi}_1^*(k_x = 1,\, t) + \tilde{\xi}^*(t)\ ,
\end{aligned} \tag{3.34}$$

with

$$\tilde{\lambda} = \tilde{\lambda}_1(k_x = 1) = \lambda\, \frac{u_0}{c_s}\, \left[1 + O(u_0^2/c_s^2)\right] \approx 4\pi^2 \varepsilon\, \frac{a_r^2 + 1}{a_r^2 (a_r^2 + 2)} \left(1 - \frac{R_c^2}{R^2}\right) \tag{3.35}$$

and

$$\tilde{\gamma} = \gamma\, \frac{c_s}{u_0}\, \left[1 + O(u_0^2/c_s^2)\right] \approx \frac{\gamma}{\varepsilon\, R}\ . \tag{3.36}$$

Here λ and γ are given by eqs. (3.7) and (3.8), respectively. The functions $\tilde{\xi}(t)$ and its complex-conjugate $\tilde{\xi}^*(t)$ are Gaussian white noises with zero means and correlations given by

$$\begin{aligned}
\left\langle \tilde{\xi}(t)\, \tilde{\xi}(t') \right\rangle &= 0\,, \\
\left\langle \tilde{\xi}(t)\, \tilde{\xi}^*(t') \right\rangle &= \tilde{\mathcal{B}}\, \delta(t - t')\,,
\end{aligned} \tag{3.37}$$

with

$$\tilde{\mathcal{B}} = \left(\frac{u_0}{c_s}\right)^3 \mathcal{B}\, \left[1 + O(u_0^2/c_s^2)\right] \approx 4\, \varepsilon\, a_r^2\, \mathcal{A}\,, \tag{3.38}$$

where $\mathcal{B}$ and $\mathcal{A}$ are given by eqs. (3.15) and (2.39), respectively.

Although the form of the Langevin equations (3.34) is the same as the one obtained for the incompressible case, eqs. (3.13), the two sets are nevertheless not equivalent since their coefficients are clearly different, even at the leading order in ε. The main reason for this apparent discrepancy is related to the fact that, for the incompressible case, the analysis has been

carried out by scaling the velocities by u_0, whereas for the compressible case they have been scaled by c_s, the velocity of sound. If we now revert to the former scaling, i.e. we perform the change of variables $t \rightarrow t\, c_s/u_0$, $\{u, v\} \rightarrow u_0/c_s\{u, v\}$, then eqs. (3.34) lead to

$$\delta\tilde{\phi}_1(t) = \frac{u_0}{c_s}\, \delta\phi_1(t)\, \left[1 + O(u_0^2/c_s^2)\right] \tag{3.39}$$

Remarkably, this result shows that, to leading order in ε, the evolution of fluctuating compressible and incompressible hydrodynamic equations are governed by the same slow mode, at least for values of the Reynolds number close to its critical value.

Let us first consider the *macroscopic* behavior. Using eqs. (3.35), (3.36) and (3.39), one can go back step by step and derive the evolution equations of the hydrodynamical velocities near the instability threshold. It can then easily be checked that, to leading order in ε, the compressible stationary velocity profiles are given by their incompressible expressions, eqs. (3.11) and (3.12). To check this important result, we have solved numerically the full nonlinear compressible hydrodynamic equations and compared the result with analytical expressions obtained for the incompressible case. A typical result is shown in figure 3.4, where $u_{st}(x, y = 1/4)$ as a function of $v_{st}(x, y = 1/4)$ is depicted for $R = 15$, $\varepsilon = 10^{-2}$ and $a_r = 2$. Given the relatively large values of the Reynolds number ($R/R_c - 1 \approx 17\%$) and ε, the agreement is very good, the discrepancy remaining below 5%.

We now concentrate on the behavior of the fluctuations, as described by the Langevin equations (3.34). The associated Fokker-Planck equation reads

$$\begin{aligned}\frac{\partial P(\delta\tilde{\phi}_1\,, \delta\tilde{\phi}_1^*\,, t)}{\partial t} &= \frac{\partial}{\partial(\delta\tilde{\phi}_1)}\left[-(\tilde{\lambda}\,\delta\tilde{\phi}_1 - \tilde{\gamma}\delta\tilde{\phi}_1^2\,\delta\tilde{\phi}_1^*)\,P + \frac{\tilde{\mathcal{B}}}{2}\frac{\partial P}{\partial(\delta\tilde{\phi}_1^*)}\right] \\ &+ \frac{\partial}{\partial(\delta\tilde{\phi}_1^*)}\left[-(\tilde{\lambda}\,\delta\tilde{\phi}_1^* - \tilde{\gamma}\delta\tilde{\phi}_1\,\delta\tilde{\phi}_1^{*2})\,P + \frac{\tilde{\mathcal{B}}}{2}\frac{\partial P}{\partial(\delta\tilde{\phi}_1)}\right].\end{aligned} \tag{3.40}$$

For the stationary distribution, one finds

$$P_{st}(\delta\tilde{\phi}_1\,, \delta\tilde{\phi}_1^*) = \mathcal{N}^{-1}\, \exp\left[\frac{2}{\tilde{\mathcal{B}}}\left(\tilde{\lambda}|\delta\tilde{\phi}_1|^2 - \frac{\tilde{\gamma}}{2}|\delta\tilde{\phi}_1|^4\right)\right]\,, \tag{3.41}$$

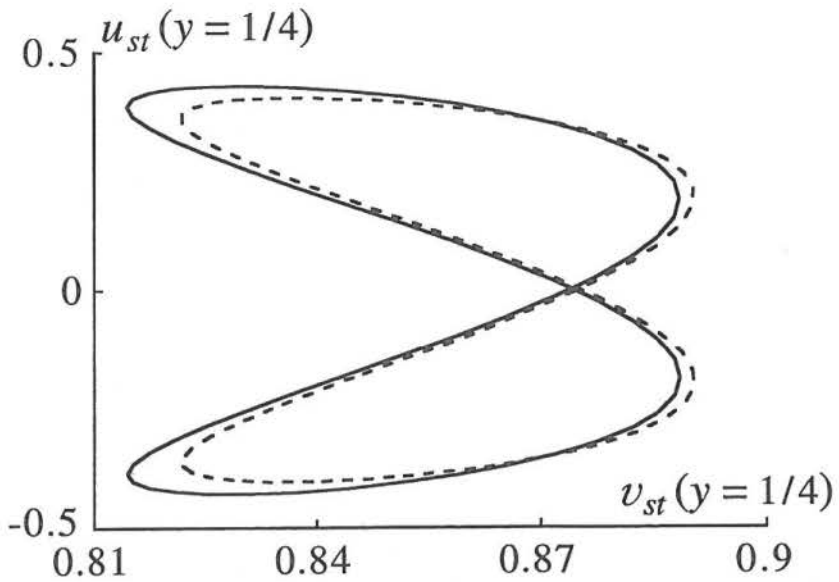

Figure 3.4: Vertical versus horizontal components of the stationary state velocity field with $y = 3/4$. The full line corresponds to theoretical predictions, as given by eqs. (3.11) and (3.12), whereas the dashed line is obtained by solving numerically the compressible nonlinear hydrodynamic equations. The parameters are $R = 15$, $a_r = 2$, $\theta_0 = 0$ and $\varepsilon = 10^{-2}$. The discrepancy is about 5%.

with

$$\mathcal{N} = \frac{1}{4}\sqrt{\pi\,\tilde{\mathcal{B}}/\tilde{\gamma}}\;\exp\left(\tilde{\lambda}^2/\,\tilde{\gamma}\tilde{\mathcal{B}}\right)\;\mathrm{erfc}\left(-\,\tilde{\lambda}\,/\sqrt{\tilde{\gamma}\,\tilde{\mathcal{B}}}\,\right) \tag{3.42}$$

where erfc denotes the complementary error function. With the help of this result, one readily gets

$$\left\langle |\delta\tilde{\phi}_1|^2 \right\rangle = \frac{1}{\tilde{\gamma}}\left(\tilde{\lambda} + \tilde{\mathcal{B}}/4\mathcal{N}\right) . \tag{3.43}$$

Away from the bifurcation point ($\tilde{\lambda} << 0$) the quartic term in (3.41) is negligible, so that the distribution is Gaussian and

$$\left\langle |\delta\tilde{\phi}_1(k_x = 1)|^2 \right\rangle_G \approx \frac{\mathcal{A}\,R^2\,a_r^4\,(a_r^2+2)}{2\,\pi^2\,(R_c^2(k_x=1) - R^2)\,(a_r^2\,+\,1)} . \tag{3.44}$$

The fluctuations thus behave as $|\delta\tilde{\phi}_1(k_x = 1)| \sim O(\mathcal{A}^{1/2})$. Recall that the parameter $\mathcal{A}$ is inversely proportional to the total number of particles in the system, so that $\mathcal{A} << 1$ (cf. eq. (2.39)). As one approaches the bifurcation point, the Gaussian character of the distribution is gradually lost. Right at the bifurcation point, $\tilde{\lambda} = 0$, one has

$$\left\langle |\delta\tilde{\phi}_1(k_x = 1)|^2 \right\rangle_{\tilde{\lambda}=0} = 2\,\varepsilon\,a_r\left[\frac{R_c(k_x=1)\,\mathcal{A}}{\gamma\,\pi}\right]^{1/2} , \tag{3.45}$$

which shows that the fluctuations now behave as $|\delta\tilde{\phi}_1(k_x = 1)| \sim O(\mathcal{A}^{1/4})$. The enhancement of fluctuations and the change of the probability law at the bifurcation point are a direct manifestation of the breaking of the spatial symmetry associated with the emergence of convective patterns.

On the other hand, the fast modes $\delta\tilde{\phi}_1(k_x \neq \pm 1)$, $\delta\tilde{\phi}_2$, $\delta\tilde{\phi}_3$ and $\delta\tilde{\phi}_4$ continue to remain Gaussian, regardless of the value of the Reynolds number. Detailed analysis shows that their contribution to nonequilibrium statistical properties of the fluid remain of the order of u_0^2/c_s^2. In other words, the fluctuation spectrum of hydrodynamic variables is determined mainly by the statistical properties of $\delta\phi_1(k_x = 1)$ and its complex conjugate. For instance, the static velocity autocorrelation function is found to satisfy the equation

$$\langle \delta\mathbf{v}_\mathbf{k} \cdot \delta\mathbf{v}_{-\mathbf{k}} \rangle - 2\mathcal{A} = \frac{\pi^2(a_r^2+1)}{a_r^2\,(a_r^2+2)^2}\left\langle |\delta\tilde{\phi}_1(k_x=1)|^2 \right\rangle \left[1 + O\left((u_0/c_s)^2\right)\right] , \tag{3.46}$$

where the second term on the left-hand side is the equilibrium contribution and $\left\langle |\delta\tilde{\phi}_1(k_x = 1)|^2 \right\rangle$ is given by eq. (3.43).

It is instructive to study the Gaussian limit, $R << R_c$, where the linearized Langevin equations, eqs. (2.33)-(2.35), remain valid. As has been shown in Section 2.2, eq.(2.52), they lead to the following expression for the static velocity autocorrelation function, in the particular case $k_x = k_y = 1$:

$$\langle \delta \mathbf{v}_{1,1} \cdot \delta \mathbf{v}_{-1,-1} \rangle_G - 2\mathcal{A} = \frac{\mathcal{A}\, R^2\, a_r^2}{2\,(R_c^2 - R^2)\,(a_r^2 + 2)} \,. \qquad (3.47)$$

Now, the insertion into eq. (3.46) of the Gaussian form of $\left\langle |\delta\tilde{\phi}_1(k_x = 1)|^2 \right\rangle$, as given by eq. (3.44), leads to precisely the same result. We thus conclude that our general expression (eq. (3.46)) remains valid in the Gaussian regime $R << R_c$, despite the fact that it has been derived for R in the close vicinity of the bifurcation point ($R \approx R_c$).

To check the validity of our theoretical results, we have simulated the nonlinear fluctuating hydrodynamic equations (2.3)-(2.5) for different values of R, setting $a_r = 2$, $\varepsilon = 10^{-2}$ and $\mathcal{A} = 10^{-3}/256 \approx 3.9 \times 10^{-6}$. The estimated statistical error remains below 5% for $R \lesssim 10$, but grows rapidly as we consider higher values of R, reaching about 13% for $R \approx R_c$. Above the bifurcation point, $R \gtrsim R_c$, the stationary distribution has two maxima, located at $\delta\tilde{\phi}_1^{\pm}(k_x = 1) = \pm\sqrt{\tilde{\lambda}/\tilde{\gamma}}$, which correspond (up to a phase factor) to the deterministic stationary solutions of the amplitude equation (3.9). Because of the presence of noise terms, the system visits these states in a rather random fashion, resulting in a sizeable dispersion. This is specially true for R close to R_c, which is precisely the situation where our theoretical predictions are expected to be applicable. Under these circumstances, obtaining reliable statistics requires prohibitively large computing times. We have therefore limited the numerical simulations to values of Reynolds numbers $R \leq R_c$.

The results are presented in figure 3.5, together with both the complete solution and the linearized solution, eqs. (3.46) and (3.47), respectively. The linear theory (Gaussian limit) shows quantitative agreement for values of R/R_c up to about 86%, but significant discrepancies start to show up as $R \to R_c$ where the theory leads to diverging correlation functions (see eq. (3.47)). This is not the case for the complete solution, eq. (3.46),

which exhibits perfect quantitative agreement for R/R_c up to 95%. A relatively small discrepancy of about 8% is however observed for higher values of R. Although this discrepancy remains within the range of the estimated statistical errors, its systematic occurrence requires some clarification: It is important to recall that the results derived in this section are valid to $O(u_0^2/c_s^2)$. Now, by definition $u_0/c_s = R\varepsilon$ (see eq. (3.25)), and since we have set $\varepsilon = 10^{-2}$, $R_c\varepsilon \approx 0.13$ at the bifurcation point. This relatively large value of $R_c\varepsilon$ might well be the source of the observed discrepancy. To check the validity of this argument, it is useful to perform the simulations all over again for a smaller value of ε. However, since the relaxation time of hydrodynamical modes grows as ε^{-1}, reaching the same degree of statistical accuracy as in the previous cases requires much longer running times. For this reason we decided to perform only one more simulation right at the critical point, $R = R_c$, setting $\varepsilon = 10^{-3}$. The theoretical prediction for the nonequilibrium part of the velocity correlation function is 2.31×10^{-6}. The simulation leads to 2.24×10^{-6} with an estimated statistical error of about 15%. The discrepancy is now about 3%, much smaller than in the case $\varepsilon = 10^{-2}$.

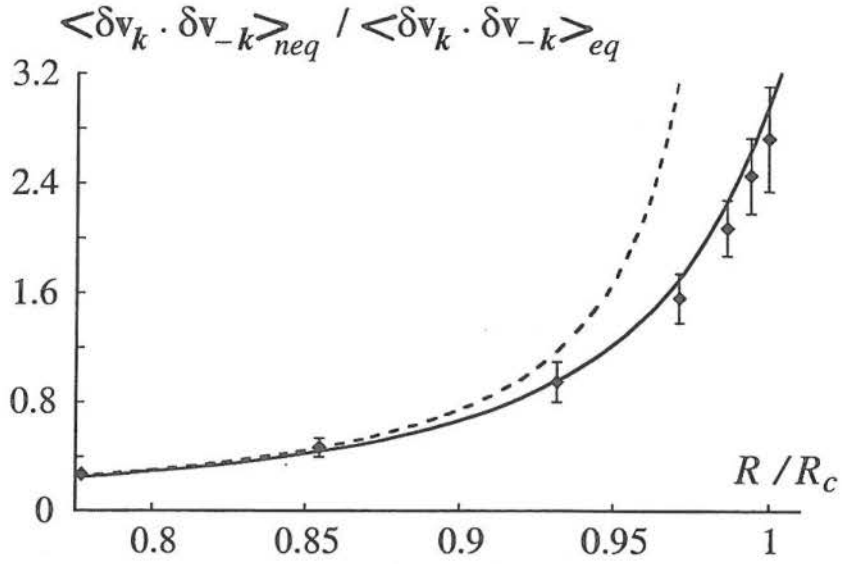

Figure 3.5: Fourier transform of the nonequilibrium part of the static velocity autocorrelation function, normalized by the corresponding equilibrium part, as a function of R/R_c. The solid and dashed curves represent the complete and the linearized solutions, eqs. (3.46) and (3.47), respectively. The black dots correspond to numerical results obtained by the simulation of the nonlinear compressible fluctuating hydrodynamic equations. The parameter values are $a_r = 2$, $\varepsilon = 10^{-2}$ and $\mathcal{A} = 10^{-3}/256$. The estimated statistical error is about 13% for the last data point.

Chapter 4

Spurious Diffusion in Particle Simulations of Kolmogorov Flow

The purpose of this chapter is to point out a subtle problem concerning the nonequilibrium fluctuations that appear in Kolmogorov flow. It is shown that the center of mass of the system undergoes a spurious diffusion that corrupts the statistical properties of the flow.

Let us return to the fluctuating hydrodynamic equations that describe the flow,

$$\frac{\partial \rho}{\partial t} = -\boldsymbol{\nabla} \cdot (\rho \mathbf{v}) \,, \tag{4.1}$$

$$\frac{\partial (\rho \mathbf{v})}{\partial t} = -\boldsymbol{\nabla} \cdot (\rho \mathbf{v}\mathbf{v}) - \boldsymbol{\nabla} p - \boldsymbol{\nabla} \cdot \boldsymbol{\sigma} + \mathbf{F}_{ext} \,. \tag{4.2}$$

We recall that ρ is the mass density, p the hydrostatic pressure and $\boldsymbol{\sigma}$ the *two-dimensional* stress tensor,

$$\sigma_{ij} = -\eta \left(\frac{\partial v_i}{\partial x_j} + \frac{\partial v_j}{\partial x_i} - \delta_{ij} \boldsymbol{\nabla} \cdot \mathbf{v} \right) - \zeta \, \delta_{ij} \boldsymbol{\nabla} \cdot \mathbf{v} + S_{ij}. \tag{4.3}$$

$\mathbf{S}$ is a random tensor whose elements $\{S_{ij}\}$ are Gaussian white noises with zero mean and covariances given by [12]

$$\begin{aligned} \langle S_{ij}(\mathbf{r},t)\, S_{k\ell}(\mathbf{r}',t') \rangle &= 2k_B T_0 \, \delta(t-t') \, \delta(\mathbf{r}-\mathbf{r}') \\ &\quad [\eta(\delta_{ik}\delta_{j\ell} + \delta_{i\ell}\delta_{jk}) + (\zeta - \eta)\delta_{ij}\delta_{k\ell}] \end{aligned} \tag{4.4}$$

where T_0 is the (uniform) temperature. For simplicity, it is assumed that the shear and bulk viscosity coefficients η and ζ are state-independent, i.e., they are constant. The external force

$$\mathbf{F}_{ext} = F_0 \sin(2\pi n y/L_y)\mathbf{1}_x \ . \tag{4.5}$$

For sufficiently small F_0 the mean stationary flow essentially follows the external field,

$$\begin{aligned} \mathbf{v}_{st} &= u_0 \sin(2\pi n y/L_y)\mathbf{1}_x \ , \\ u_0 &= \frac{F_0 L_y^2}{4\pi^2 n^2 \eta} \ . \end{aligned} \tag{4.6}$$

For sufficiently high F_0 this laminar flow becomes unstable and gives rise to the familiar rotating convective patterns.

As we have already pointed out in Section 2.1, when imposing a force field, one has to keep in mind that in microscopic simulations as well as in real systems, the fluid is made up of individual particles. Hence what one can impose is not a bulk force, but rather an acceleration field acting on the particles. Since the density of particles is fluctuating, we conclude that the external field in the momentum equation (4.2) is *also* a fluctuating quantity:

$$\mathbf{F}_{ext} = \rho(x,y)\, a_0 \sin\left(2\,\pi\, n\, y/L_y\right) \mathbf{1}_x, \tag{4.7}$$

where a_0 is the amplitude of the imposed acceleration field. Moreover, since the external field in Kolmogorov flow is space-dependent, the force acting on a particle depends on its exact position so that the total force $F(t)$ in the x-direction will also be fluctuating, even though the total number of particles is conserved. As a result, the center of mass linear momentum $J_x(t)$ undergoes a stochastic motion driven by a scalar force $F(t)$:

$$\frac{\partial J_x(t)}{\partial t} = \frac{a_0}{L_x\, L_y} \int_0^{L_x} dx \int_0^{L_y} dy\, \rho(x,y,t) \sin\left(2\,\pi\, n\, y/L_y\right) \equiv F(t). \tag{4.8}$$

In strictly subsonic regimes the flow behaves essentially as an incompressible fluid (as follows from the preceding chapters), so that the average density is uniform in space, $\langle\rho\rangle = \rho_0$. It then follows from eq. (4.8) that $\langle F(t)\rangle = 0$.

To find the correlation function $\langle F(t)F(t')\rangle$, we consider the spatial average of the hydrodynamical equations (4.1) and (4.2) over x. The corresponding spatially averaged density $\rho(y,t) = \frac{1}{L_x}\int_0^{L_x} dx\,\rho(x,y,t)$, and the y-component of the velocity $v(y,t) = \frac{1}{L_x}\int_0^{L_x} dx\,v_y(x,y,t)$, are not affected by the external constraints, i.e., they assume their equilibrium form. In particular, in the *stationary* regime one has $\langle\rho\rangle = \rho_0$ and $\langle v\rangle = 0$, independent of the value of a_0. To study the fluctuations around this state, we introduce the deviations $\delta\rho(y,t) = \rho(y,t) - \rho_0$, $\delta v(y,t) = v(y,t)$ and $\delta p(y,t) = p(y,t) - \langle p\rangle$. These obey the following linearized equations :

$$\frac{\partial\,\delta\rho}{\partial t} = -\rho_0\frac{\partial\,\delta v}{\partial y}\,, \tag{4.9}$$

$$\rho_0\frac{\partial\,\delta v}{\partial t} = -\frac{\partial\,\delta p}{\partial y} + (\eta+\zeta)\frac{\partial^2\,\delta v}{\partial y^2} - \frac{\partial\,S_{yy}}{\partial y}\,, \tag{4.10}$$

with

$$\left\langle S_{yy}(y,t)\,S_{yy}(y',t')\right\rangle = 2\,\frac{k_BT_0}{L_x}\,(\eta+\zeta)\,\delta(t-t')\,\delta(y-y')\,. \tag{4.11}$$

To close this set of equations, we need to specify the equation of state. Since the fluid is isothermal, we simply set

$$\delta p = c_s^2\,\delta\rho\,, \tag{4.12}$$

where c_s is the isothermal speed of sound.

The stochastic differential equation for the fluctuating force $F(t)$ now follows easily by multiplication of (4.9) and (4.10) by $\sin(2\pi n y/L_y)$ and $\cos(2\pi n y/L_y)$, respectively, followed by integration over y. One obtains:

$$\frac{d^2F(t)}{dt^2} + \frac{\eta+\zeta}{\rho_0}\frac{4\pi^2n^2}{L_y^2}\frac{dF(t)}{dt} + \frac{4\pi^2n^2c_s^2}{L_y^2}F(t) = \theta(t)\,, \tag{4.13}$$

where $\theta(t)$ is a Gaussian white noise with zero mean and variance given by

$$\left\langle\theta(t)\,\theta(t')\right\rangle = \frac{k_B\,T_0}{L_xL_y}\,(\eta+\zeta)\,a_0^2\left(\frac{2\pi\,n}{L_y}\right)^4\delta(t-t')\,. \tag{4.14}$$

We conclude that $F(t)$ is a Gaussian non-Markovian process, that obeys the equation of a Brownian damped harmonic oscillator. The exact form of the

force correlation is easily obtained from (4.13) and (4.14), but the final expression is rather lengthy. On the other hand, the validity of hydrodynamics can only be guaranteed if the parameter

$$\varepsilon = \frac{\eta}{\rho_0 c_s L_y} \tag{4.15}$$

remains small [43]. Accordingly, to leading order in ε, the force correlation reads:

$$\langle F(t)F(0)\rangle = \rho_0^2 a_0^2 \frac{k_B T_0}{2 m N c_s^2} \exp\left(-\frac{4\pi^2 n^2 \Gamma_s t}{L_y^2}\right) \cos\left(\frac{2\pi n c_s t}{L_y}\right) \quad (t \geq 0) , \tag{4.16}$$

where $\Gamma_s = (\eta + \zeta)/2\rho_0$ is the two-dimensional sound damping coefficient, N is the total number of particles and m their individual mass.

Turning to $J_x(t)$, which is nothing but the time integral of $F(t)$, we conclude that it is a Gaussian stochastic process with zero average and a second moment given (again to leading order in ε) by

$$\begin{aligned} \langle J_x^2(t)\rangle = \quad & \rho_0^2 a_0^2 \frac{k_B T_0}{m N c_s^4} \times \\ & \left\{ \Gamma_s\, t \;+\; \left(\frac{L_y}{2\pi n}\right)^2 \left[1 - \exp\left(-\frac{4\pi^2 n^2 \Gamma_s t}{L_y^2}\right) \cos\left(\frac{2\pi n c_s t}{L_y}\right)\right] \right\} . \end{aligned} \tag{4.17}$$

As stated, $J_x(t)$ behaves diffusively (in momentum space) with a diffusion coefficient given by

$$D = \lim_{t\to\infty} \frac{\langle J_x^2(t)\rangle}{2t} = \rho_0^2 a_0^2 \frac{k_B T_0}{2 m N c_s^4} \Gamma_s . \tag{4.18}$$

It is important to note that in real macroscopic systems the actual diffusion of the center of mass remains questionable for the following reason. The imposition of periodic boundary conditions is one of the basic simplifying features of Kolmogorov flow. This is all right for a system of infinite extent, consisting of periodically repeated Kolmogorov units, as long as only macroscopic properties are concened. However, when the fluctuations are under investigation, it is essential to realize that periodic boundary conditions imply a perfect correlation of the fluctuating forces in the different units. This

is obviously unphysical (except for the theoretical case of a system defined on a torus). In any case, *the diffusion coefficient D is unobservable in macroscopic systems*[1].

The situation is entirely different in *microscopic simulations* where the total number of particles N barely exceeds 10^5. To estimate the importance of the diffusion of the center of mass, and the corresponding effect on the statistical properties of the system in numerical simulations, we first note that the ratio $k_B T_0/m\, c_s^2$ is of the order of unity. Next, we observe that there is a minimum run time for simulations, namely the hydrodynamic relaxation time $\tau_h \approx L_x L_y/\Gamma_s$; typical runs last for several times τ_h. It then follows from eq. (4.17) that for large t (i.e., $t > \tau_h$) the velocity fluctuation $\langle J_x^2 \rangle / \rho_0^2$ of the center of mass is

$$\langle v_x^2(t) \rangle = \frac{\langle J_x^2(t) \rangle}{\rho_0^2} \approx \frac{a_0^2}{n_0\, c_s^2}\, \frac{t}{\tau_h}, \tag{4.19}$$

where $n_0 = N/L_x L_y$ is the number density. This quantity has to be compared with the spatial average of the mean square flow velocity $\bar{u}_m^2$, which is of the order of $u_0^2/2$ (see eq. (4.6)). The relative importance of the center of mass diffusion can thus be quantified by the square root of the ratio $\langle v_x^2(t) \rangle / \bar{u}_m^2$. Using the explicit form of u_0 (eq. (4.6)), one finds that for $t > \tau_h$,

$$\mu(t) = \left(\langle v_x^2(t) \rangle / \bar{u}_m^2 \right)^{1/2} \approx \left(2/n_0 \right)^{1/2} a_r\, \frac{4\pi^2\, n^2\, \eta}{m\, N\, c_s}\, \left(t/\tau_h \right)^{1/2} \tag{4.20}$$

where $a_r = L_x/L_y$ is the aspect ratio.

As an example, consider a two dimensional Boltzmann gas for which there exists an efficient algorithm, proposed two decades ago by Bird [52], that is about 3 orders of magnitude faster than the corresponding traditional molecular dynamics simulation. A typical case is a system involving 20 000 hard disks of diameter d, with $L_x \times L_y = 2000 \times 1000\, d^2$ (i.e. $a_r = 2$ and $n_0 = 10^{-2}$ particles per d^2), $n = 2$, $c_s \approx 1$ and $\eta \approx 0.3$ (in system units, where lengths, masses and velocities are scaled by the disk diameter d, the

[1] Let us take the example of a liquid under normal conditions, for which typically $k_B T_0/m c_s^2 \sim 1$, $c_s \sim 10^3\ m/s$, $L_y \sim 10^{-3}\ m$, $\varepsilon \sim 10^{-6}$, $\Gamma_s \sim 10^{-6}\ m^2/s$, $\rho_0 \sim 10^{-3}\ kg/m^2$, $\rho_0 a_0 \sim 10^{-4}\ kg/ms^2$, and $N \sim 10^{18}$. These values lead to $D \sim 10^{-38}\ kg^2/m^2 s^3$.

particle mass m and the thermal velocity, $\sqrt{k_B T_0/m}$, respectively). It then follows from eq. (4.20) that after only one relaxation time, $\mu(\tau_h) \approx 7 \times 10^{-2}$ which is certainly not negligible, all the more so since typical running times are 10 to 100 times larger than τ_h.

One way to avoid this problem is to increase the number of particles, while keeping the number density $n_0 = 10^{-2}$ particles per d^2, since the Bird algorithm is then applicable. However, to reach reasonably small values of μ, for instance $\mu(\tau_h) \approx 10^{-4}$, one has to consider a simulation involving over 10^7 particles. Such simulations would require a prohibitively long running time with present day computers.

The only other alternative is to increase the number density as well. For a given number of particles, the best strategy is to choose n_0 so that the Reynolds number is as high as possible, since this is precisely one of the main objectives of numerical simulations [53]. In the case of subsonic hard disk flows, the appropriate number density turns out to be about $n_0 = 0.27$ particles per d^2 [54]. For a system containing $5 \cdot 10^5$ particles, $L_x \times L_y = 960 \times 1920\ d^2$, $c_s \approx 1.6$ and $\eta \approx 0.4$; $\mu(\tau_h)$ is then about 4×10^{-4}, which is quite satisfactory. However, a number density $n_0 \approx 0.27$ corresponds to a moderately dense Enskog gas for which the Bird algorithm is no longer applicable [55]. Instead, one has to use the traditional hard disk molecular dynamics method which, as mentioned before, is about 3 orders of magnitude slower than the corresponding dilute gas simulation. Moreover, the collision frequency grows linearly with the number density, which further increases the run time by at least another order of magnitude. Under these conditions, pursuing the simulation for a single relaxation time τ_h is about the best one can achieve with present day computer performances. Although such a relatively short simulation might be satisfactory to study the average properties of the system, it is certainly not enough to extract the associated fluctuation spectrum.

The discussion above highlights the usefulness of lattice-particle simulations for the study of the relatively high Reynolds number flows. But these model simulations have their own limitations. Because the motion of particles takes place within a restricted geometry (4 or 6 linear directions), with the corresponding restricted number of velocities, reaching local equilibrium now requires many more collisions than in the case of hard disk dynamics [56]. As far as macroscopic properties of the system are concerned, this is only a

minor problem, since lattice-particle simulations typically run seven orders of magnitude faster than hard disk molecular dynamics. The major drawback however is that such a long time simulation inevitably increases the effect of the center of mass diffusion reported here. This spurious diffusion has also been noted very recently by Boon et al. [57] in a study of the turbulent diffusion in Kolmogorov flow.

In conclusion, while the foregoing diffusion of the center of mass in Kolmogorov flow does not affect the average macroscopic behavior of the system, it does vitiate the other statistical properties, and to a significant degree under conditions that are typical for many microscopic simulations. The best way to get around this problem is to include in the simulation algorithm an *ad hoc* mechanism that prevents the momentum fluctuations of the center of mass. This can be accomplished rather easily in lattice-particle simulations [58], but its counterpart in molecular dynamics simulations is rather less obvious.

Chapter 5

Conclusions

In this brief final chapter, we summarize the main results of Part II of this thesis.

Our initial motivation was to find a solution to the problem of using fluctuating hydrodynamics or the incompresibility assumption for the study of a fluid in the vicinity of the onset of a hydrodynamic instability, as explained in the Introduction. The idea was to choose a model that, on the one hand, would exhibit hydrodynamic instabilities analogous to those encountered in real systems, and, on the other hand, would be simple enough to be amenable to a complete analytical treatment. Our choice was Kolmogorov flow, mainly because of the periodic boundary conditions associated with it. Also, this model exhibits a primary hydrodynamic instability through which laminar flow undergoes a transition to a rotating convective pattern [1]. A detailed, comparative analysis of this simple model flow has been presented for both the compressible and incompressible cases, from equilibrium up to the vicinity of the first instability threshold. The objective has been to understand at a more quantitative level the roles of compressibility and fluctuations in the onset of the instability, and to deduce some general conclusions regarding this aspect.

Chapter 2 dealt with the study of the statistical properties of the linearized Kolmogorov flow. Following a description of the model and a review of its

[1] If the nonequilibrium constraint imposed on the fluid is progressively increased, other successive, increasingly complex bifurcations appear - leading, finally, to chaotic behavior. We have not been concerned here with these secondary bifurcations.

macroscopic behavior, a linear stability analysis indicated the location of the instability threshold R_c in terms of the Reynolds number R of the flow. The simplicity of the model permits a detailed analysis of the fluctuation spectrum from near equilibrium up to the vicinity of the first instability leading to convective rolls. For the latter case, the analytical calculations were based on a three-mode approximation in which only the Fourier modes with wavenumber $|k_y| \leq 1$ are retained; while for the former case we have set up a perturbation scheme around the equilibrium. Extensive numerical calculations allow us to delineate clearly the limits of validity of both regimes. In particular, we have shown that the three-mode approximation holds already for $R/R_c \geq 0.65$ and leads to a divergence of the velocity autocorrelation as $R \to R_c$. On the other hand, the simulation of the full nonlinear fluctuating hydrodynamic equations indicates that the validity of the linearized hydrodynamic equations can be guaranteed for Reynolds numbers as high as $R \approx 0.9\, R_c$.

It was also shown that the dynamic structure factor of the fluid is practically unaffected by nonequilibrium constraints. This is not surprising: as already discussed in the Introduction, the nonequilibrium constraints are expected to affect mainly the viscous, slow modes of the system (the ones that are connected to the onset of the instability); or, in terms of the structure factor, to affect the central (Rayleigh) peak. However, because of the strictly isothermal character of Kolmogorov flow, this peak is completely absent in the present instance. Therefore, the form factor does not yield any information about the nonequilibrium regime. This is compensated for by the behaviour of the velocity autocorrelation function, which exhibits a purely dissipative viscous regime, together with a "sound propagation" regime. While the latter is not affected by the nonequilibrium constraints, the former yields valuable information about the nonequilibrium state of the system. Also, the static velocity autocorrelation function is found to be long-ranged in space, even in the vicinity of equilibrium.

Another interesting result concerns the validity of the incompressibility assumption which greatly simplifies the mathematical analysis of the problem. The compressibility of a fluid mainly affects fast sound modes whereas the dynamics of the system near an instability is governed mainly by dissipative slow modes. This intuitive argument has been used by many authors who have considered fluctuating incompressible hydrodynamic equations, or even directly the corresponding normal form amplitude equations to which

random noise terms are added [59]. In these approaches, the characteristics of the noise remain arbitrary, because they cannot be related to equilibrium statistical properties of the fluid. A more satisfactory approach would be to start with the compressible fluctuating hydrodynamic equations. Such a procedure, however, proves to be extremely difficult mainly because of the problem of boundary conditions. Here again, the relative simplicity of Kolmogorov flow allows some further progress to be made in this important issue. In this respect, we have shown that in the long-time limit the flow behaves as an incompressible fluid, regardless of the value of the Reynolds number. However, this does not hold good for the short-time behavior. In particular, the incompressibility assumption in general leads to an incorrect form of the static correlation functions. The only exception is near the convective instability, where we have shown that the incompressibility assumption remains valid.

The problem with this conclusion is that the linearized fluctuating hydrodynamic equations, on which the analysis in Chapter 2 is based, are no longer valid close to the instability threshold. Although extensive numerical simulations have basically confirmed our predictions, a full answer to this important problem requires nevertheless a nonlinear analysis of the fluctuating Kolmogorov flow. This was dealt with in Chapter 3. The case of an incompressible fluid was considered first. A deterministic analysis enables one to identify the slow modes and adiabatically eliminate the fast modes, to obtain the nonlinear normal form amplitude equation. We could then derive the explicit form of the stationary stream function, as well as the corresponding velocity profiles, in real space. Numerical studies of the nonlinear hydrodynamical equations confirm the theoretical predictions. Next, we considered the stochastic behaviour in the limit of a weak noise. Using a suitable singular rescaling of the variables and a "stochastic adiabatic elimination" of the fast modes, we showed that the stochastic evolution in the vicinity of the threshold is essentially given by two coupled nonlinear Langevin equations in Fourier space. Their solutions can be cast in the form of the exponential of a Landau-Ginzburg functional. The case of compressible Kolmogorov flow was considered afterwards. The analysis is simplified by noticing that the evolution of a compressible fluid is generally characterized by two different time scales: a slow one, related to the dissipative viscous modes; and a fast one, expressing the propagation of (damped) sound modes. The ratio ε of these time scales must be a small quantity to ensure the validity of the hydrodynamic approach. We thus have at our disposal a natural small

parameter, which is used to set up a perturbative formalism. As already mentioned, this method represents an advantageous alternative to the multiple time scale theory [51] that was generalized by Schmitz and Cohen [20] in order to study the Bénard instability in a compressible fluid. Using this perturbation technique, we have shown that the macroscopic behavior of the fluid is not affected, up to $O(\varepsilon^2)$, by the compressibility, in agreement with the intuitive arguments presented in the Introduction. We then established that, to the same degree of precision, the stochastic dynamics of the compressible system is also identical to the one obtained for the case of the incompressible fluid. These theoretical predictions have been confirmed by numerical simulations of the nonlinear fluctuating hydrodynamic equations.

Finally, in Chapter 4 we discussed a rather subtle problem concerning the nonequilibrium fluctuations that appear in the model: owing to the density fluctuations in the system, the density of the applied external force is also a fluctuating quantity. This leads to a stochastic motion of the center of mass of the system in phase space, which, in turn, affects the statistical properties of the flow. An analytical expression is derived for the corresponding diffusion coefficient in phase space. The effect turns out to be completely insignificant for macroscopic systems, while it dramatically affects the particle simulations. Analysing different situations, we showed that its influence cannot be eliminated in practice in molecular dynamics simulations, while in lattice-particle simulations one may use *ad hoc* algorithmic procedures to diminish its effects.

Appendix A

Light Scattering by Hydrodynamic Modes

An electromagnetic wave propagating in a transparent medium is *scattered*, i.e., it gives birth to small-intensity *scattered waves*, with frequencies and directions that are different, in general, from those of the incident wave. Scattering is due to the *changes* in the disordered motion of the electric charges of the medium under the influence of the field of the incident wave, resulting in the emission of scattered waves. The variations in the frequency of the scattered waves with respect to the incident wave can then be seen as Doppler shifts determined by the movement of the particles.

The fact that the wavelength of visible light is very large compared to molecular sizes and intermolecular distances allows us to formulate a *macroscopic* description of this phenomenon. Light scattering is then regarded as a result of local fluctuations in the dielectric constant of the medium, which in turn are caused by *hydrodynamic density fluctuations*[1], and this is precisely

[1] A simple reasoning to show this: A light beam incident on a medium polarizes it; the electric charges, accelerated in the field of the wave, radiate light. All the particles in an infinitesimal volume element ΔV experience essentially the same incident electric field; this differs from one ΔV to another by a phase factor. If all these small regions were optically identical, then the total scattered field (the sum of all the fields scattered by these volume elements) would vanish: the waves scattered from these volumes would be identical except for a phase factor, leading to their mutual cancellation when summed. Hence a non-vanishing scattered field arises when there are variations in the optical properties of different volume elements, i.e., when there are density inhomogeneities (fluctuations) in the medium.

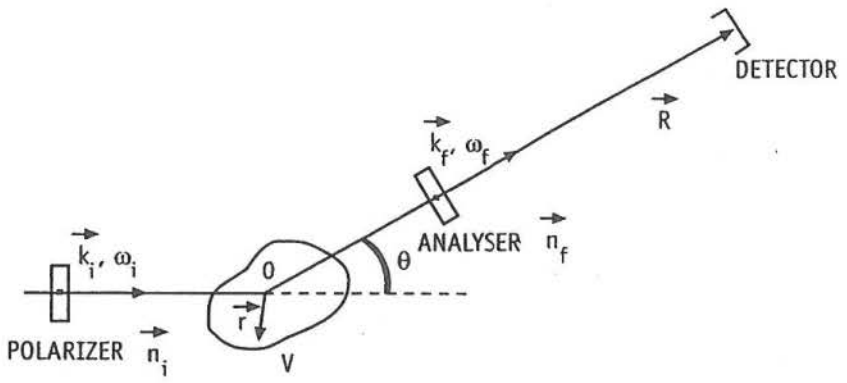

Figure A.1: Schematic representation of a light scattering experiment

the point of interest to us. In general, for a fluid (in or out of equilibrium) these density fluctuations may diffuse in the medium or may propagate as damped sound waves. The latter will result in a shift in the frequency of the scattered waves, while the diffusion will only result in a dispersion of the frequencies of the scattered waves around the frequency of the incident wave. These are the features the Doppler effect is expected to present in this case. We present below a simplified macroscopic theory of light scattering, that enables us to see how such an optical experiment can be used to get information about the hydrodynamic state of a fluid.

Consider a simple scattering experiment as shown schematically in fig. A.1. A non-magnetic, non-conducting, non-absorbing fluid of volume V, with average dielectric constant ε, is placed in the field of a plane, monochromatic, polarized incident wave ($\mathbf{E}_i$, $\mathbf{D}_i$, $\mathbf{H}_i$, $\mathbf{B}_i$) given by

$$\begin{aligned} &\mathbf{E}_i(\mathbf{r}, t) = E_0\ \mathbf{n}_i\ \exp\left[i(\mathbf{k}_i \cdot \mathbf{r} - \omega_i t)\right]\ , \\ &\mathbf{D}_i = \varepsilon\, \mathbf{E}_i\ ; \quad \mathbf{B}_i = \mu_0\, \mathbf{H}_i\ , \end{aligned} \tag{A.1}$$

and the source-free Maxwell equations

$$\begin{aligned} &\nabla \times \mathbf{E}_i = -\frac{\partial \mathbf{B}_i}{\partial t}\ ; \quad \nabla \times \mathbf{H}_i = \frac{\partial \mathbf{D}_i}{\partial t}\ ; \\ &\nabla \cdot \mathbf{D}_i = 0\ ; \quad \nabla \cdot \mathbf{B}_i = 0\ . \end{aligned} \tag{A.2}$$

Let $(\mathbf{E}_s, \mathbf{D}_s, \mathbf{H}_s, \mathbf{B}_s)$ denote the scattered field at a point of the medium with an instantaneous dielectric coefficient

$$\varepsilon(\mathbf{r}, t) = \varepsilon + \delta\varepsilon(\mathbf{r}, t) \ . \tag{A.3}$$

The scattered fields also satisfy Maxwell's equations, of course. Further,

$$\mathbf{B}_s = \mu_0 \mathbf{H}_s \ , \tag{A.4}$$

while

$$\mathbf{D}_s = \varepsilon \mathbf{E}_s + \delta\varepsilon(\mathbf{r}, t) \mathbf{E}_i \ , \tag{A.5}$$

the term $\delta\varepsilon(\mathbf{r}, t) \mathbf{E}_s$ being negligibly small. We will assume, for simplicity, that the detector is immersed in a medium with the same dielectric constant ε. After some simple manipulations, eqs. (A.2)-(A.5) give for the polarized scattered field at the detector

$$\mathbf{E}_s(\mathbf{R}, t) = \mathbf{n}_f \mathbf{n}_f \cdot \left\{ \boldsymbol{\nabla} \times \boldsymbol{\nabla} \times \left[\frac{E_0 \mathbf{n}_i}{4\pi\varepsilon} \int_V \frac{\delta\varepsilon(\mathbf{r}, t')}{|\mathbf{R} - \mathbf{r}|} \exp\left[i(\mathbf{k}_i \cdot \mathbf{r} - \omega_i t') \right] d\mathbf{r} \right] \right\} \ , \tag{A.6}$$

where t' is the retarded time

$$t' = t - \sqrt{\varepsilon\mu_0} \, |\mathbf{R} - \mathbf{r}| \ . \tag{A.7}$$

If the detector is at a large distance R from the scattering medium, we have

$$|\mathbf{R} - \mathbf{r}| \approx R - \mathbf{r} \cdot \frac{\mathbf{R}}{R} \ , \tag{A.8}$$

so that (A.6) finally leads to

$$\mathbf{E}_s(\mathbf{r}, t) = \mathbf{n}_f \, \mathbf{n}_f \cdot (\mathbf{k}_f \times \mathbf{k}_f \times \mathbf{n}_i) \frac{E_0}{4\pi\varepsilon R} \exp\left[i(\mathbf{k}_f \cdot \mathbf{R} - \omega_i t) \right] \cdot \int_V d\mathbf{r} \exp(i\mathbf{q} \cdot \mathbf{r}) \delta\varepsilon(\mathbf{r}, t) \ , \tag{A.9}$$

where

$$\mathbf{k}_f \equiv k_i \frac{\mathbf{R}}{R} \tag{A.10}$$

is the scattered wavevector and

$$\mathbf{q} \equiv \mathbf{k}_f - \mathbf{k}_i \tag{A.11}$$

is the momentum transfer, related to the scattering angle θ by

$$q = 2\, k_i\, \sin(\theta/2)\ . \tag{A.12}$$

The fluctuations of the dielectric constant can be expressed in terms of the polarizability μ of the molecules of the medium, their molecular mass m and the fluctuations of the density:

$$\delta\varepsilon(\mathbf{r},\, t) = \frac{\mu}{m}\, \delta\rho(\mathbf{r},\, t)\ . \tag{A.13}$$

Introducing the spatial Fourier transform of the density fluctuations,

$$\delta\rho(\mathbf{q},\, t) = \int_V d\mathbf{r}\, \exp(i\mathbf{q}\cdot\mathbf{r})\, \delta\rho(\mathbf{r},\, t)\ , \tag{A.14}$$

and working out the cross products in eq.(A.9), we finally get

$$\mathbf{E}_s(\mathbf{r},\, t)\ = -\,\mathbf{n}_f\,(\mathbf{n}_i\cdot\mathbf{n}_f)\,\frac{k_f^2\, E_0\, \mu}{4\,\pi\,\varepsilon\, m\, R}\, \exp\left[i(\mathbf{k}_f\cdot\mathbf{R} - \omega_i t)\right]\, \delta\rho(\mathbf{q},\, t)\ . \tag{A.15}$$

The time correlation function of $\mathbf{E}_s$ can be evaluated as

$$\langle \mathbf{E}_s^*(\mathbf{R},\, 0)\cdot\mathbf{E}_s(\mathbf{R},\, t)\rangle = \frac{k_f^4 E_0^2 \mu^2}{16\pi^2 m^2 \varepsilon^2 R^2}(\mathbf{n}_i\cdot\mathbf{n}_f)^2 \exp(-i\omega_i t)\langle\delta\rho(\mathbf{q},\, 0)\delta\rho(\mathbf{q},\, t)\rangle. \tag{A.16}$$

Finally, the spectral density of the light scattered into the detector such that

$$(\mathbf{n}_i,\, \mathbf{k}_i,\, \omega_i) \rightarrow (\mathbf{n}_f,\, \mathbf{k}_f,\, \omega_f)$$

is simply one half the Fourier transform of the temporal correlation function of the electric field $\mathbf{E}_s$, namely,

$$I(\mathbf{q}, \omega_f, R) = \frac{k_f^4 E_0^2 \mu^2}{32\pi^2 m^2 \varepsilon^2 R^2}(\mathbf{n}_i\cdot\mathbf{n}_f)^2 S_{\mathbf{q}}(\omega_f - \omega_i)\ , \tag{A.17}$$

where the spectral density of the hydrodynamic density fluctuations,

$$S_{\mathbf{q}}(\omega) = \frac{1}{2\pi}\int_{-\infty}^{\infty} dt\, \exp(i\omega t)\langle\delta\rho(\mathbf{q},\, t)\delta\rho^*(\mathbf{q},\, 0)\rangle\ , \tag{A.18}$$

is the *dynamic structure factor*. This is the relation sought: the scattering that produces a wavevector difference $\mathbf{q}$ and frequency shift ω in the scattered light with respect to the incident one is due to the hydrodynamic density fluctuations of wavevector $\mathbf{q}$ and frequency ω. What is usually measured in light scattering spectroscopy is $I(\mathbf{q}, \omega_f, R)$ for a given geometry (fixed $\mathbf{q}$, R) as a function of ω (ω_f). Also, the integrated intensity

$$I(\mathbf{q}, R) = \int_{-\infty}^{\infty} d\omega_f I(\mathbf{q}, \omega_f, R) = \frac{k_f^4 E_0^2 \mu^2}{32\pi^2 m^2 \varepsilon^2 R^2} (\mathbf{n}_i \cdot \mathbf{n}_f)^2 S_{\mathbf{q}} , \qquad (A.19)$$

with

$$S_{\mathbf{q}} = \langle |\delta\rho(\mathbf{q})|^2 \rangle , \qquad (A.20)$$

yields information about the mean-square fluctuations of the density for a given value of the wavevector.

As an example, we will focus in what follows on the dynamic structure factor for a simple fluid *in equilibrium* [2]: $\mathbf{v} = 0$ (fluid at rest), $\rho = \rho_0$ (uniform density), $T = T_0$ (uniform temperature), and $\mathbf{F}_{ext} = 0$ (no external forcing). This will enable us to understand how the hydrodynamic processes that take place in a fluid affect the form of the dynamic structure factor. *Small* fluctuations around equilibrium are described by the linearized hydrodynamic equations

$$\begin{aligned}
\frac{\partial \delta\rho}{\partial t} &= -\rho_0 \nabla \cdot \delta\mathbf{v} , \\
\rho_0 \frac{\partial \delta\mathbf{v}}{\partial t} &= -\nabla \delta p + \eta \Delta \delta\mathbf{v} + \left(\zeta + \frac{\eta}{3}\right) \nabla(\nabla \cdot \delta\mathbf{v}) + \mathbf{F} \quad (\text{in } 3D) , \\
\rho_0 \frac{\partial \delta\mathbf{v}}{\partial t} &= -\nabla \delta p + \eta \Delta \delta\mathbf{v} + \zeta \nabla(\nabla \cdot \delta\mathbf{v}) + \mathbf{F} \quad (\text{in } 2D) , \\
\frac{\partial \delta T}{\partial t} &= -\frac{\beta T_0}{\rho_0 c_v} \nabla \cdot \delta\mathbf{v} + \frac{\kappa}{\rho_0 c_v} \Delta \delta T + F_T , \qquad (A.21)
\end{aligned}$$

where $\mathbf{F}(\mathbf{r}, t) = -\nabla \cdot \mathbf{S}(\mathbf{r}, t)$, $F_T(\mathbf{r}, t) = -\nabla \cdot \mathbf{g}(\mathbf{r}, t)/\rho_0 c_v$, $\beta = (\partial p/\partial T)_\rho$, and c_v is the isochoric specific heat. $\mathbf{S}(\mathbf{r}, t)$ is the fluctuating part of the viscous pressure tensor, and $\mathbf{g}(\mathbf{r}, t)$ the fluctuating part of the heat flow. They are Gaussian white noises with zero mean and covariances that are

[2] This entails a *direct calculation* of the temporal correlation functions from the *linear* Langevin equations. This method is used in Chapter 2.

prescribed by the Landau-Lifshitz theory of hydrodynamic fluctuations according to

$$
\begin{aligned}
&\langle S_{ik}(\mathbf{r}\,,t)\rangle \;=\; 0\;,\\
&\langle g_i(\mathbf{r},\,t)\rangle \;=\; 0\;,\\
&\langle S_{ij}(\mathbf{r},\,t)S_{kl}(\mathbf{r}',\,t')\rangle \;=\\
&\quad=\;\frac{2k_BT}{\rho}\left[\eta\left(\delta_{ik}\delta_{jl}+\delta_{il}\delta_{jk}\right)+\left(\zeta-\frac{\eta}{3}\right)\delta_{ij}\delta_{kl}\right]\delta(\mathbf{r}-\mathbf{r}')\delta(t-t')\quad(3D),\\
&\langle S_{ij}(\mathbf{r},\,t)S_{kl}(\mathbf{r}',\,t')\rangle \;=\\
&\quad=\;\frac{2k_BT}{\rho}\left[\eta\left(\delta_{ik}\delta_{jl}+\delta_{il}\delta_{jk}\right)+\left(\zeta-\eta\right)\delta_{ij}\delta_{kl}\right]\delta(\mathbf{r}-\mathbf{r}')\delta(t-t')\quad(2D),\\
&\langle g_i(\mathbf{r},\,t)g_k(\mathbf{r}',\,t')\rangle \;=\; 2\kappa k_BT\delta(\mathbf{r}-\mathbf{r}')\delta(t-t')\;,\\
&\langle S_{ij}(\mathbf{r},\,t)g_k(\mathbf{r}',\,t')\rangle \;=\; 0\;.
\end{aligned}
\tag{A.22}
$$

Eqs.(A.21) is modified slightly by taking into account the fact that

$$
\delta p=\alpha\delta\rho\;+\;\beta\delta T\;, \tag{A.23}
$$

where

$$
\alpha=\left(\frac{\partial p}{\partial\rho}\right)_T=\gamma c_s^2\,,\quad \beta=\left(\frac{\partial p}{\partial T}\right)_\rho=\rho_0c_s(c_v/T_0)^{1/2}\left(\frac{\gamma-1}{\gamma}\right)^{1/2}\;, \tag{A.24}
$$

$c_s=(\partial p/\partial\rho)_s$ being the velocity of the sound and $\gamma=c_p/c_v$. We take the divergence of the momentum equation and introduce the new variable

$$
\delta\chi\equiv\boldsymbol{\nabla}\cdot\delta\mathbf{v}\;. \tag{A.25}
$$

Then

$$
\frac{\partial\delta\rho}{\partial t}\;=\;-\rho_0\delta\chi\;,
$$

$$
\begin{aligned}
\rho_0\frac{\partial\delta\chi}{\partial\delta t}\;&=\;-\gamma c_s^2\Delta\delta\rho-\rho_0c_s\left(\frac{c_v}{T_0}\right)^{1/2}\left(\frac{\gamma-1}{\gamma}\right)^{1/2}\Delta\delta T+\\
&+\;\left(\zeta+\frac{4}{3}\eta\right)\Delta\delta\chi+\boldsymbol{\nabla}\cdot\mathbf{F}\;\;(\text{in }\;3D)\;,
\end{aligned}
$$

$$
\begin{aligned}
\rho_0\frac{\partial\delta\chi}{\partial\delta t}\;&=\;-\gamma c_s^2\Delta\delta\rho-\rho_0c_s\left(\frac{c_v}{T_0}\right)^{1/2}\left(\frac{\gamma-1}{\gamma}\right)^{1/2}\Delta\delta T+\\
&+\;(\zeta+\eta)\,\Delta\delta\chi+\boldsymbol{\nabla}\cdot\mathbf{F}\;\;(\text{in }\;2D)\;,
\end{aligned}
$$

$$\frac{\partial \delta T}{\partial t} = -c_s \left(\frac{T_0}{c_v}\right)^{1/2} \left(\frac{\gamma - 1}{\gamma}\right)^{1/2} \delta\chi + \frac{\kappa}{\rho_0 c_v} \Delta \delta T + F_T \ . \qquad \text{(A.26)}$$

Taking the Fourier transform of these equations,

$$\frac{\partial \delta\rho(\mathbf{q}, t)}{\partial t} = -\rho_0 \delta\chi(\mathbf{q}, t) \ ,$$

$$\begin{aligned} \frac{\partial \delta\chi(\mathbf{q}, t)}{\partial t} &= \frac{c_s^2}{\gamma\rho_0} q^2 \delta\rho(\mathbf{q}, t) + q^2 c_s \left(\frac{c_v}{T_0}\right)^{1/2} \left(\frac{\gamma - 1}{\gamma}\right)^{1/2} \delta T(\mathbf{q}, t) - \\ &- \frac{\zeta + 4\eta/3}{\rho_0} q^2 \delta\chi(\mathbf{q}, t) + i\mathbf{q} \cdot \mathbf{F}(\mathbf{q}, t) \quad (\text{in } 3D) \ , \end{aligned}$$

$$\begin{aligned} \frac{\partial \delta\chi(\mathbf{q}, t)}{\partial t} &= \frac{c_s^2}{\gamma\rho_0} q^2 \delta\rho(\mathbf{q}, t) + q^2 c_s \left(\frac{c_v}{T_0}\right)^{1/2} \left(\frac{\gamma - 1}{\gamma}\right)^{1/2} \delta T(\mathbf{q}, t) - \\ &- \frac{\zeta + \eta}{\rho_0} q^2 \delta\chi(\mathbf{q}, t) + i\mathbf{q} \cdot \mathbf{F}(\mathbf{q}, t) \quad (\text{in } 2D) \ , \end{aligned}$$

$$\begin{aligned} \frac{\partial \delta T(\mathbf{q}, t)}{\partial t} &= -c_s \left(\frac{T_0}{c_v}\right)^{1/2} \left(\frac{\gamma - 1}{\gamma}\right)^{1/2} \delta\chi(\mathbf{q}, t) - \\ &- \frac{\kappa}{\rho_0 c_v} q^2 \delta T(\mathbf{q}, t) + F_T(\mathbf{q}, t) \ . \end{aligned} \qquad \text{(A.27)}$$

The variances of the noises $\mathbf{F}(\mathbf{q}, t)$ and $F_T(\mathbf{q}, t)$ can be deduced from the Fourier transforms of the expressions in (A.22) for $\langle S_{ij}(\mathbf{r}, t) S_{kl}(\mathbf{r}', t') \rangle$ and $\langle g_i(\mathbf{r}, t) g_k(\mathbf{r}', t') \rangle$.

We are interested in the correlation function $\langle \delta\rho(\mathbf{q}, t) \delta\rho^*(\mathbf{q}, 0) \rangle$; therefore, we solve the *linear* Langevin-type equations (A.27) through the so-called *direct method*, i.e., we find directly the correlation functions

$$\begin{aligned} C_{\rho\rho}(\mathbf{q}, t) &\equiv \langle \delta\rho(\mathbf{q}, t) \delta\rho^*(\mathbf{q}, 0) \rangle \ , \\ C_{\chi\rho}(\mathbf{q}, t) &\equiv \langle \delta\chi(\mathbf{q}, t) \delta\rho^*(\mathbf{q}, 0) \rangle \ , \\ C_{T\rho}(\mathbf{q}, t) &\equiv \langle \delta T(\mathbf{q}, t) \delta\rho^*(\mathbf{q}, 0) \rangle \ . \end{aligned} \qquad \text{(A.28)}$$

Multiplying eqs.(A.27) by $\delta\rho^*(\mathbf{q}, t)$ and taking averages (for $t > 0$) leads to

$$\begin{aligned}
\frac{\partial C_{\rho\rho}}{\partial t} &= -\rho_0 C_{\chi\rho} \ , \\
\frac{\partial C_{\chi\rho}}{\partial t} &= \frac{c_s^2 q^2}{\rho_0 \gamma} C_{\rho\rho} - 2\Gamma q^2 C_{\chi\rho} + q^2 c_s \left(\frac{c_v}{T_0}\right)^{1/2} s C_{T\rho} \\
&\qquad \text{(in both } 3D \text{ and } 2D) \ , \\
\frac{\partial C_{T\rho}}{\partial t} &= -c_s \left(\frac{T_0}{c_v}\right)^{1/2} s C_{\chi\rho} - \gamma \Lambda_T q^2 C_{T\rho} \ ,
\end{aligned} \tag{A.29}$$

where

$$\begin{aligned}
s &= \left(\frac{\gamma - 1}{\gamma}\right)^{1/2} \ , \\
\Gamma &= \frac{\zeta + \frac{4}{3}\eta}{2\rho_0} \ \text{(in } 3D) \ , \\
\Gamma &= \frac{\zeta + \eta}{2\rho_0} \ \text{(in } 2D) \ ,
\end{aligned} \tag{A.30}$$

and the *thermal diffusivity coefficient*

$$\Lambda_T \equiv \frac{\kappa}{\rho_0 c_p} \ . \tag{A.31}$$

We obtained (A.29) using the relations

$$\begin{aligned}
\langle F_i(\mathbf{q}, t)\delta\rho^*(\mathbf{q}, 0)\rangle &= 0 \ \ (t > 0) \ , \\
\langle F_T(\mathbf{q}, t)\delta\rho^*(\mathbf{q}, 0)\rangle &= 0 \ \ (t > 0)
\end{aligned} \tag{A.32}$$

implied by causality. The linear system of equations (A.32) allows us to express the correlations $C_{\rho\rho}$, $C_{\chi\rho}$, and $C_{T\rho}$ as functions of their initial values, i.e., their static, *equilibrium* values.

It is not necessary to find the exact (and rather complicated) solution of the system of equations, as long as we are only interested in the hydrodynamic regime. Let us first consider the underlying physics, in order to understand the relative importance of the different terms. Γq^2, $\Lambda_T q^2$, and $c_s q$ have the dimensions of inverse time. The first two are related to the

dissipative viscous and thermal processes, while the third is connected to sound propagation. For a dilute system, elementary kinetic theory gives

$$\Gamma\,,\quad \Lambda_T \sim c_s l\,, \tag{A.33}$$

where l is the mean free path. That is, the hydrodynamic equations are valid for spatial lengths

$$|\mathbf{r}| \approx \frac{1}{q} >> l\,, \tag{A.34}$$

i.e., as long as

$$\Gamma q^2\,,\quad \Lambda_T q^2 << c_s q\,. \tag{A.35}$$

Introducing the parameter

$$\varepsilon = \frac{2\,\Gamma\, q}{c_s}\,, \tag{A.36}$$

we see that *the hydrodynamic description is valid as long as*

$$\varepsilon << 1\,. \tag{A.37}$$

Although this criterion was justified for the case of a dilute fluid, experiments show that its validity extends to dense fluids as well.
We will simplify eqs.(A.29) by introducing, besides ε, the parameter

$$a = \frac{\gamma\,\Lambda_T}{2\,\Gamma} = O(1)\,. \tag{A.38}$$

We also scale time according to

$$t = \frac{\tau}{c_s\, q}\,, \tag{A.39}$$

and use the dimensionless variables

$$\begin{aligned}
\delta\tilde{\rho} &= \frac{1}{\rho_0}\delta\rho\,,\\
\delta\tilde{\chi} &= \frac{1}{c_s q}\delta\chi\,,\\
\delta\tilde{T} &= \frac{1}{c_s}\left(\frac{c_v}{T_0}\right)^{1/2}\delta T\,.
\end{aligned} \tag{A.40}$$

Then eqs. (A.29) become

$$\frac{\partial}{\partial\tau}\begin{pmatrix} C_{\tilde{\rho}\tilde{\rho}} \\ C_{\tilde{\chi}\tilde{\rho}} \\ C_{\tilde{T}\tilde{\rho}} \end{pmatrix} = \begin{pmatrix} 0 & -1 & 0 \\ 1/\gamma & -\varepsilon & s \\ 0 & -s & -a\varepsilon \end{pmatrix} \cdot \begin{pmatrix} C_{\tilde{\rho}\tilde{\rho}} \\ C_{\tilde{\chi}\tilde{\rho}} \\ C_{\tilde{T}\tilde{\rho}} \end{pmatrix} , \tag{A.41}$$

whose eigenvalues and eigenvectors will be found *perturbatively.* The characteristic polynomial

$$\Lambda^3 + \varepsilon(1+a)\Lambda^2 + (1+a\varepsilon^2)\Lambda + a\varepsilon/\gamma = 0 \tag{A.42}$$

has, to $O(\varepsilon^2)$, the solutions

$$\begin{aligned} \Lambda_1 &= -\frac{\varepsilon a}{\gamma} , \\ \Lambda_{2,3} &= \pm i + \frac{\varepsilon a}{2\gamma} - \frac{\varepsilon(a+1)}{2} . \end{aligned} \tag{A.43}$$

The corresponding left eigenvectors are, to $O(\varepsilon)$,

$$\Phi_1 = \begin{pmatrix} 1 \\ 0 \\ -\frac{1}{\gamma s} \end{pmatrix} , \quad \Phi_2 = \begin{pmatrix} 1 \\ -i \\ s \end{pmatrix} , \quad \Phi_3 = \begin{pmatrix} 1 \\ i \\ s \end{pmatrix} , \tag{A.44}$$

while the right eigenvectors are

$$\begin{aligned} \Phi_1^* &= s^2\left(1, 0, -\frac{1}{s}\right) , \\ \Phi_2^* &= \frac{1}{2\gamma}(1, i\gamma, \gamma s) , \\ \Phi_3^* &= \frac{1}{2\gamma}(1, -i\gamma, \gamma s) . \end{aligned} \tag{A.45}$$

It can be shown easily that the first eigenvalue is associated with the diffusive propagation of entropy; hence Φ_1 is called *entropic* or *thermal diffusivity* mode. The second and third eigenvalues are associated with the propagation of damped pressure (sound) waves, and therefore Φ_2 and Φ_3 are called *sound modes. The condition $\varepsilon << 1$ is therefore just the condition that sound waves propagate faster than they are damped.*

Finally,

$$\begin{pmatrix} C_{\tilde{\rho}\tilde{\rho}}(\mathbf{q},\,\tau) \\ C_{\tilde{\chi}\tilde{\rho}}(\mathbf{q},\,\tau) \\ C_{\tilde{T}\tilde{\rho}}(\mathbf{q},\,\tau) \end{pmatrix} = \sum_{j=1}^{3} C_j(\mathbf{q},\,0)\exp(\Lambda_j\tau)\Phi_j \ ,$$

$$C_j(\mathbf{q},\,\tau) = \Phi_j^* \cdot \begin{pmatrix} C_{\tilde{\rho}\tilde{\rho}}(\mathbf{q},\,0) \\ C_{\tilde{\chi}\tilde{\rho}}(\mathbf{q},\,0) \\ C_{\tilde{T}\tilde{\rho}}(\mathbf{q},\,0) \end{pmatrix} \ . \tag{A.46}$$

In particular, reverting to the original variables,

$$\begin{aligned} C_{\rho\rho}(\mathbf{q},\,t) \;=\; & \left[\frac{\gamma-1}{\gamma}\exp(-\Lambda_T q^2 t) + \frac{1}{\gamma}\exp(-\Gamma_s q^2 t)\cos(c_s q t)\right] C_{\rho\rho}(\mathbf{q},\,0) \\ - \; & \frac{\rho_0}{c_s q}\exp(-\Gamma_s q^2 t)\sin(c_s q t) C_{\chi\rho}(\mathbf{q},\,0) \\ + \; & \frac{\rho_0}{c_s}\left(\frac{c_v}{t_0}\right)^{1/2}\left(\frac{\gamma-1}{\gamma}\right)^{1/2}\left[-\exp(-\Lambda_T q^2 t) + \right. \\ & \left. + \; \exp(-\Gamma_s q^2 t)\cos(c_s q t)\right] C_{T\rho}(\mathbf{q},\,0) \ . \end{aligned} \tag{A.47}$$

Here

$$\Gamma_s = \Gamma + \frac{\gamma-1}{2}\Lambda_T \tag{A.48}$$

is the so-called *sound damping coefficient.* The standard procedure now is to use eqs.(A.27) (multiplied, respectively, by $\delta\rho^*(\mathbf{q},\,t)$, $\delta\chi^*(\mathbf{q},\,t)$ and $\delta T(\mathbf{q},\,t)$ and averaged), as well as Stratonovich's relationships[3] to find the values of the *static* moments and correlators $\langle|\delta\rho(\mathbf{q})|^2\rangle$, $\langle\delta\chi(\mathbf{q})\delta\rho^*(\mathbf{q})\rangle$, $\langle\delta T(\mathbf{q})\delta\rho^*(\mathbf{q})\rangle$, $\langle|\delta\chi(\mathbf{q})|^2\rangle$, etc. But here we shall simply take advantage of the fact that we

[3]Consider a set of n Langevin equations:

$$\frac{d\alpha_i}{dt} \;=\; f_i(\alpha_1,\ldots,\alpha_n) + \xi_i(t) \ \ ,i=1,\ldots n$$

where $\xi_i(t)$ are Gaussian white noises with zero mean and covariances

$$\langle\xi_i(t)\xi_j(t')\rangle \;=\; Q_{ij}\delta(t-t') \ ,$$

and f_i are analytic functions of $\alpha_1,\ldots,\alpha_n$. Then:

$$\langle\alpha_i(t)\xi_j(t')\rangle \;=\; \begin{cases} Q_{ij}/2\,, & t=t' \\ 0\,, & t<t' \end{cases}$$

are concerned with the fluctuations *around equilibrium*, so that $C_{\rho\rho}(\mathbf{q}, 0)$, $C_{\chi\rho}(\mathbf{q}, 0)$ and $C_{T\rho}(\mathbf{q}, 0)$ have their equilibrium values[4]

$$\begin{aligned} C_{\rho\rho}(\mathbf{q}, 0) &= \rho_0^2 k_B T_0 \chi_T V \ , \\ C_{\chi\rho}(\mathbf{q}, 0) &= 0 \ , \\ C_{T\rho}(\mathbf{q}, 0) &= 0 \ . \end{aligned} \tag{A.49}$$

Hence

$$\begin{aligned} C_{\rho\rho}(\mathbf{q}, t) &= \rho_0^2 k_B T_0 \chi_T V \left[\frac{\gamma - 1}{\gamma} \exp(-\Lambda_T q^2 t) \right. \\ &\quad \left. + \frac{1}{\gamma} \exp(-\Gamma_s q^2 t) \cos(c_s q t) \right] \ , \end{aligned} \tag{A.50}$$

and the structure factor reads:

$$\begin{aligned} S_{\mathbf{q}}(\omega) &= \rho_0^2 k_B T_0 \chi_T V \left\{ \frac{\gamma - 1}{\gamma} \frac{2\Lambda_T q^2}{\omega^2 + (\Lambda_T q^2)^2} \right. \\ &+ \left. \frac{1}{\gamma} \left[\frac{\Gamma_s q^2}{(\omega + c_s q)^2 + (\Gamma_s q^2)^2} + \frac{\Gamma_s q^2}{(\omega - c_s q)^2 + (\Gamma_s q^2)^2} \right] \right\} \ . \end{aligned} \tag{A.51}$$

---

[4]Consider a function $f(\mathbf{r}, \mathbf{r}') = f(\mathbf{r} - \mathbf{r}')$ and its Fourier transform

$$f(\mathbf{q}, -\mathbf{q}) = \int_V \int_V e^{i\mathbf{q}\cdot\mathbf{r}} e^{-i\mathbf{q}\cdot\mathbf{r}'} f(\mathbf{r} - \mathbf{r}') d\mathbf{r} d\mathbf{r}' \ .$$

With a change of variables (for a simplex domain V)

$$\mathbf{R} = \frac{\mathbf{r} + \mathbf{r}'}{2} \ , \ \mathbf{s} = \mathbf{r} - \mathbf{r}' \ , V \times V \to V \times V' \ ,$$

we obtain

$$f(\mathbf{q}, -\mathbf{q}) = \int_V d\mathbf{R} \int_{V'} e^{i\mathbf{q}\cdot\mathbf{s}} f(\mathbf{s}) d\mathbf{s} = \frac{V}{(2\pi)^3} \int_{V'} e^{i\mathbf{q}\cdot\mathbf{s}} f(\mathbf{s}) d\mathbf{s} \ .$$

In particular, if $f(\mathbf{r} - \mathbf{r}') = \delta(\mathbf{r} - \mathbf{r}')$,

$$f(\mathbf{q}, -\mathbf{q}) = V \ .$$

For the equilibrium correlation functions [60]

$$\begin{aligned} \langle \delta\rho(\mathbf{r}) \delta\rho(\mathbf{r}') \rangle &= \rho_0^2 k_B T_0 \chi_T \delta(\mathbf{r} - \mathbf{r}') \ , \\ \langle \delta\rho(\mathbf{r}) \delta\mathbf{v}(\mathbf{r}') \rangle &= 0 \ , \\ \langle \delta\rho(\mathbf{r}) \delta T(\mathbf{r}') \rangle &= 0 \ . \end{aligned}$$

This leads directly to eqs. (A.49).

The spectrum of the scattered light thus consists of *three Lorentzians* - the so-called *Rayleigh-Brillouin spectrum.* The central peak at $\omega = 0$ (width $\Lambda_T q^2$), called the *Rayleigh peak*, arises from diffusive entropy fluctuations (i.e., it corresponds to the thermal diffusivity mode). The two symmetric spectral lines that are shifted in frequency by $\pm c_s q$ respectively (and have a width $\Gamma_s q^2$) are the Stokes and anti-Stokes components of the *Brillouin doublet*; they correspond to (thermally excited) propagating sound waves. As may be seen directly, the Rayleigh-Brillouin spectrum gives information on both thermodynamic quantities (γ, c_s, χ_T) as well as transport coefficients (Λ_T, κ, Γ_s). As already pointed out at the beginning of this Appendix, this structure of the spectrum can easily be understood in terms of the Doppler effect. Indeed, a perturbation in density of wavevector $\mathbf{q}$ propagates in the fluid through two mechanisms. The first is *sound propagation* with velocity c_s, parallel and anti-parallel to $\mathbf{q}$, which leads to a Doppler shift $\pm c_s q$ in the frequency of the scattered light (i.e., to the Brillouin peaks). Also, the microscopic mechanism responsible for the damping of the sound waves (the *diffusion* of the sound wavefront) results in a finite width of the spectral lines (i.e., a dispersion of the frequencies of the scattered waves around the peaks $\omega_i \pm c_s q$). This is, of course, also a Doppler effect, but one arising from a disordered motion. The second mechanism of *thermal diffusion* of density does not modify the frequency (i.e., the peak is centered at $\omega = 0$), but leads to a finite width of the spectral line. For more details, we cite Refs. [61], [62], and [63].

We note that this form of the scattered spectrum is obtained as long as the fluid is far from any critical point, i.e., the fluctuations are small and the linear formalism is valid. In the vicinity of a critical point, fluctuations are greatly enhanced and become long-ranged; the linear formalism breaks down and the hydrodynamic modes become coupled nonlinearly. This is reflected in the spectrum of the scattered light through the appearance of critical opalescence. We also note that the boundary effects have been neglected in the above formalism.

It is interesting to ask what happens in *nonequilibrium* systems. As soon as the fluid is driven out of equilibrium, the hydrodynamic fluctuations become long-ranged in space and time, and this will affect the structure of the dynamic form factor in a specific manner that carries information on the nonequilibrium constraints imposed on the system. For example, let us consider a case that has been extensively studied both theoretically and

experimentally, namely, a fluid subjected to a stationary temperature gradient. In the first approximation, the temperature gradient may be expected to cause an asymmetry in the Brillouin lines, since the sound waves propagating parallel to the temperature gradient will probe regions of different temperatures (an effect that is proportional to the temperature gradient). For sufficiently large temperature gradients, the Rayleigh line is also modified (an effect of the second order); it is found to be a superposition of two Lorentzians centered at $\omega = 0$. One of these is still caused by a heat mode and has a width $\Lambda_T q^2$, though its amplitude is enhanced; the other Lorentzian has a width $\eta q^2/\rho_0$ and is due to a viscous mode that couples to the density in the presence of the temperature gradient.

Many of the theoretical predictions of the Landau-Lifshitz fluctuating hydrodynamics have been well verified through light scattering experiments [15]. There remains, however, a paucity of experimental results, because of numerous practical and technical complications. Given these limitations on laboratory experiments, another useful approach is by direct computer simulations [19]. The overall conclusion arrived at is that, except for certain extreme conditions (e.g., high Mach number shock waves [64]), the hydrodynamic equations remain surprisingly robust [5]. Hence they may be used in describing fluids far from equilibrium, with the added advantage of their relative simplicity as compared to more fundamental approaches [9, 11].

[5] See, however, Ref. [65] which reports on the failure of the hydrodynamic theory in describing plane Poiseuille flow for a dilute gas.

Appendix B

Adiabatic Elimination of Fast Variables

The fluctuations of the hydrodynamic variables can be studied by adopting a Langevin approach and incorporating the effect of thermal agitation in a phenomenological manner, by the addition of a purely stochastic term to the macroscopic hydrodynamic equations. This term is not arbitrary, of course: for fluctuations around equilibrium it must be consistent with standard linear response theory and the fluctuation-dissipation relationships that follow from this. Its amplitude is inversely proportional to the square root of the system size, and therefore this term is *small* in any macroscopic system (i.e., we are in the so-called *weak noise limit*); its effect is small as long as the macroscopic state of the system is stable, but becomes *macroscopically* important when the stability of the system is altered, e.g., in the vicinity of a bifurcation. One can say, in general, that the relative fluctuations are greatly enhanced in the vicinity of an instability point, but the concrete way in which this happens depends essentially on the form of the nonlinearities in the system.

The study of the behavior of the system in the vicinity of a critical point is greatly simplified because the actual dynamics takes place in a restricted, low-dimensional geometry (on the so-called *center manifold*), and the governing dynamical laws also get simplified, as will be explained below. While these effects can be understood relatively unambiguously in a deterministic system, their settlement and interpretation are more difficult in the case of stochastic evolution. In order to clarify these ideas, we start by review-

ing some basic elements from the theory of deterministic dynamical systems, and subsequently turn to the more complicated case of stochastic dynamical systems *in the limit of weak noise.*

B.1 Deterministic Systems

Consider a general autonomous n-dimensional dynamical system

$$\dot{x} = f(x) \ , \quad x = \{x_i\}_{i=1,\dots,n} \in I\!R^n, \ f : I\!R^n \to I\!R^n \ , \tag{B.1}$$

where f is a nonlinear function of the x_i's. Suppose that (B.1) admits a *steady-state* solution (a *fixed* or *critical point*) x_0,

$$f(x_0) = 0 \ . \tag{B.2}$$

An important question concerning the fixed point is that of its *stability*; this can usually be reduced to the study of the stability of the trivial solution of the associated *linear* system

$$\dot{y} = Df(x_0)y \equiv Ay \ , \quad y = x - x_0 \ , \tag{B.3}$$

where $Df(x_0)$ is the Jacobian matrix of f at the point x_0. The critical point x_0 is *asymptotically* stable if all the eigenvalues of the *stability matrix* A have negative real parts.

Another questions refers to the *form* of the phase trajectories of the dynamical system (B.1) in the vicinity of the fixed point. There is a great difference between a *hyperbolic* fixed point (i.e., for which none of the eigenvalues of A has a real part that is zero) and that of a *non-hyperbolic* fixed point. In any case, the central role in the analysis is played by the *invariant manifolds.* A surface $S \subset I\!R^n$ is called an *invariant manifold* [1] for the dynamics (B.1) if any phase trajectory that intersects S at a certain instant of time is entirely contained in S. We look first at the invariant manifolds of the associated linear dynamics (B.2), as they are relevant to the structure of the invariant manifolds of (B.1). Obviously, each sub-space spanned by an eigenvector of the stability matrix A is an invariant manifold for the linear dynamics around x_0. It is useful to regroup these elementary manifolds into

[1] S has to have the structure of a differentiable manifold of some rank ≥ 1, but we do not go into these technicalities here.

three larger invariant manifolds E^s, E^u and E^c, of dimensions s, u and c respectively:

$$\mathbb{R}^n = E^s \oplus E^u \oplus E^c \ . \tag{B.4}$$

E^s, E^u and E^c are spanned by the s, u and c eigenvectors of the stability matrix A that correspond, respectively, to eigenvalues of A with positive, negative and zero real parts. They are called the *stable, unstable* and *center* manifolds, as the trajectories on them respectively approach the fixed point, flow away from it, and neither approach nor move away from it in the long-time limit. It is useful to introduce a linear transformation of (B.2) that separates these behaviors,

$$T\dot{y} \equiv \begin{pmatrix} \dot{u} \\ \dot{v} \\ \dot{w} \end{pmatrix} = \begin{pmatrix} A_s & 0 & 0 \\ 0 & A_u & 0 \\ 0 & 0 & A_c \end{pmatrix} \cdot \begin{pmatrix} u \\ v \\ w \end{pmatrix} \ , \tag{B.5}$$

where A_s is a $s \times s$ matrix that only has eigenvalues with negative real parts. Corresponding statements apply to the matrices A_u and A_c. Returning to the nonlinear dynamics specified by (B.1), this can be written down in a simpler form by shifting the fixed point to the origin and then using the transformation T to change variables to u, v, w:

$$\begin{pmatrix} \dot{u} \\ \dot{v} \\ \dot{w} \end{pmatrix} = \begin{pmatrix} A_s & 0 & 0 \\ 0 & A_u & 0 \\ 0 & 0 & A_c \end{pmatrix} \cdot \begin{pmatrix} u \\ v \\ w \end{pmatrix} + \begin{pmatrix} N_s(u, v, w) \\ N_u(u, v, w) \\ N_c(u, v, w) \end{pmatrix} \ , \tag{B.6}$$

where the N's stand for the nonlinear terms. It can then be demonstrated, in general, that the fixed point $(u, v, w) = (0, 0, 0)$ possesses an s-dimensional *local* stable invariant manifold W^s, a u-dimensional *local* unstable invariant manifold W^u, and a c-dimensional *local* invariant center manifold W^c, that intersect at the origin and to which the Euclidean spaces E^s, E^u, and E^c are respectively tangent at the origin. More precisely,

$$\begin{aligned}
W^s &= \{(u, v, w) \in \mathbb{R}^s \times \mathbb{R}^u \times \mathbb{R}^c | \, v = h^s_v(u), \, w = h^s_w(u), \\
&\quad h^s_{v,w}(0) = 0, \, Dh^s_{v,w}(0) = 0, \, ||u|| \text{ sufficiently small}\} \ , \\
W^u &= \{(u, v, w) \in \mathbb{R}^s \times \mathbb{R}^u \times \mathbb{R}^c | \, u = h^u_u(v), \, w = h^u_w(v), \\
&\quad h^u_{u,w}(0) = 0, \, Dh^u_{u,w}(0) = 0, \, ||v|| \text{ sufficiently small}\} \ , \\
W^c &= \{(u, v, w) \in \mathbb{R}^s \times \mathbb{R}^u \times \mathbb{R}^c | \, u = h^c_u(w), \, v = h^c_v(w), \\
&\quad h^c_{u,v}(0) = 0, \, Dh^c_{u,v}(0) = 0, \, ||w|| \text{ sufficiently small}\} \ .
\end{aligned} \tag{B.7}$$

Moreover, W^s and W^u have the asymptotic properties of their local tangent spaces E^s and E^u respectively. Note that if the fixed point is hyperbolic (E^c is a null space), then the solutions of the nonlinear vector field (B.6) in a sufficiently small neighbourhood of the origin behave in essentially the same way as the solutions of the associated linear vector field. For a non-hyperbolic fixed point, however, the nature of the solutions in the center manifold W^c cannot in general be inferred from the nature of the solutions in the local tangent space E^c. A deeper analysis is required, along the lines described below.

We will assume, for simplicity, that there is no unstable dynamics in the neighbourhood of the origin, i.e., $W^u = \emptyset$; this is a rather drastic limitation, but it can be shown [66] that the inclusion of the unstable directions does not modify in any essential manner the *formal* aspects of the theory to be presented. Therefore, consider vector fields of the form

$$\begin{aligned} &\dot{w} = A_c w + N_c(w, u) \ , \\ &\dot{u} = A_s u + N_s(w, u) \ , \\ &(w, u) \in I\!R^c \times I\!R^s \ , \\ &N_c(0, 0) = 0, N_s(0, 0) = 0 \ , \\ &DN_c(0, 0) = 0, \ DN_s(0, 0) = 0 \ . \end{aligned} \tag{B.8}$$

Here A_c [resp., A_s] is a $c \times c$ [resp.,$s \times s$] matrix whose eigenvalues have zero [negative] real parts, and the N's represent nonlinear terms. As we have seen, there exists a local invariant center manifold for (B.8),

$$\begin{aligned} W^c \ = \ &\{(w, u) \in I\!R^c \times I\!R^s | \, u = h(w), \, h(0) = 0, \, Dh(0) = 0, \\ &||w|| \text{ sufficiently small}\} \ . \end{aligned} \tag{B.9}$$

The dynamics of (B.8) restricted to the center manifold is given, for $||w||$ sufficiently small, by the c-dimensional vector field w satisfying

$$\dot{w} = A_c w + N_c(w, h(w)) \ . \tag{B.10}$$

The dynamics of (B.10) near $w = 0$ determines that of (B.8) near $(w, u) = (0, 0)$. Indeed, the type of stability of the zero solution of (B.10) (whether it is stable, or asymptotic stable, or unstable) dictates the stability of the zero solution of (B.8). Further, if $(w(t), u(t))$ is some solution of (B.8) starting

sufficiently close to the origin, then there exists a solution $\psi(t)$ of (B.10) such that, in the long-time limit,

$$\begin{aligned} w(t) &= \psi(t) + O(e^{-\gamma t}) \ , \\ u(t) &= h(\psi(t)) + O(e^{-\gamma t}) \ , \end{aligned} \tag{B.11}$$

where γ is the smallest absolute value of the (negative) real parts of the eigenvalues λ_{A_s} of A_s,

$$\gamma = \min\{-[Re(\lambda_{A_s}]\} \ . \tag{B.12}$$

The meaning of all this is that for trajectories which start outside the center manifold, the dynamics in the initial stages evolves rapidly, being dictated by the eigenvalues of A_s in directions normal to the center manifold. Consequently, these trajectories "contract" onto the center manifold on a fast time scale of the order of γ^{-1}. The subsequent evolution takes place on the center manifold, on a slow time scale, and is governed by the nonlinear terms $N_c(w, h(w))$.

The equation of the center manifold is obtained by imposing the condition that it be invariant with respect to the dynamics (B.8),

$$Dh(w)[A_c w + N_c(w, h(w)] - A_s h(w) - N_s(w, h(w)) = 0 \ , \tag{B.13}$$

which is in general a complicated nonlinear partial differential equation. However, for most physical applications, the nonlinear terms are generally polynomials; (B.13) then admits a solution in powers of w, to any desired degree of accuracy. We note in this context that this polynomial expansion, in its lowest order, is equivalent to that obtained through the *adiabatic elimination of variables* [46, 47]. This method takes into account the rapid contraction of the phase space trajectories onto the center manifold, and exploits the fact that, at each instant of time, the "fast-variables" u "follow" the movement of the "slow variables" w - i.e., they relax rapidly to values dictated by the instantaneous, slowly varying values of the w's. This permits one to set $\dot{u} \approx 0$ in eq.(B.8), to obtain

$$A_s u + N_s(w, u) = 0 \ . \tag{B.14}$$

This is solved for u (iteratively in powers of w), and the result is inserted in the first equation in (B.8), to obtain the evolution equation for the slow variables w.

Some of the low-order nonlinear terms in (B.10) can sometimes be eliminated through a nonlinear transformation on w (a *similarity transformation*), leading to the so-called *normal form* for (B.10).

B.1.1 Center Manifolds Depending on Parameters

In many physical situations, the dynamical system (B.8) depends on a set of p parameters collectively denoted by μ, i.e.,

$$\begin{aligned}
&\dot{w} = A_c w + N_c(w, u, \mu) \ , \\
&\dot{u} = A_s u + N_s(w, u, \mu) \ , \\
&(w, u, \mu) \in I\!R^c \times I\!R^s \times I\!R^p \ , \\
&N_c(0, 0, 0) = 0, \ N_s(0, 0, 0) = 0 \ , \\
&DN_c(0, 0, 0) = 0, \ DN_s(0, 0, 0) = 0 \ .
\end{aligned} \tag{B.15}$$

The eventual dependence of the matrices A_c and A_s on μ can be circumvented, as will be shown below.

In order to handle such a parametrized system, one considers the parameters μ as new *dependent variables*, i.e.,

$$\begin{aligned}
&\dot{w} = A_c w + N_c(w, u, \mu) \ , \\
&\dot{\mu} = 0 \ , \\
&\dot{u} = A_s u + N_s(w, u, \mu) \ .
\end{aligned} \tag{B.16}$$

Although this seems to be just a formal operation, it is fact an important step from the point of view of *bifurcation theory*. According to the discussion in the foregoing, there exists a local center manifold of the fixed point $(w, \mu, u) = (0, 0, 0)$ of the dynamical system (B.16), given by

$$\begin{aligned}
W^c \ = \ &\{(w, \mu, u) \in I\!R^c \times I\!R^p \times I\!R^s | \, u = h(w, \mu), \, h(0, 0) = 0, \\
&Dh(0, 0) = 0, \, ||w|| \text{ sufficiently small}, \ ||\mu|| \text{ sufficiently small}\} \ .
\end{aligned} \tag{B.17}$$

The vector field (B.16) relaxes rapidly to the center manifold dynamics,

$$\begin{aligned}
&\dot{w} = A_c w + N_c(w, h(w, \mu), \mu) \ , \\
&\dot{\mu} = 0 \ .
\end{aligned} \tag{B.18}$$

It is very important that the center manifold exists in a sufficiently small neighbourhood of the origin (0, 0) in *both* w and μ. Indeed, it is possible that *bifurcations* of the point (0, 0) appear (see below), i.e., stationary solutions can be created or destroyed by perturbing nonhyperbolic fixed points. The fact to remember is that *all the bifurcating solutions will be contained in the center manifold.* For computing the center manifold $u = h(w, \mu)$, we impose the condition that it be invariant under the dynamics (B.16): this gives

$$D_x h(w, \mu)\,[A_c w + N_c(w, h(w, \mu), \mu)] - A_s h(w, \mu) - N_s(w, h(w, \mu), \mu) = 0\ , \tag{B.19}$$

which is very similar to eq. (B.13).

Finally, note that when the parameters are considered as new dependent variables, terms like μw and μu become *nonlinear* terms and get included in N_c and N_s, respectively, and not in A_c and A_s.

B.1.2 Local Bifurcation of a Fixed Point

Let us assume for simplicity that the local center manifold of the fixed point $(w, \mu, u) = (0, 0, 0)$ of the dynamical system (B.15) is one-dimensional ($c = 1$), and also that there is only one parameter in the system ($p = 1$). Then the orbit structure near (0, 0, 0) is determined by the associated center manifold equation (B.18), that takes the simple form

$$\dot{w} = f(w, \mu)\ , \tag{B.20}$$

with

$$f(0, 0) = 0 \tag{B.21}$$

(the fixed point condition) and

$$\frac{\partial f}{\partial w}(0, 0) = 0 \tag{B.22}$$

(the zero eigenvalue condition). Depending on the values of μ, eq.(B.20) admits, in general, different stationary points

$$\dot{w} = 0 \rightarrow f(w, \mu) = 0 \rightarrow w = w(\mu) \tag{B.23}$$

of different stabilities. We say that the hyperbolic fixed point $(w, \mu) = (0, 0)$ of a one-parameter family of the one-dimensional vector field (B.20) undergoes a bifurcation at $\mu = 0$ if the flow for w near zero and μ *near* zero is not qualitatively the same as the flow *at* $\mu = 0$.

- Two flows
$$\dot{x} = f(x)\,, \quad \dot{y} = g(y) \quad (x,\, y \in I\!R)$$
are said to be *qualitatively equivalent* if there is a diffeomorphism that transforms orbits of the first flow to orbits of the second flow, preserving the time-orientation (but not necessarily the parametrization by time). Therefore, the existence of bifurcating solutions means the existence of at least two types of trajectories that are not qualitatively equivalent - those for $\mu = 0$ and those for $\mu \neq 0$.

- In practice, the hyperbolic fixed point $(w,\, \mu) = (0,\, 0)$ of a one-dimensional vector field is a bifurcation point if
- either more than one curve of fixed points (B.23) passes through $(0,\, 0)$ in the $(w,\, \mu)$ plane,
or
- only one curve of fixed points passes through $(0,\, 0)$, and it lies entirely on one side of the line $\mu = 0$ in the $(w,\, \mu)$ plane.

- The condition that a fixed point is hyperbolic is a necessary but not sufficient condition for a bifurcation to occur in one-parameter families of vector fields.

The foregoing comprises the fundamentals to be recalled before we go on to the case of stochastic dynamic evolution in the presence of a weak noise. The connection of the latter to the deterministic case will become clear as we proceed. For further details we cite Refs. [66]-[68].

B.2 Adiabatic Elimination of Stochastic Variables in the Limit of a Weak Noise

As mentioned in the beginning of this Appendix, in studying the stochastic behavior of a macroscopic system, one is generally led to a set of parameter-dependent nonlinear Langevin equations in the limit of a weak noise:

$$\begin{aligned} &\dot{W}_i = f_i(W,\, \mu) + \varepsilon^{1/2} F_i(t)\,, \quad i = 1, \ldots n\,, \\ &W = \{W_i\}_{i=1,\ldots n}\,, \quad \varepsilon << 1\,, \\ &\langle F_i(t) \rangle = 0\,, \quad \langle F_i(t) F_j(t') \rangle = Q_{ij}\delta(t - t')\,. \end{aligned} \tag{B.24}$$

The corresponding Fokker-Planck equation reads

$$\frac{\partial P(W,t)}{\partial t} = -\frac{\partial}{\partial W_i}\left[f_i(W,\, \mu) P(W,\, t)\right] + \frac{\varepsilon}{2} Q_{ij} \frac{\partial^2}{\partial W_i \partial W_j} P(W,\, t)\,. \tag{B.25}$$

One is usually interested in the asymptotic, *stationary* behavior of the system, in the limit of a vanishingly small noise. For *finite* times t it has been proven [69] that the stochastic trajectory $W(t)$ and the deterministic (macroscopic) trajectory $\bar{W}(t)$, given by

$$\dot{\bar{W}}_i(t) = f_i(\bar{W}, \mu) \ , \tag{B.26}$$

stay close to each other almost everywhere, at least if this is initially the case. More precisely,

$$||W(t) - \bar{W}(t)|| \sim O(\varepsilon^{1/2}) \ , \quad \forall \ t \geq t_{initial} \ , \quad t \ finite \ . \tag{B.27}$$

Moreover, for the case of a $1D$ system, the stochastic trajectory tends to the deterministic one in the limit $\varepsilon \to 0$ for *any* time - *including* the asymptotic limit $t \to \infty$ - *provided* that the macroscopic state is unique and globally stable (this includes states of marginal stability). However, nothing can be said, in general, about the *way* in which the stochastic trajectory approaches the deterministic one in the long time limit,

$$\lim_{t\to\infty} ||W(t) - \bar{W}(t)|| \sim O(\varepsilon^{?}) \ . \tag{B.28}$$

Things are even more complicated when the deterministic counterpart exhibits a *critical behavior*, i.e., in the vicinity of a bifurcation point. (See [48] for a clear illustration of this point through a simple example.) As long as the system is far from a critical point, the fluctuations of all the variables *have a Gaussian character and behave like* $\varepsilon^{1/2}$. When the critical point is approached, the fluctuations get amplified and eventually lose their Gaussian character. Also, the fluctuations of the slow modes and of the fast modes acquire different ε-scaling behaviors.

In order to clarify this problem, we shall limit ourselves to the case that is relevant for our study of Kolmogorov flow in Chapter 3. (We refer to [48] for more general cases.) The stochastic dynamics of concern is described by the set of nonlinear Langevin equations

$$\begin{aligned}
\frac{\partial W_1}{\partial t} &= \lambda_1 W_1 - \alpha_1 W_1 \left(W_2 + W_2^*\right) - \beta_1 W_1^* W_3 + \varepsilon^{1/2} F_1 \ , \\
\frac{\partial W_2}{\partial t} &= \lambda_2 W_2 + \alpha_2 W_1 W_1^* + \varepsilon^{1/2} F_2 \ , \\
\frac{\partial W_3}{\partial t} &= \lambda_3 W_3 - \beta_2 W_1^2 + \varepsilon^{1/2} F_3 \ ,
\end{aligned} \tag{B.29}$$

and their complex conjugates [2]. Here the α's and β's are constants (usually positive), λ_2 and λ_3 are always strictly negative, and λ_1 is negative below the critical point and becomes zero at the critical point. F_1, F_2, F_3 and their complex conjugates are Gaussian white noises with zero mean and covariances given by

$$\begin{aligned}
&\langle F_i(t)F_j(t')\rangle = 0 \ , \\
&\langle F_i(t)F_j^*(t')\rangle = Q_i\delta_{ij}\delta(t-t') \ , i,\, j = 1,2,3 \ .
\end{aligned} \tag{B.30}$$

The corresponding Fokker-Planck equation for the associated (transition) probability reads

$$\begin{aligned}
&\frac{\partial P(W_1,\, W_2,\, W_3,\, W_1^*,\, W_2^*,\, W_3^*, t)}{\partial t} = \\
&-\frac{\partial}{\partial W_1}\left\{[\lambda_1 W_1 \, - \, \alpha_1(W_2 + W_2^*)W_1 - \beta_1 W_1^* W_3]\, P\right\} + \text{c.c.} \\
&-\frac{\partial}{\partial W_2}\left[(\lambda_2 W_2 \, + \, \alpha_2|W_1|^2)\, P\right] + \text{c.c.} \\
&-\frac{\partial}{\partial W_3}\left[(\lambda_3 W_3 \, - \, \beta_2 W_1^2)\, P\right] + \text{c.c.} \\
&+\varepsilon\left(Q_1\frac{\partial^2}{\partial W_1 \partial W_1^*} + Q_2\frac{\partial^2}{\partial W_2 \partial W_2^*} + Q_3\frac{\partial^2}{\partial W_3 \partial W_3^*}\right) P \ ,
\end{aligned} \tag{B.31}$$

where c.c. stands for the complex conjugate of the corresponding preceding expression. We find the correct ε-behavior of W_1, W_2, W_3 by introducing the scaled variables

$$x = \varepsilon^{a-1}W_1, \; y = \varepsilon^{b-1}W_2, \; z = \varepsilon^{b-1}W_3 \ , \tag{B.32}$$

and choosing the exponents a and $b < 1$ such that the following requirements are satisfied at all times, including the asymptotic limit $t \to \infty$:

- $C1$: $P(x,\, y,\, z,\, x^*,\, y^*,\, z^*,\, t)$ is normalizable in the limit $\varepsilon \to 0$;
- $C2$: P does not factorize trivially into a product of δ-functions in the variables;
- $C3$: all the moments of x, y and z are *finite* for $\varepsilon \to 0$.
  Note that this condition excludes the possibility of Brownian processes (with or without drift) for the variables x, y, z.

[2] An asterisk denotes the complex conjugate.

Also, in order to explore the vicinity of the critical point, we set

$$\lambda_1 = \varepsilon^c \Lambda \ , \tag{B.33}$$

where Λ is some negative constant, and the exponent c is a measure of the distance to the critical point. When $c = 0$, we are far away from the critical point, and increasing c means an approach to the threshold; there exists a critical value of c (yet to be determined) which delimits the critical regime from the noncritical one.

Let us first consider a Gaussian initial condition for P, i.e., a scaling $a = b = 1/2$. Then, to leading order in ε, eq.(B.31) reduces to a linear Fokker-Planck equation for the scaled variables,

$$\begin{aligned}\frac{\partial P(x,\, y,\, z,\, x^*,\, y^*,\, z^*,\, t)}{\partial t} &= \left[-\frac{\partial}{\partial x}(\lambda_1 x P)\right. \\ &\left. -\frac{\partial}{\partial y}(\lambda_2 y P) - \frac{\partial}{\partial z}(\lambda_3 z P)\right] + \text{c.c.} \\ &+ \left(Q_1 \frac{\partial^2}{\partial x \partial x^*} + Q_2 \frac{\partial^2}{\partial y \partial y^*} + Q_3 \frac{\partial^2}{\partial z \partial z^*}\right) P \ . \end{aligned} \tag{B.34}$$

Therefore the probability distribution retains its Gaussian nature. The evolution equations for the variances are easily deduced to be

$$\begin{aligned}&\frac{d}{dt}\langle x_i x_j \rangle = (\lambda_i + \lambda_j)\langle x_i x_j \rangle \ , \\ &\frac{d}{dt}\langle x_i x_j^* \rangle = (\lambda_i + \lambda_j)\langle x_i x_j \rangle + Q_i \delta_{ij} \ , \ \{x,\, y,\, z\} = \{x_i\}_{i=1,2,3}. \end{aligned} \tag{B.35}$$

It is then seen that the scaling $a = b = 1/2$ is still valid for the asymptotic stationary state, provided the variances of the scaled variables *do not diverge*. This clearly depends on the eigenvalues λ_i, $i = 1, 2, 3$. Indeed, for $t \to \infty$,

$$\langle x_i x_j \rangle_{st} = 0, \qquad \langle x_i x_j^* \rangle_{st} = 0 \quad \text{for } i \neq j \ ,$$

$$\langle |x_i|^2 \rangle_{st} = -\frac{Q_i}{2\lambda_i} \qquad (i, j = 1, 2, 3) \ , \tag{B.36}$$

and so *the Gaussian law is valid as long as the stationary state is asymptotically stable.* At the critical point we have $\lambda_1 = 0$, and therefore $\langle |x|^2 \rangle_{st} \to \infty$

according to the above formulas; it is clear that a different scaling behavior now comes into play.

We now introduce the scaled variables defined in (B.32) and (B.33) in (B.31), to obtain

$$\begin{aligned}
&\frac{\partial P(x,\, y,\, z,\, x^*,\, y^*,\, z^*,\, t)}{\partial t} = \\
&\left\{ -\frac{\partial}{\partial x}\left\{\left[\Lambda\varepsilon^c x - \alpha_1\varepsilon^{1-b}x(y+y^*) - \beta_1\varepsilon^{1-b}x^*z\right]P\right\}\right. \\
&-\frac{\partial}{\partial y}\left[\left(\lambda_2 y + \alpha_2\varepsilon^{1+b-2a}|x|^2\right)P\right] \\
&\left.-\frac{\partial}{\partial z}\left[\left(\lambda_3 z - \beta_2\varepsilon^{1+b-2a}x^2\right)P\right]\right\} + \text{c.c.} \\
&+\left(Q_1\varepsilon^{2a-1}\frac{\partial^2}{\partial x\partial x^*} + Q_2\varepsilon^{2b-1}\frac{\partial^2}{\partial y\partial y^*} + Q_3\varepsilon^{2b-1}\frac{\partial^2}{\partial z\partial z^*}\right)P\,.
\end{aligned} \tag{B.37}$$

Consider also the evolution equation for the reduced distribution $P(x,\, x^*,\, t)$ obtained from (B.37) by integrating with respect to y, z, y^* and z^*:

$$\begin{aligned}
\frac{\partial P(x,\, x^*,\, t)}{\partial t} &= -\frac{\partial}{\partial x}\left\{\left[\Lambda\varepsilon^c x - \alpha_1\varepsilon^{1-b}x\left(\langle y|x,\, x^*\rangle + \langle y^*|x,\, x^*\rangle\right)\right.\right. \\
&- \left.\left.\beta_1\varepsilon^{1-b}x^*\langle z|x,\, x^*\rangle\right]P(x,\, x^*,\, t)\right\} \\
&+ Q_1\varepsilon^{2a-1}\frac{\partial^2 P(x,\, x^*,\, t)}{\partial x\partial x^*}\,,
\end{aligned} \tag{B.38}$$

where $\langle y|x,\, x^*\rangle$ [resp., $\langle y^*|x,\, x^*\rangle$, $\langle z|x,\, x^*\rangle$] is the mean of y [resp., y^*, z] given x, x^*. That is,

$$\begin{aligned}
\langle y|x,\, x^*\rangle &= \int y P(x,\, y,\, z,\, x^*,\, y^*,\, z^*,\, t)dy\, dz\, dy^*\, dz^* \\
&= P(x,\, x^*,\, t)\int y P(y,\, z,\, y^*,\, z^*,\, t|x,\, x^*)dy\, dz\, dy^*\, dz^*\,.
\end{aligned} \tag{B.39}$$

Analogous expressions hold good for $\langle y^*|x,\, x^*\rangle$ and $\langle z|x,\, x^*\rangle$.

Imposing the conditions $(C1) - (C3)$ on $P(x,\, y,\, z,\, x^*,\, y^*,\, z^*,\, t)$, $P(x,\, x^*,\, t)$ and $P(y,\, z,\, y^*,\, z^*,\, t|x,\, x^*)$, it is found that a and b satisfy the following set of inequalities:

(*i*)

$$\frac{1}{2} \leq a,\, b < 1 \tag{B.40}$$

Proof: Let us suppose the contrary - for example, that $b < 1/2$ and a is arbitrary (the case $a < 1/2$ and b arbitrary is analogous). $(C2)$ requires that the processes are not dominated by the noise, and therefore

$$1 + b - 2a < 0 \rightarrow a > 1/2\ .$$

The equation for the conditional probability, as deduced from (B.37) to leading order in ε, reduces to

$$\begin{aligned} \frac{\partial P(y,\, z,\, y^*,\, z^*,\, t|x,\, x^*)}{\partial t} &= \varepsilon^{1+b-2a}\left(-\alpha_2|x|^2\frac{\partial}{\partial y} + \beta_2 x^2\frac{\partial}{\partial z}\right)P + \text{c.c.} \\ &+ \varepsilon^{2b-1}\left(Q_2\frac{\partial^2}{\partial y\partial y^*} + Q_3\frac{\partial^2}{\partial z\partial z^*}\right)P\ , \end{aligned} \tag{B.41}$$

and this (with a fixed drift term) is a Brownian process for $\{y(t),\, z(t),\, y^*(t),\, z^*(t)\}$, contrary to the condition $(C3)$.

(*ii*)

$$a > \frac{1}{2} \tag{B.42}$$

Otherwise, the process $\{x(t),\, x^*(t)\}$ is purely stochastic, as seen from (B.38).

(*iii*)

$$b < a \tag{B.43}$$

Otherwise, as seen from (B.37), the process $\{x(t),\, y(t),\, z(t),\, x^*(t),\, y^*(t),\, z^*(t)\}$ is purely deterministic.

Taking these constraints into account, the leading terms in ε in (B.37) are

$$\begin{aligned} \frac{\partial P(x,\, y,\, z,\, x^*,\, y^*,\, z^*,\, t)}{\partial t} &= \left\{\left\{-\frac{\partial}{\partial y}\left[\left(\lambda_2 y + \alpha_2\varepsilon^{1+b-2a}|x|^2\right)P\right]\right.\right. \\ &+ \left.\left.\frac{\partial}{\partial z}\left[\left(\lambda_3 z - \beta_2\varepsilon^{1+b-2a}x^2\right)P\right]\right\} + \text{c.c.}\right. \\ &+\varepsilon^{2b-1}\left(Q_2\frac{\partial^2}{\partial y\partial y^*} + Q_3\frac{\partial^2}{\partial z\partial z^*}\right)P\Bigg\}\left[1 + O(\varepsilon^r)\right], \end{aligned} \tag{B.44}$$

with some $r > 0$. Therefore, integrating with respect to y, z, y^* and z^*,

$$\frac{\partial P(x,\, x^*,\, t)}{\partial t} = O(\varepsilon^r) \ . \tag{B.45}$$

It is seen that at this order in ε the variables x and x^* do not evolve in time: we will call them *slow* variables, while y, z, y^*, z^* are the *fast* variables. Combining (B.44) and (B.45), one obtains for the conditional probability

$$\begin{aligned}\frac{\partial P(y,\, z,\, y^*,\, z^*,\, t|x,\, x^*)}{\partial t} &= \left\{\left\{-\frac{\partial}{\partial y}\left[\left(\lambda_2 y + \alpha_2 \varepsilon^{1+b-2a}|x|^2\right) P\right]\right.\right. \\ &+ \left.\left.\frac{\partial}{\partial z}\left[\left(\lambda_3 z - \beta_2 \varepsilon^{1+b-2a} x^2\right) P\right]\right\} + \text{c.c.}\right. \\ &+ \left.\varepsilon^{2b-1}\left(Q_2 \frac{\partial^2}{\partial y \partial y^*} + Q_3 \frac{\partial^2}{\partial z \partial z^*}\right) P\right\} \left[1 + O(\varepsilon^r)\right] ,\end{aligned} \tag{B.46}$$

which describes the way in which the fast variables y, z, y^*, z^* follow the slow ones x, x^*. If we are only concerned with the evolution of the slow variables, it suffices to consider the stationary solution to which the conditional probability relaxes on a time of the order of unity, namely,

$$\begin{aligned}P_{st}(y,\, z,\, y^*,\, z^*|x,\, x^*) &= \left(\frac{\varepsilon^{1-2b}}{\pi}\right)^3 \left(\frac{\lambda_2 \lambda_3}{Q_2 Q_3}\right)^{3/2} \\ &\times \exp\left[\frac{\lambda_2 \varepsilon^{1-2b}}{Q_2}\left|y + \frac{\alpha_2}{\lambda_2}\varepsilon^{1+b-2a}|x|^2\right|^2\right] \\ &\times \exp\left[\frac{\lambda_3 \varepsilon^{1-2b}}{Q_3}\left|z - \frac{\beta_2}{\lambda_3}\varepsilon^{1+b-2a} x^2\right|^2\right] .\end{aligned} \tag{B.47}$$

In order to get a nonsingular behavior in the limit $\varepsilon \to 0$, it is necessary that

$$1 - 2b = 0 \ , \quad \text{or } b = \frac{1}{2} \ . \tag{B.48}$$

We also note that if

$$1 + b - 2a = 0 \ , \quad \text{or } a = \frac{3}{4} \ , \tag{B.49}$$

these values of a and b satisfy all the restrictions involved. One can therefore adopt them as the relevant scaling laws. Correspondingly, (B.47) becomes

$$P_{st}(y,\, z,\, y^*,\, z^*|x,\, x^*) = \left(\frac{\lambda_2\lambda_3}{\pi^2 Q_2 Q_3}\right)^{3/2} \exp\left(\frac{\lambda_2}{Q_2}\left|y + \frac{\alpha_2}{\lambda_2}|x|^2\right|^2\right) \times \exp\left(\frac{\lambda_3}{Q_3}\left|z - \frac{\beta_2}{\lambda_3}x^2\right|^2\right) . \tag{B.50}$$

This allows us to calculate the conditional averages that appear in eq.(B.38) for the slow variables, namely,

$$\langle y|x,\, x^*\rangle = \langle y^*|x,\, x^*\rangle = \frac{-\alpha_2}{\lambda_2}|x|^2 ,$$
$$\langle z|x,\, x^*\rangle = \frac{\beta_2}{\lambda_3}x^2 . \tag{B.51}$$

We thus obtain, finally, a closed equation for $P(x,\, x^*,\, t)$:

$$\frac{\partial P(x,\, x^*,\, t)}{\partial t} = \varepsilon^{1/2}\left\{-\frac{\partial}{\partial x}\left\{\left[\Lambda\varepsilon^{c-1/2}x - \gamma|x|^2 x\right] P(x,\, x^*,\, t)\right\} + Q_1\frac{\partial^2 P(x,\, x^*,\, t)}{\partial x \partial x^*}\right\} , \tag{B.52}$$

where

$$\gamma \equiv \frac{-2\alpha_1\alpha_2}{\lambda_2} + \frac{\beta_1\beta_2}{\lambda_3} . \tag{B.53}$$

It is now obvious that the critical value of the exponent c is

$$c_{critical} = \frac{1}{2} , \tag{B.54}$$

i.e., the critical behavior manifests itself when $\lambda_1 = O(\varepsilon^{1/2})$.

We are ready, now, to compare these results with those presented earlier for the deterministic system. First of all, we distinguish between two time scales: a slow one for the variables x and x^*; and a fast one for y, z, y^* and z^*. In the vicinity of the bifurcation point, for $\lambda_1 = O(\varepsilon^{1/2})$, we obtain a closed equation for the probability density of the slow variables x, x^*, by taking into account the way in which the fast variables follow the slow ones,

eqs.(B.50) and (B.51). The expressions in (B.51) for the conditional averages correspond to the deterministic adiabatic elimination of fast variables (as described in the foregoing Section, and according to the deterministic part of eqs.(B.29)). Finally,

$$P_{st}(x,\, x^*) = \mathcal{N}^{-1} \exp\left[\frac{2}{Q_1}\left(\Lambda\varepsilon^{c-1/2}|x|^2 - \frac{\gamma}{2}|x|^4\right)\right] \tag{B.55}$$

with

$$\mathcal{N} = \frac{1}{4}\sqrt{\pi\, Q_1/\gamma}\ \exp\left(\Lambda^2\varepsilon^{2c-1}/\,\gamma Q_1\right)\ \mathrm{erfc}\left(-\,\Lambda\varepsilon^{c-1/2}/\sqrt{\gamma Q_1}\,\right)\,, \tag{B.56}$$

where erfc stands for the complementary error function. It can easily be shown that *the Gaussian character of the fast variables is preserved*, but their critical fluctuations are enhanced relative to their "far-from-critical" expressions (B.36). Therefore, only *the slow variable is characterized by critical non-Gaussian fluctuations*, eqs.(B.51), (B.54) and (B.55), when $c \approx 1/2$.

Bibliography

[1] One can find a list of the most famous hydrodynamic instabilities in S. Chandrasekhar, *Hydrodynamic and Hydromagnetic Stability*, Clarendon Press, Oxford (1961).

[2] R. Schmitz, Phys. Rep. **171**, 1 (1998).

[3] A. M. Tremblay, in *Recent Developments in Nonequilibrium Thermodynamics*, eds. J. Casas-Vasquez, D. Jou and G. Lebon, Springer-Verlag, Berlin (1984).

[4] N. N. Bogoliubov, in *Studies in Statistical Mechanics*, Vol. I, eds. G. E. Uhlenbeck and J. de Boer, North-Holland, Amsterdam (1962).

[5] G. E. Uhlenbeck, in *Probability and Related Topics in Physical Sciences*, ed. M. Kac, Wiley, New York (1959).

[6] J. R. Dorfman, T. R. Kirkpatrick, and J. V. Sengers, Ann. Rev. Phys. Chem. **45**, 213 (1994).

[7] M. Fixman, J. Chem. Phys. **47**, 2808 (1967); L. P. Kadanoff and J. Swift, Phys. Rev. **166**, 89 (1968); K. Kawasaki, Ann. Phys. (NY) **61**, 1 (1970); K. Kawasaki, in *Phase Transitions and Critical Phenomena*, Vol. 5A, eds. C. Domb and M. S. Green, Academic Press, New York (1976).

[8] J. R. Dorfman and E. G. D. Cohen, Phys. Rev. Lett. **16**, 124 (1965); J. Weinstock, Phys. Rev. A **140**, 460 (1965); E. G. D. Cohen, Physica A **194**, 229 (1993).

[9] A. Onuki, J. Stat. Phys. **18**, 475 (1978); T. R. Kirckpatrick, E. G. D. Cohen, and J. R. Dorfman, Phys. Rev. Lett. **42**, 862 (1979); *ibid.* **44**, 472 (1980); *ibid.*, Phys. Rev. A **26**, 950 (1982); *ibid.*, 972 (1982); *ibid.*,

995 (1982); T. Kirckpatrick and E. G. D. Cohen, Phys. Lett. **78 A**, 350 (1980); J. Stat. Phys. **33**, 639 (1983).
For binary fluid mixtures, see A. Campa and E. G. D. Cohen, Phys. Rev. Lett. **61**, 853 (1988); *ibid.*, Phys. Rev. A **39**, 4909 (1989); *ibid.*, Phys. Rev. A **41**, 5451 (1990); *ibid.* Physica A **174**, 214 (1991).

[10] I. Procaccia, D. Ronis, M. A. Collins, J. Ross, and I. Oppenheim, Phys. Rev. A **19**, 1290 (1979); D. Ronis, I. Procaccia, and I. Oppenheim, Phys. Rev. A **19**, 1307 (1979); *ibid.*, 1324 (1979); *ibid.*, Phys. Rev. A **26**, 1812 (1982); I. Procaccia, D. Ronis, and I. Oppenheim, Phys. Rev. Lett. **42**, 287 (1979).

[11] K. Kawasaki and J. Gunton, Phys. Rev. A **8**, 2048 (1973) ; K. Kawasaki, Prog. Theor. Phys. **51**, 1064 (1974) ; T. Yamada and K. Kawasaki, Prog. Theor. Phys. **53**, 111 (1975); R. Graham and H. Pleiner, Phys. Fluids, **18**, 130 (1975); J. Dufty, Phys. Rev. Lett. **51**, 2159 (1983); J. Dufty, in *Spectral Line Shapes*, ed. P. Wende, De Kruger, Berlin (1981); J. Dufty, Phys. Rev. A **30**, 1465 (1984); J. Lutsko and J. Dufty, Phys. Rev. A **32**, 1229 (1985).

[12] L. D. Landau and E. M. Lifshitz, *Fluid Mechanics*, Pergamon Press, Oxford (1984).

[13] A. M. Tremblay, E. Siggia, and M. Aray, Phys. Rev. Lett. **42**, 287 (1979); A. M. Tremblay, M. Aray and E. Siggia, Phys. Rev. A **23**, 1451 (1981) ; D. Ronis and S. Putterman, Phys. Rev. A **22**, 733 (1980); G. Van der Zwan, D. Bedeaux, and P. Mazur, Physica A **107**, 491 (1981); R. Schmitz and E.G.D. Cohen, J. Stat. Phys. **39**, 285 (1985); *ibid.*, **40**, 431 (1985); *ibid.*, **46**, 319 (1987); *ibid.*, Phys. Rev. A **35**, 2602 (1987).

[14] J. Machta, I. Procaccia and I. Oppenheim, Phys. Rev. Lett. **42**, 1368 (1979); J. Machta, I. Oppenheim, and I. Procaccia, Phys. Rev. A. **22**, 2809 (1980).

[15] B. M. Law and J. V. Sengers, J. Stat. Phys. **57**, 531 (1989); J. V. Sengers and B. M. Law, in *Lectures on Thermodynamics and Statistical Mechanics*, eds. M. Lopez de Haro and C. Varea, World Scientific, Singapore (1990); J. V. Sengers and B. M. Law, in *Nonlinear and Chaotic Phenomena in Plasmas, Solids, and Fluids*, eds. W. Rozmes and S. A. Tuszynski, World Scientific, Singapore (1991); P. N. Segrè, R. W. Gammon, and J. V. Sengers, Phys. Rev. **A 45**, 714 (1992); Phys. Rev. **E 47**,

1026 (1993); P. N. Segrè and J. V. Sengers, Physica **A 198**, 46 (1993); P. N. Segrè, R. Schmitz, and J. V. Sengers, Physica **A 195**, 31 (1993); W. B. Li, P. N. Segrè, R. Gammon, and J. V. Sengers, Physica **A 204**, 399 (1994); W. B. Li, P. N. Segrè, J. V. Sengers, and R. Gammon, J. Phys. Cond. Matt. **6**, A119 (1994); K. J. Zhang, M. E. Briggs, R. W. Gammon, and J. V. Sengers, J. Chem. Phys. **104**, 6881 (1996); W. B. Li, K. J. Zhang, J. V. Sengers, R. W. Gammon, and J. M. Ortiz de Zarate, Phys. Rev. Lett. **81**, 5580 (1998); J. Chem. Phys. **112**, 9139 (2000).

[16] M. Malek Mansour, A. L. Garcia, G. Lie, and E. Clementi, Phys. Rev. Lett., **58**, 874 (1987); M. Mareschal, M. Malek Mansour, G. Sonino, and E. Kestemont, Phys. Rev. A **45**, 7180 (1992).

[17] A. Suarez, J. P. Boon, and P. Grosfils, Phys. Rev. E **54**, 1208 (1996).

[18] A. L. Garcia, M. Malek Mansour, G. Lie, M. Mareschal, and E. Clementi, Phys. Rev. A **36**, 4348 (1987).

[19] A. L. Garcia, Phys. Rev. **A 34**, 1454 (1986); M. Malek Mansour, A. L. Garcia, G. C. Lie, and E. Clementi, Phys. Rev. Lett. **58**, 874 (1987); A. L. Garcia, M. Malek Mansour, G. C. Lie, and E. Clementi, J. Stat. Phys. **47**, 209 (1987); M. Malek Mansour, J. W. Turner, and A. L. Garcia, J. Stat. Phys. **48**, 1157 (1987); A. L. Garcia, M. Malek Mansour, G. C. Lie, M. Mareschal, and E. Clementi, Phys. Rev. **A 36**, 4348 (1987); M. Malek Mansour, A. L. Garcia, J. W. Turner, and M. Mareschal, J. Stat. Phys. **52**, 295 (1988); M. Mareschal, M. Malek Mansour, A. Puhl, and E. Kestemont, Phys. Rev. Lett. **61**, 2550 (1988); A. Puhl, M. Malek Mansour, and M. Mareschal, Phys. Rev. **A 40**, 1999 (1989); A. L. Garcia and C. Penland, J. Stat. Phys. **64**, 1121 (1991); M. Malek Mansour, M. Mareschal, G. Sonnino, and E. Kestemont, in *Microscopic Simulations of Complex Hydrodynamic Phenomena*, eds. M. Mareschal and B. Holian, NATO ASI Series, Vol. 292, Plenum, London (1992).

[20] R. Schmitz and E. G. D. Cohen, J. Stat. Phys. **39**, 285 (1985); *ibid.*, **40**, 431 (1985).

[21] H. Van Beijeren and E. D. G. Cohen, Phys. Rev. Lett. **60**, 1208 (1988); J. Stat. Phys. **53**, 77 (1988).

[22] V. M. Zaitsev, and M. I. Shliomis, Sov. Phys. JETP **32**, 866 (1971).

[23] R. Graham, Phys. Rev. A **10**, 1762 (1974); R. Graham and H. Pleiner, Phys. Fluids **18**, 130 (1975); J. Swift and P. C. Hohenberg, Phys. Rev. A **15**, 319 (1977).

[24] A. M. Obukhov, Russ. Math. Surveys **38**, 113 (1983).

[25] R. H. Kraichnan, Phys. Fluids **10**, 1417 (1967).

[26] L. Meshalkin and Ya. G. Sinai, J. Appl. Math. Mech. **25**, 1140 (1961).

[27] J. S. A. Green, J. Fluid. Mech. **62**, 273 (1974).

[28] E. N. Lorenz, J. Fluid Mech. **55**, 545 (1972).

[29] A. A. Nepomniaschichii, J. Appl. Math. Mech. **40**, 836 (1976).

[30] G. I. Sivashinsky, Physica D **17**, 243 (1985).

[31] Z. S. She, Phys. Lett. A **124**, 161 (1987); Ph.D. Thesis, University of Paris VII (1987) (unpublished).

[32] R. Benzi, S. Succi, and M. Vergassola, Phys. Rep. **222**, 147 (1992).

[33] U. Frisch, B. Hasslacher, and Y. Pomeau, Phys. Rev. Lett. **56**, 1505 (1986) ; G. Doolen, ed., *Lattice Gas Methods for PDE's*, Physica D **47**, 1 (1991).

[34] M. Hénon and H. Scholl, Phys. Rev. A **43**, 5365 (1991).

[35] R. Benzi and S. Succi, J. Stat. Phys. **56**, 69 (1989) ; U. Frisch, B. Legras, and B. Villone, Physica D **94**, 36 (1996).

[36] E. Vanden Eijnden, D. Hanon, and J. P. Boon, in *Advances in Turbulence*, ed. U. Frisch, **VII**, p. 183 (1998); D. Hanon, Ph.D. Thesis, Université Libre de Bruxelles (2000) (unpublished).

[37] I. Bena, M. Malek Mansour, and F. Baras, Phys. Rev. E **59**, 5503 (1999).

[38] I. Bena, F. Baras, and M. Malek Mansour, Phys. Rev. E **62**, 6560 (2000).

[39] M. Malek Mansour, C. Van den Broeck, I. Bena, and F. Baras, Europhys. Lett. **47**, 8 (1999).

[40] S. Gama, M. Vergassola, and U. Frisch, J. Fluid Mech. **260**, 95 (1994).

[41] This result is not new and has been obtained earlier by several authors: Nepomniaschichii [29], Meshalkin and Sinai [26], and Lorenz [28].

[42] C. Machioro, Commun. Math. Phys. **105**, 99 (1986).

[43] See, for instance, W. E. Alley and B. J. Alder, Phys. Rev. A **27**, 3158 (1983) ; W. E. Alley, B. J. Alder, and S. Yip, Phys. Rev. A **27**, 3174 (1983).

[44] A. L. Garcia, M. Malek Mansour, G. Lie, and E. Clementi, J. Stat. Phys. **47**, 209 (1987).

[45] M. Malek Mansour, J. W. Turner, A. L. Garcia, J. Stat. Phys. **48**, 1157 (1987).

[46] H. Haken, *Synergetics - An Introduction*, Springer Verlag, Berlin (1983).

[47] G. Nicolis, *Introduction to Nonlinear Science*, Cambridge University Press, Cambridge (1995).

[48] F. Baras, M. Malek Mansour, and C. Van den Broeck, J. Stat. Phys. **28**, 557 (1982).

[49] G. M. Zaslavsky, R. Z. Sagdeev, D. A. Usikov, and A. A. Chernikov, *Weak Chaos and Quasi-Regular Patterns*, Cambridge University Press, Cambridge (1991), Ch. 9.

[50] C.-Y. Chow, *An Introduction to Computational Fluid Mechanics*, Seminole Publications, Boulder (1983).

[51] U. Geigenmüller, U. M. Titulaer, and B. U. Felderhof, Physica **119 A**, 41 (1983).

[52] G. A. Bird, *Molecular Gas Dynamics*, Clarendon, Oxford (1976) ; *ibid.*, *Gas Dynamics and the Direct Simulation of Gas Flows*, Clarendon, Oxford (1994).

[53] A Bird algorithm with adjustable transport coefficients has been proposed in F. Baras, M. Malek Mansour, A. Garcia, and M. Mareschal, J. Comp. Phys. **119**, 94 (1994).

[54] A. Puhl, M. Malek Mansour, and M. Mareschal, Phys. Rev. A **40**, 1999 (1989).

[55] An extension of the Bird algorithm dealing with dense systems has been reported in F. Alexander, A. Garcia, and B. Alder, Phys. Rev. Lett. **74**, 5212 (1995).

[56] D. H. Rothman and S. Zaleski, *Lattice-Gas Cellular Automata*, Cambridge University Press, Cambridge (1997).

[57] J. P. Boon, E. Vanden Eijnden and D. Hanon , to appear in *Chaos, Solitons and Fractals.*

[58] D. Hanon (private communication).

[59] R. Graham, Phys. Rev. A **10**, 1762 (1974) ; R. Graham and H. Pleiner, Phys. Fluids, **18**, 130 (1975); J. Swift and P. C. Hohenberg, Phys. Rev. A **15**, 319 (1977).

[60] L. D. Landau and E. M. Lifshitz, *Statistical Physics*, Pergamon, Oxford (1980), Ch. XII.

[61] L. D. Landau and E. M. Lifshitz, *Electrodynamics of Continuous Media*, Pergamon, Oxford (1982), Ch. XIV.

[62] B. J. Berne and R. Pecora, *Dynamic Light Scattering*, Wiley, New York (1976).

[63] J. P. Boon and S. Yip, *Molecular Hydrodynamics*, Dover, New York (1980).

[64] W. G. Hoover, Phys. Rev. Lett. **42**, 1531 (1979); B. L. Hoolian, W. G. Hoover, B. Moran, and G. K. Straub, Phys. Rev. A **22**, 2798 (1980); B. L. Holian, Phys. Rev. A **37**, 2562 (1988).

[65] M. Malek Mansour, F. Baras, and A. L. Garcia, Physica A **240**, 255 (1997).

[66] S. Wiggins, *Introduction to Applied Nonlinear Systems and Chaos*, Springer Verlag, New York (1990).

[67] J. Guckenheimer and P. Holmes, *Nonlinear Oscillations, Dynamical Systems and Bifurcations of Vector Fields*, Springer Verlag, New York (1983).

[68] E. Knobloch and K. A. Wiesenfeld, J. Stat. Phys. **33**, 611 (1983).

[69] T. G. Kurtz, J. Appl. Prob. **8**, 344 (1971); Stoch. Proc. Appl. **6**, 223 (1978).

List of Publications

- I. Bena, C. Misbah, and A. Valance, "Nonlinear evolution of a terrace edge during step-flow growth", Phys. Rev. B **47**, 7408 - 7419 (1993).
- G. Bourceanu, P. Joulain, A. Birzu, I. Birzu (Bena), and V. Melnig, "Thermodynamic considerations on the partial miscibility of liquids", Entropie (France) **97**, 47 - 51 (1996) (in French).
- I. Birzu (Bena), "New demonstration for the minimum entropy production theorem", Entropie (France) **97**, 59 - 64 (1996) (in French).
- I. Bena, M. Malek Mansour, and F. Baras, "Hydrodynamic fluctuations in the Kolmogorov flow: Linear regime", Phys. Rev. E **59**, 5503 - 5510 (1999).
- M. Malek Mansour, C. Van den Broeck, I. Bena, and F. Baras, "Spurious diffusion in particle simulations of the Kolmogorov flow", Europhys. Lett. **47**, 8 - 13 (1999).
- I. Bena and C. Van den Broeck, "Coupled parametric oscillator", Europhys. Lett. **48**, 498 - 504 (1999).
- A. Birzu, I. Birzu (Bena), G. Bourceanu, and J. Vatamanu, "Properties of the thermodynamic coefficients in the case of chemical reactions ", Romanian Chemistry Review **50**, 647 - 655 (1999) (in Romanian).
- I. Bena, M. Copelli, and C. Van den Broeck, "Stokes' drift: a rocking ratchet", J. Stat. Phys. **101**, 415 - 424 (2000).

- I. Bena, F. Baras, and M. Malek Mansour, "Hydrodynamic fluctuations in the Kolmogorov flow: Nonlinear regime", Phys. Rev. E **62**, 6560 - 6570 (2000).
- C. Van den Broeck, I. Bena, P. Reimann, and J. Lehmann, "Coupled Brownian motors on a tilted washboard", Ann. Phys. (Leipzig) **9**, 713 - 720 (2000).
- C. Van den Broeck and I. Bena, "Parametric resonance revisited", in *Stochastic Processes in Physics, Chemistry, and Biology*, eds. J. A. Freund and T. Pöschel, Lecture Notes in Physics Vol. 557, Springer Verlag, Berlin (2000).
- I. Bena, R. Kawai, C. Van den Broeck, M. Copelli, and K. Lindenberg, "On the collective behavior of parametric oscillators", submitted to Phys. Rev. E.